Characterization of the coherence of ultra-cold atoms with nonlinear matter-wave optics methods

Von der Fakultät Mathematik und Physik der Universität Stuttgart

zur Erlangung der Würde eines Doktors der Naturwissenschaften

(Dr. rer. nat.) genehmigte Abhandlung

Vorgelegt von

Dominic Meiser

aus Stennweiler

Hauptberichter:	Prof. Dr. H. Giessen
Zweitberichter:	Prof. Dr. G. Mahler
Tag der mündlichen Prüfing:	28.7.2006

4. Physikalisches Institut der Universität Stuttgart

2006

ACKNOWLEDGEMENTS

This dissertation would not have been possible without the help and support from many people. I would like to thank

- my coworkers and fellow students in Bonn and Tucson: Dietmar, Jörn, Diana, Florian, Taka, Markku, Chris, Wenzhou, Hermann, Omjyoti.
- the many members of the administration at the University of Tucson and the Universität Stuttgart who have always been friendly and helpful and who have made this graduation as smooth as possible: Pat Gransie, Dottie Sherwood-Cooney, Donna Swibold, Gabi Feuerle and Christa Nagel.
- Harald Giessen for giving me the opportunity to go to Tucson and for the great support over the last five years.
- Pierre Meystre for being such a patient teacher, for letting me travel as much as I did and for doing whatever it takes to help me in every respect.

Ganz besonderer Dank gilt meiner Familie und Sarah für die bedingungslose Unterstützung und Rückhalt.

Parts of this dissertation have been published in the following articles:

A. Nunnenkamp, D. Meiser, and P. Meystre, “Full counting statistics of heteronuclear molecules from Feshbach-assisted photoassociation”, New J. Phys. **8**, 88 (2006).

D. Meiser, T. Miyakawa, H. Uys, und P. Meystre, “Quantum optics of ultracold molecules”, in *Advances in Atomic, Molecular and Optical Physics*, vol. 53, Hrsg. G. Rempe und M. O. Scully, Academic Press (2006).

H. Uys, T. Miyakawa, D. Meiser, and P. Meystre, “Passage time statistics in the formation of ultra-cold dimers from fermionic atoms”, Phys. Rev. A **72**, 53616 (2005).

D. Meiser and P. Meystre, “Reconstruction of the phase of matter-wave fields using a momentum resolved cross-correlation technique”, Phys. Rev. A **71**, 023605 (2005).

D. Meiser and P. Meystre, “Number statistics of molecules formed by ultracold atoms”, Phys. Rev. Lett. **94**, 093001 (2005).

D. Meiser, C. P. Search, and P. Meystre, “Molecule formation as a diagnostic tool for second-order correlations of ultra-cold gases”, Phys. Rev. A **71**, 033621 (2005).

Notation and conventions

Throughout this dissertation we use SI units. The complex conjugate of a complex number z is denoted by z^*. All operators are designated with a hat, e.g. $\hat{a}$. Vectors are written in bold face letters, e.g. $\mathbf{x}$.

We define the Fourier transform of any c-number valued or operator valued function $f(\mathbf{x})$ as

$$\tilde{f}(\mathbf{q}) = \frac{1}{\sqrt{V}} \int_V d^3x e^{-i\mathbf{q}\mathbf{x}} f(\mathbf{x}), \tag{0.1}$$

so that the inverse Fourier transform is

$$f(\mathbf{x}) = \frac{1}{\sqrt{V}} \sum_{\mathbf{q}} d^3q e^{i\mathbf{q}\mathbf{x}} \tilde{f}(\mathbf{x}). \tag{0.2}$$

Here V is a cube in three dimensional space, often referred to as quantization volume, and the allowed wavevectors $\mathbf{q}$ are determined such that the exponentials $e^{i\mathbf{q}\mathbf{x}}$ are periodic in V. The definitions Eq. (0.1) and Eq. (0.2) are immediately clear for integrable functions f with compact support if V is chosen large enough, i.e. $\operatorname{supp} f \subset V$. If f does not have compact support, the limit $V \to \infty$ is taken at the end of the calculation, i.e. we use finite volume regularization. For all the fields encountered in this thesis this procedure is well defined.

The following symbols have special meanings:

constants:	
c	speed of light
$\hbar$	Planck's constant divided by 2π
k_B	Boltzmann's constant
others:	
H.C.	Hermitian conjugate of the expression immediately to the left
$\langle \ldots \rangle$	Quantum mechanical average for quantum objects and ensemble average for classical quantities
tr	trace of an operator

CONTENTS

LIST OF FIGURES

ABSTRACT

In this dissertation we make use of the many analogies between quantum optical and ultra-cold atomic and molecular systems in order to study the coherence properties of the latter with methods of non-linear optics.

We adapt the XFROG method that has first been developed for the characterization of ultra-short laser pulses, to the problem of reconstructing both amplitude and phase of the condensate wavefunction of a Bose-Einstein-condensate (BEC). Using the example of a vortex state we study the dependence of the reconstruction quality on the number of measurements and different sources of noise and we find that the method is feasible with available experimental technology.

Exploiting the similarity between the coherent formation of ultra-cold molecules and optical sum frequency generation we devise a scheme for measuring second-order correlations of atoms through density measurements of molecules. We use perturbation theory in the cases of weak and strong coupling between atoms and molecules to calculate the momentum distribution of the molecules for the cases where the molecules are formed from a BEC, a normal Fermi gas and a Fermi gas with superfluidity in a Bardeen-Cooper-Schrieffer (BCS) state. These calculations are supplemented by exact integrations of Schrödinger's equation in the single mode approximation for the molecules. Atoms in a BEC are collectively transformed into molecules with a narrow momentum distribution reflecting the long coherence length of atoms in the BEC. For the normal Fermi gas molecules are formed non-collectively and their momentum distribution is much wider. The momentum distribution of molecules from a BCS state looks similar to the BEC case: The superfluid component leads to collectively formed molecules with a very narrow momentum distribution and the unpaired fraction gives rise to non-collectively formed molecules with a much wider momentum distribution similar to the normal Fermi gas case. The counting statistics of the molecules from a BEC is that of a coherent state, from a normal Fermi gas it is that of a thermal state and the BCS case interpolates between the two.

1. INTRODUCTION

The degree of coherence is a very important property of wave phenomena in general. It characterizes the ability of the wave field to exhibit interference.

Interference is closely related to the superposition principle that many wave phenomena obey. Two waves with amplitudes E_1 and E_2 give rise to a total field that is simply given by the sum of the two, $E_1 + E_2$. Because the relative phase between E_1 and E_2 can vary, the two waves can add up or they can be subtracted from each other. The first case is called constructive interference and the latter destructive interference. In many cases of practical importance the two fields can be written as the product of a rapidly varying carrier wave, e.g. of the form $\cos(\mathbf{k}_{1,2}\mathbf{x} - \omega_{1,2}t)$, with $\mathbf{k}_{1,2}$ the wavevectors of the fields 1 and 2 and $\omega_{1,2}$ their frequencies, and an envelop $\tilde{E}_{1,2}(\mathbf{x}, t)$ that modulates the carrier wave and varies very little over a wavelength $\lambda_{1,2} = 2\pi/|\mathbf{k}_{1,2}|$. Then the superposition of the two fields will give rise to an intensity pattern $|E_1 + E_2|^2$ that varies over distances of order $\lambda_{1,2}$ between fully destructive and fully constructive interference.

In a classical theory the relative phase between the two fields can fluctuate over time and if time averages of the intensity are observed the contrast of the interference fringes may be reduced. The reduction of the contrast from the maximum possible value leads directly to a quantitative measure for coherence for classical fields [13]. Obviously, coherence is intimately related to correlations and fluctuations.

Soon after the introduction of lasers it became obvious that a more careful definition of coherence was required for quantized light fields. Roughly speaking, for a full characterization of coherence, knowledge of the correlations of the field at an arbitrary number of space-time points is required. In the classical case all these correlations can be reduced to the two point field correlations. For a quantized field this is no longer true. E.g. even if two interfering mode functions have a perfectly stable relative phase, the contrast of the interference pattern can still fluctuate because the number of field quanta in the two modes may be uncertain. This difference between classical and quantized fields, as far as their coherence properties are concerned, was first fully recognized by Glauber and this lead him to introduce a hirarchy of coherence functions of various orders that are the basis of his quantum theory of coherence. He first explained these ideas in two seminal papers in 1963 [47, 46] and this work has been rewarded with a share of the Nobel

prize in 2005.

It is well known that matter also possesses wave character [29, 28] and hence can interfere. For over fifty years interference experiments with matter were limited to single particle interference. Consequently, all the observed effects could be readily explained with classical coherence theory. In a sense, these experiments were analogous to optical experiments in the pre-laser era using light from classical thermal sources, which has at most one photon per quantum state as well. The dramatic progress in the cooling of atoms has made it possible to increase their phase space density and to ultimately achieve Bose-Einstein condensation (BEC) [3, 15, 27] which is a state in which a macroscopic number of atoms occupy a single quantum state. Similar to lasers in optics, the advent of quantum degenerate atomic gases has made it necessary to extend the quantum theory of coherence to matter waves.

Matter waves introduce several new aspects to the coherence theory. The first is related to interactions. Photons usually do not interact strongly with each other and in most cases their interaction with matter is also weak. This leads to their coherence properties being mostly simple and rather easy to understand. Atoms on the other hand interact strongly with each other and can be efficiently manipulated with external magnetic or optical fields. This gives rise to an intriguing variety of different many-particle quantum states and their different coherence properties are an important means to classify them.

Secondly, atoms can also obey Fermi-Dirac statistics. The extension of the optical coherence theory, which is a theory for bosons, to fermions is still an open question.

Despite their tremendous value in classifying and characterizing manyparticle quantum states, measurements of higher order correlations of matter fields have not very often been performed[1]. The reason for this lies without question in the technical difficulties that such a measurement poses, which stem mostly from the fact that the atom detection is more difficult than e.g. photon detection and cannot be achieved with the same level of accuracy and reliability, at least not yet. As a consequence, studies of ultracold atoms have to date mostly relied on measurements of the atomic density, i.e. first order correlations.

The need to characterize higher order correlations of ultracold atoms combined with the experimental difficulties in detecting them have provided the main motivation for the work summarized in this dissertation. We have adapted two methods well known in nonlinear and quantum optics to matter wave optics.

The first scheme is based on the so called XFROG method that is used in optics for the characterization of the amplitude and phase of ultrashort laser pulses. The proposed method aims at measuring the condensate wavefunction of BECs. The

[1] Exceptions where higher order correlations have been measured are discussed in chapter 4.

second method relies on the formal similarities between optical sum frequency generation and the coherent formation of molecules from ultra-cold atoms and aims at a characterization of second order correlations of atomic states. Both methods rely on density measurements, which, with the difficulties with the measurements of higher order correlations of atomic states in mind, was one of our "design goals".

The rest of this dissertation is organized as follows: In chapter 2 we review the optical coherence theory for classical and quantum fields. Besides giving an exposition of the theoretical framework we provide a number of examples of states of the light field that will serve as valuable reference points for the atom optical case in later chapters.

Chapter 3 gives an overview of the formalism necessary for the description of ultracold atoms and molecules. We employ an approach that we found particularly well suited for the study of coherence properties and we explain the consequences of certain approximations as far as coherence and correlations are concerned. Specifically, we discuss the mean field approximation for BECs and the inclusion of fluctuations within the Bogoliubov approximation. For Fermions we describe the local density approximations for Fermions in the normal state and the Bardeen-Cooper-Schrieffer (BCS) theory for superfluidity in the weakly interacting regime. A feature of ultra-cold atomic systems is that they are typically confined in an external trapping potential so that their theoretical description necessarily needs to include spatial inhomogeneity. To this end we have devised a simple formalism that is based on the splitting of the atomic state into a part with long range correlations and in a fluctuations part whose correlations decay on a rather short length scale. We describe this method in detail for the case of a BEC with thermal and quantum fluctuations as well as for the BCS state. We also describe the physics of ultra-cold molecules as it is needed for the scope of this dissertation. We discuss the two-body physics that gives rise to these molecules and Feshbach resonances and we show how the molecules can be introduced into an effective many-body theory, highlighting the similarities with optical three-wave mixing.

In chapter 4 we review the status of the field of coherence for matter waves. We discuss several experiments that have been performed so far using various approaches and we outline how the optical coherence theory has been adapted to matter waves by several researchers.

In chapter 5 we discuss a number of analogies between quantum optical and atom optical systems. These analogies can often be used to obtain a qualitative understanding of the atomic system in question without explicit calculations. Furthermore it allows one to transfer the powerful theoretical methods that have been developed in quantum optics to the ultra-cold atoms arena.

In chapter 6 we show how the XFROG method can be adapted for the recon-

struction of the amplitude and phase of condensate wavefunctions using momentum resolved cross-correlations. We discuss general properties of the resulting method and use the example of the reconstruction of a vortex state to illustrate the procedure. We analyze the feasibility of the method by studying how the accuracy of the field reconstruction changes with the number of measurements and how it is affected by noise in the measurements.

Chapter 7 describes how ultracold molecules can be used as a probe of second order correlations in atomic gases. Using perturbation theory we calculate the momentum distribution of molecules formed from a BEC with fluctuations, from a normal Fermi gas and from a BCS state. The BEC and normal Fermi gas cases serve as reference points and our main interest lies in showing that the molecules can be used to detect the superfluid order parameter in the BCS state, an effect of second order correlations that is very difficult to analyze through measurements of the atomic density.

In chapter 8 we use a simplified single mode model for the coupled atom molecule system to solve its quantum dynamics exactly and thus we obtain the full counting statistics of the molecular field. Through this full quantum treatment we gain a deeper understanding of the statistical aspects of the molecule formation process. We show that the counting statistics of the molecular field strongly depends on the statistics of the original atomic state and this way we can get additional information about the atomic state.

We conclude and give some indications on work we intend to do in the future in chapter 9.

2. OPTICAL COHERENCE THEORY

The field of optical coherence is very highly developed and mature. Without question part of the reason for that lies in the importance of a good unterstanding of coherence for many optical devices such as interferometers that play important roles both in fundamental research as well as in technological applications. Especially since the invention of the laser, experimentalists have gained tremendous control over many properties of light and have been able to manufacture light sources with custom made properties.

Since it will be our goal in later chapters to transfer part of the knowledge and methods of optical coherence theory to atom optical situations, it is natural that we first take a closer look at coherence in optics.

In this chapter we thus first review the classical coherence theory of optical fields and then describe quantum optical coherence theory. We first discuss Glauber's analysis of the photodetector since it plays an important role in the construction of Glauber's coherence theory. We show how correlation functions of various orders naturally arise from coincidence measurements and how they serve to define the different orders of coherence.

Finally, we discuss several examples that serve a dual purpose. First, they allow us to illustrate the concept of coherence as it is introduced in this chapter. Second, these examples are of a representative nature and we will use them as reference points to compare the atom optical states with in later chapters. Specifically, we discuss coherent states of light, which are the quantum mechanical analogs of a perfectly stable classical wave, number states, which have a well defined intensity, and thermal fields, which are a good model for the light created in classical, i.e. non-laser, light sources. We also discuss the light field generated by an ensemble of independent radiators, wich is an important model system for many fields. We conclude the chapter by introducing the counting statistics of a field. We calculate the counting statistics for the coherent, number and thermal state.

2.1 Classical coherence theory

Even though we will ultimately be interested in the coherence properties of quantum fields it is valuable to first study the classical theory since the quantum theory

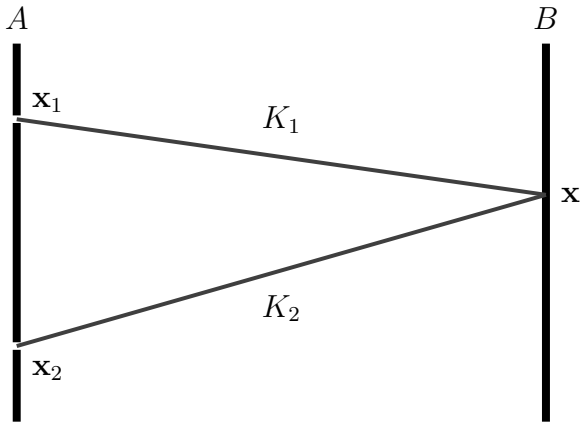

Fig. 2.1: Schematic of interference of light originating from two pinholes at positions $\mathbf{x_1}$ and $\mathbf{x_2}$.

is to some degree modelled after it. Thus it is interesting to see on the one hand the similarities between quantum and classical coherence and recognize the effects that could in principle be understood in the framework of a classical theory and to see on the other hand the effects that are inherently quantal and have no classical analog.

The classical theory of optical coherence was put on a solid foundation by E. Wolf in the 1950s, see chapter 10 in [13], also [83, 85, 89]. In this section we closely follow E. Wolf's original discussion. We consider a prototypical interference experiment in which light originating from two pinholes at positions $\mathbf{x_1}$ and $\mathbf{x_2}$ in an opaque screen A falls onto another screen B where it is detected, see Fig. 2.1. We assume that the light is perfectly polarized in one common plane so that we can describe it by a scalar field.

The field at position $\mathbf{x}$ is

$$E^{(+)}(\mathbf{x}) = K_1 E^{(+)}(\mathbf{x_1}, t_1) + K_2 E^{(+)}(\mathbf{x_2}, t_2), \tag{2.1}$$

where

$$t_{1,2} = \frac{|\mathbf{x} - \mathbf{x_{1,2}}|}{c} \tag{2.2}$$

are the times it takes the light field to travel from the pinholes to $\mathbf{x}$ and $K_{1,2}$ are amplitudes that describe how the light field propagates from the openings to $\mathbf{x}$. $K_{1,2}$ depend on the geometry of the pinholes and the the light field incident on the pinholes from the left of screen A.

Light detectors are sensitive to the cycle averaged intensity. The cycle aver-

aged intensity is found from the Poynting vector of the light field as [83, 59]

$$I = \frac{1}{2} c\varepsilon_0 |E^{(+)}|^2, \tag{2.3}$$

where $E^{(+)}$ is the positive frequency part of the light field[1].

We find for the light intensity at $\mathbf{x}$

$$I(\mathbf{x}) = \frac{1}{2} c\varepsilon_0 |K_1|^2 |E^{(+)}(\mathbf{x_1}, t_1)|^2 + \frac{1}{2} c\varepsilon_0 |K_2|^2 |E^{(+)}(\mathbf{x_2}, t_2)|^2 + c\varepsilon_0 |K_1 K_2| \mathrm{Re}(E^{(-)}(\mathbf{x_1}, t_1) E^{(+)}(\mathbf{x_2}, t_2)), \tag{2.8}$$

where we have used that $K_{1,2}$ are purely imaginary and that $E^{(+)*} = E^{(-)}$. Light detectors have a finite response time and the signal they record represents the average of the intensity over some time interval. We denote this averaging by $\langle \ldots \rangle$. For simplicity we assume that the light field is stationary and the detector averages over a long enough time interval (much longer than the coherence time defined below) so that the measured intensities do not depend on time any more[2].

[1] In general, if

$$V^{(r)}(t) = \int_0^\infty d\omega a(\omega) \cos(\phi(\omega) - \omega t) \tag{2.4}$$

is a real signal, the positive frequency part is defi ned as

$$V^{(+)}(t) = \int_0^\infty d\omega a(\omega) e^{i(\phi(\omega) - \omega t)} \tag{2.5}$$

with the same real function $a(\omega)$. The form of the real signal Eq. (2.4) has the advantage that the reality of $V(r)$ is obvious. Sometimes it is however advantageous to introduce the Fourier transform

$$V^{(r)}(t) = \frac{1}{\sqrt{2\pi}} \int_{-\infty}^\infty d\omega v(\omega) e^{-i\omega t} \tag{2.6}$$

where the reality of $V^{(r)}$ is now ensured by $v(-\omega) = v^*(\omega)$. In therms of the Fourier transform the positive frequency part can be written as

$$V^{(+)}(t) = \sqrt{\frac{2}{\pi}} \int_0^\infty d\omega v(\omega) e^{-i\omega t} \tag{2.7}$$

Because only positive frequencies are involved this function is analytic in the lower half of the complex omega plane.

[2] Wolf's original theory always considered stationary fi elds of this kind and accordingly the "detector-averages" where always temporal. An objection frequently raised against this theory in the early days was that this requirement is too restrictive since it cannot capture situations in which light pulses are brought to interference. Note however that through a reinterpretation of the averages as ensemble averages his theory can also be applied to light pulses. Thus, with the light fi elds considered as stochastic fi elds taken from certain ensembles, Wolf's theory gives a complete description of fi rst order coherence phenomena.

Introducing

$$G^{(1)}(\mathbf{x_1}, t_1; \mathbf{x_2}, t_2) = \langle E^{(-)}(\mathbf{x_1}, t_1) E^{(+)}(\mathbf{x_2}, t_2) \rangle \tag{2.9}$$

and

$$g^{(1)}(\mathbf{x_1}, t_1; \mathbf{x_2}, t_2) = \frac{G^{(1)}(\mathbf{x_1}, t_1; \mathbf{x_2}, t_2)}{\sqrt{G^{(1)}(\mathbf{x_1}, t_1; \mathbf{x_1}, t_1) G^{(1)}(\mathbf{x_2}, t_2; \mathbf{x_2}, t_2)}} \tag{2.10}$$

we can write the intensity as

$$\langle I(\mathbf{x}) \rangle = \langle I_1(\mathbf{x}) \rangle + \langle I_2(\mathbf{x}) \rangle + 2\sqrt{\langle I_1(\mathbf{x}) \rangle \langle I_2(\mathbf{x}) \rangle} |g^{(1)}(\mathbf{x_1}, t_1; \mathbf{x_2}, t_2)| \cos \phi(x_1, x_2) \tag{2.11}$$

where $\phi(x_1, x_2)$ is the phase of $g^{(1)}(\mathbf{x_1}, t_1; \mathbf{x_2}, t_2)$ and

$$\langle I_{1,2}(\mathbf{x}) \rangle = \frac{1}{2} c \varepsilon_0 G^{(1)}(\mathbf{x_{1,2}}, t_{1,2}; \mathbf{x_{1,2}}, t_{1,2}).$$

$g^{(1)}(\mathbf{x_1}, t_1; \mathbf{x_2}, t_2)$ depends only on the time difference $t_1 - t_2$ due to the assumed stationarity of the light field. The intensities $I_{1,2}(\mathbf{x})$ are the intensities of the field at position $\mathbf{x}$ if only one of the sources was present. They are assumed to change slowly compared to an optical wavelength. The phase $\phi(\mathbf{x_1}, \mathbf{x_2})$ on the other hand changes appreciably over distances of the order of an optical wavelength. Therefore it is clear that $|g^{(1)}(\mathbf{x_1}, t_1; \mathbf{x_2}, t_2)|$ determines the contrast of the interference fringes. Consequently, $|g^{(1)}(\mathbf{x_1}, t_1; \mathbf{x_2}, t_2)|$ is used to characterize the degree of coherence of a wave field in Wolfs classical coherence theory . The waves interfere maximally if $|g^{(1)}(\mathbf{x_1}, t_1; \mathbf{x_2}, t_2)| = 1$ and in this case the fields are called fully coherent. Due to the Cauchy-Schwartz inequality a value of $|g^{(1)}(\mathbf{x_1}, t_1; \mathbf{x_2}, t_2)|$ larger than one is impossible. If $|g^{(1)}(\mathbf{x_1}, t_1; \mathbf{x_2}, t_2)| = 0$ on the other hand the intensities from the two sources add without any interference at all and the fields are called incoherent. If $|g^{(1)}(\mathbf{x_1}, t_1; \mathbf{x_2}, t_2)|$ is between zero and one the fields are called partially coherent.

2.2 Quantum optical coherence theory

In the quantum theory of light the electrical field is replaced by a field operator $\hat{E}(\mathbf{x}, t)$. Details on the field quantization can be found in the many textbooks on the subject, e.g. [89, 83, 20, 19].

Due to the quantization of the light field the definitions and concepts of the previous section cannot be immediately applied, since they involve expectation values of classical, or possibly stochastic, fields. The quantum optical coherence theory was first developed by Glauber. His concept of coherence is very operational and is based on his analysis of the photodetector, which we will outline first.

2.2.1 Glauber's theory of the photodetector

Just like the field amplitude in the classical case, the field operator can be decomposed into a positive and a negative frequency part,

$$\hat{E}(\mathbf{x},t) = \hat{E}^{(+)}(\mathbf{x},t) + \hat{E}^{(-)}(\mathbf{x},t) \tag{2.12}$$

$$\equiv \sum_{\mathbf{k},\varepsilon} \mathcal{E}_{\mathbf{k},\varepsilon}(\mathbf{x})\varepsilon\, \hat{a}_{\mathbf{k},\varepsilon} e^{-i\omega_{\mathbf{k},\varepsilon}t} + \sum_{\mathbf{k},\varepsilon} \mathcal{E}^{*}_{\mathbf{k},\varepsilon}(\mathbf{x})\varepsilon\, \hat{a}^{\dagger}_{\mathbf{k},\varepsilon} e^{i\omega_{\mathbf{k},\varepsilon}t}. \tag{2.13}$$

$\mathcal{E}_{\mathbf{k},\varepsilon}(\mathbf{x})$ are the orthogonal modes of the electromagnetic field labeled by the wave vector $\mathbf{k}$ and the polarization ε, $\omega_{\mathbf{k},\varepsilon}$ are the corresponding eigenfrequencies and $\hat{a}_{\mathbf{k},\varepsilon}$ and $\hat{a}^{\dagger}_{\mathbf{k},\varepsilon}$ are the bosonic annihilation and creation operators for a photon in mode $\mathcal{E}_{\mathbf{k},\varepsilon}$. As we can see from Eq. (2.13) the positive frequency part annihilates a photon and the negative frequency part creates one.

As a model for a photodetector we consider an atom at position $\mathbf{x}$. At optical frequencies we can assume that the atom is initially in its ground state. Then the atom can only absorb photons from the light field. Photon detection is achieved by transitions of the atom from the initial state to some other state. Assuming first that the light field is in a pure state $|\psi\rangle$, the initial state of light field and detector atom is

$$|i\rangle = |\psi\rangle|i_{\text{detector}}\rangle, \tag{2.14}$$

where $|i_{\text{detector}}\rangle$ is the ground state of the atom. In first order perturbation theory the transition rate to state $|\psi_f\rangle|f_{\text{detector}}\rangle$ is proportional to

$$|\langle\psi_f|\langle f_{\text{detector}}|\hat{H}_{\text{int}}|\psi\rangle|i_{\text{detector}}\rangle|^2 \tag{2.15}$$

where the interaction Hamiltonian $\hat{H}_{\text{int}}$ describes the coupling of the atom to the light field. Assuming that the final state of the detector atom is not observed, we can sum over all atomic states and we find that the detector current is proportional to

$$|\langle\psi_f|\hat{E}^{(+)}(\mathbf{x},t)|\psi\rangle|^2, \tag{2.16}$$

where we have assumed that the interaction Hamiltonian is linear in the electric field, as is normally the case. Since the final state of the light field is typically not observed we have to trace over it so that we finally obtain the detector signal as

$$\text{Signal} \propto \sum_{|\psi_f\rangle} |\langle\psi_f|\hat{E}^{(+)}(\mathbf{x},t)|\psi\rangle|^2 = \langle\psi|\hat{E}^{(-)}(\mathbf{x},t)\hat{E}^{(+)}(\mathbf{x},t)|\psi\rangle. \tag{2.17}$$

If the light field is in a mixture of states described by the density matrix

$$\hat{\rho} = \sum_{|\psi\rangle} P_\psi |\psi\rangle\langle\psi| \tag{2.18}$$

with probabilities P_ψ for the different states $|\psi\rangle$, the same reasoning leads to the detector signal

$$\text{Signal} \propto \text{tr}\hat{\rho}\, \hat{E}^{(-)}(\mathbf{x},t)\hat{E}^{(+)}(\mathbf{x},t) = \langle \hat{E}^{(-)}(\mathbf{x},t)\hat{E}^{(+)}(\mathbf{x},t)\rangle. \tag{2.19}$$

Similarly one finds for the joint probability of detecting n photons at positions $\mathbf{x_1},\ldots,\mathbf{x_n}$ and times $t_1,\ldots,t_n$,

$$\text{Signal} \propto \langle \hat{E}^{(-)}(\mathbf{x_1},t_1)\ldots\hat{E}^{(-)}(\mathbf{x_n},t_n)\hat{E}^{(+)}(\mathbf{x_n},t_n)\ldots\hat{E}^{(+)}(\mathbf{x_1},t_1)\rangle. \tag{2.20}$$

We see that the signals of photodetectors are given by expectation values of the electrical field operator in which all annihilation operators occur to the right of all the creation operators. This property is called normal ordering. The proportionality of photodetector signals to normally ordered expectation values of the electric field is a consequence of them working by means of absorption.

The form of the detector signal is very similar to the classical case. In the quantum theory the time or ensemble averages are replaced by quantum mechanical averages of normally ordered products of the electrical field operator.

2.2.2 *n*-th order coherence

As the starting point of his coherence theory, Glauber considers the outcome of a general n-photon delayed coincidence measurement. As outlined in the previous section the n-photon correlations measured in such an experiment are characterized by the expectation values

$$G^{(n)}(\mathbf{x}_1,t_1,\ldots,\mathbf{x}_n,t_n;\mathbf{x}_{n+1},t_{n+1},\ldots,\mathbf{x}_{2n},t_{2n}) = \langle \hat{E}^{(-)}(\mathbf{x_1},t_1)\ldots\hat{E}^{(-)}(\mathbf{x_n},t_n)\hat{E}^{(+)}(\mathbf{x_{n+1}},t_{n+1})\ldots\hat{E}^{(+)}(\mathbf{x_{2n}},t_{2n})\rangle. \tag{2.21}$$

In analogy to the classical case it is convenient to also introduce the normalized n-th order correlation functions

$$g^{(n)}(\mathbf{x}_1,t_1,\ldots,\mathbf{x}_n,t_n;\mathbf{x}_{n+1},t_{n+1},\ldots,\mathbf{x}_{2n},t_{2n}) = \frac{G^{(n)}(\mathbf{x}_1,t_1,\ldots,\mathbf{x}_n,t_n;\mathbf{x}_{n+1},t_{n+1},\ldots,\mathbf{x}_{2n},t_{2n})}{\sqrt{\prod_{j=1,\ldots,2n} G^{(1)}(\mathbf{x}_j,t_j;\mathbf{x}_j,t_j)}}. \tag{2.22}$$

$G^{(1)}$ and $g^{(1)}$ are the quantum analogs of the correlation functions considered in the classical theory of coherence.

Inspired by the classical coherence theory it is natural to associate

$$|g^{(n)}(\mathbf{x}_1t_1,\ldots,\mathbf{x}_nt_n;\mathbf{x}_{n+1}t_{n+1},\ldots,\mathbf{x}_{2n}t_{2n})| = 1 \tag{2.23}$$

with a coherent field. Fields for which the correlation functions factorize in the form

$$g^{(n)}(\mathbf{x}_1, t_1, \ldots, \mathbf{x}_n, t_n; \mathbf{x}_{n+1}, t_{n+1}, \ldots, \mathbf{x}_{2n}, t_{2n}) = \mathcal{E}^*(\mathbf{x}_1, t_1)\ldots\mathcal{E}^*(\mathbf{x}_n, t_n)\mathcal{E}(\mathbf{x}_{n+1}, t_{n+1})\ldots\mathcal{E}(\mathbf{x}_{2n}, t_{2n}) \quad (2.24)$$

obviously satisfy Eq. (2.23) and it is this factorization property that Glauber takes as the defining property of a coherent field: A field is called coherent to order n if all correlation functions of order $m \leq n$ can be written in the form Eq. (2.24) with the same function $\mathcal{E}(\mathbf{x}, t)$ and fully coherent, or simply coherent, if it is coherent to all orders. From this perspective the classical definition of coherence corresponds to first order coherence. As we will see, classical light sources never have coherence beyond the first order.

Before we move on two comments are in order. First, the factorization of the correlation functions in the form Eq. (2.24) means that measurements of photons at different space time points are independent of each other. Second, in general the electromagnetic field is a vector field and to obtain full generality one should also consider its polarization degrees of freedom. This can easily be done but in this dissertation we restrict ourselves to an electric field with just one polarization component.

2.2.3 Examples

The following examples' main purpose is to illustrate the coherence properties of states commonly encountered in nature. In presenting the examples we strive for simplicity rather than generalitiy.

Coherent states

For the notion of coherence introduced in this section to be meaningful we should show that states with the factorization property Eq. (2.24) exist in nature. To this end we consider one polarization component of the electrical field in vacuum, see comment above. From the Maxwell equations one can easily deduce the wave equation for the electromagnetic field [59],

$$\nabla^2 E(\mathbf{x}, t) = \frac{1}{c^2}\frac{\partial^2 E(\mathbf{x}, t)}{\partial t^2}. \quad (2.25)$$

Let $E_0(\mathbf{x}, t)$ be a solution of this equation. At every time t the single photon Hilbert space $L^2(\mathbf{R}^3)$ can be decomposed into $E_0(\mathbf{x}, t)$ and its orthogonal complement.

The decomposition of the single photon Hilbert space into E_0 and the orthogonal complement brings about an analogous decomposition of the field operator,

$$\hat{E}(\mathbf{x}, t) = \hat{a}E_0(\mathbf{x}, t) + \hat{E}_\perp(\mathbf{x}, t), \quad (2.26)$$

where $\hat{a}$ is the annihilation operator for a photon in the mode $E_0(\mathbf{x}, t)$. It is possible to choose $\hat{a}$ time independent because we are in vacuum [3]. We will consider states $|\psi\rangle$ where only photons of type $E_0(\mathbf{x}, t)$ are present, i.e. if $\{\mathcal{E}^{(\perp)}_{\mathbf{k},\varepsilon}(\mathbf{x}, t)\}$ is a complete basis for the orthogonal complement at time t and $\hat{a}_{\mathbf{k},\varepsilon}$ the corresponding annihilation operators, we have

$$\hat{a}_{\mathbf{k},\varepsilon}|\psi\rangle = 0 \tag{2.27}$$

for all $\mathbf{k}$ and ϵ. Then the state of the light field $|\psi\rangle$ can be described in a number basis for the photons in the E_0 mode,

$$|n\rangle = \frac{\hat{a}^\dagger}{\sqrt{n!}}|0\rangle, \tag{2.28}$$

where $|0\rangle$ is the vacuum.

We easily verify that

$$|\alpha\rangle = e^{-|\alpha|/2}\sum_{n=0}^{\infty}\frac{\alpha^n}{n!}|n\rangle, \tag{2.29}$$

with α an arbitrary complex number, is an eigenstate of $\hat{a}$,

$$\hat{a}|\alpha\rangle = \alpha|\alpha\rangle. \tag{2.30}$$

These states are called coherent states for reasons that will become obvious shortly. Coherent states were first considered by E. Schrödinger in the context of the quantum mechanical harmonic oscillator [39]. Since Glauber's groundbreaking work on coherence they are ubiquitus in all of quantum optics and mathematical physics in general.

Assuming that the mode E_0 is in the coherent state $|\alpha\rangle$ we easily find the n-th normally ordered correlation function as

$$G^{(n)}(\mathbf{x}_1t_1, \ldots, \mathbf{x}_nt_n; \mathbf{x}_{n+1}t_{n+1}, \ldots, \mathbf{x}_{2n}t_{2n}) = |\alpha|^{2n}E_0^*(\mathbf{x}_1t_1)\cdots E_0^*(\mathbf{x}_nt_n)E_0(\mathbf{x}_{n+1}t_{n+1})\cdots E_0(\mathbf{x}_{2n}t_{2n}), \tag{2.31}$$

i.e. the light field is fully coherent. In any multiphoton coincidence measurement the quantum mechanical light field in this state yields exactly the same results as a perfectly phase stabilized classical field with amplitude E_0.

As a specific example that will become important later we consider the normalized second order correlation $g^{(2)}(\mathbf{x}t, \mathbf{x}t+\tau; \mathbf{x}t+\tau, \mathbf{x}t)$ at a single position $\mathbf{x}$ and with a variable delay τ. For a coherent state we find

$$g^{(2)}(\mathbf{x}t, \mathbf{x}t+\tau; \mathbf{x}t+\tau, \mathbf{x}t) = 1. \tag{2.32}$$

[3] At relativistic energies photons can interact with each other even in vacuum through the creation of virtual electron positron pairs. At the low energies we are considering here these effects can be neglected and the photons are noninteracting in the absence of charges.

It is interesting that even for coherent states, which in a certain sense are the best quantum mechanical approximation to a classical wave, differences exist between the classical field and quantum case. For instance one could consider a perfectly monochromatic field inside an optical resonator, $E_0(\mathbf{x},t) = E_0'(\mathbf{x})\cos(\omega t)$ with some E_0' that does not depend on time. Then, classically, the intensity of the light field does not show any fluctuations [4],

$$\langle(\Delta I(\mathbf{x}))^2\rangle_{\text{class.}} \equiv \langle I^2(\mathbf{x})\rangle_{\text{class.}} - \langle I(\mathbf{x})\rangle^2_{\text{class.}} = 0. \tag{2.33}$$

In the quantum mechanical case we find on the other hand

$$\begin{aligned}\langle(\Delta\hat{I}(\mathbf{x}))^2\rangle_{\text{quant.}} &= \left(\frac{1}{2}\varepsilon_0 c|E_0(\mathbf{x})|^2\right)^2\left(\langle\hat{a}^\dagger\hat{a}\hat{a}^\dagger\hat{a}\rangle - \langle\hat{a}^\dagger\hat{a}\rangle^2\right) &(2.34)\\ &= \left(\frac{1}{2}\varepsilon_0 c|E_0(\mathbf{x})|^2\right)^2|\alpha|^2. &(2.35)\end{aligned}$$

This finite intensity noise is intrinsically quantum mechanical and cannot be present in the classical case. It originates from the possibility of the light field to be in a superposition of states with different intensities *at the same time*. In the classical theory on the other hand the light field has no choice but to assume different intensities at different times if it is to exhibit any fluctuations in intensity at all, and this is clearly impossible for a strictly monochromatic field. The relative intensity noise $\Delta I/I$ vanishes as the magnitude of the coherent amplitude α goes to infinite so that the quantum mechanical coherent state goes over into a classical stable wave in that limit.

Number states

Using the same decomposition of the Hilbert space discussed in the previous example we can consider states containing exactly n photons, $|\psi\rangle = |n\rangle$. For these states the normally ordered n-th order correlation function becomes

$$\begin{aligned}G^{(m)}(\mathbf{x}_1,t_1,\ldots,\mathbf{x}_m,t_m;\mathbf{x}_{m+1},t_{m+1},\ldots,\mathbf{x}_{2m},t_{2m}) = \\ \frac{n!}{(n-m)!}E_0^*(\mathbf{x}_1,t_1)\cdots E_0^*(\mathbf{x}_m,t_m)E_0(\mathbf{x}_{m+1},t_{m+1})\cdots E_0(\mathbf{x}_{2m},t_{2m}).\end{aligned} \tag{2.36}$$

This means that number states with n photons are approximately coherent to orders m that are much smaller than n. For small photon number the difference between coherent states and number states can become important while they are

[4] Of course we mean the cycle averaged intensity as discussed in the section on the classical coherence theory.

largely indistinguishable for large photon numbers [5]. Number states are states with a well defined intensity, $\langle n|(\Delta\hat{I})^2|n\rangle \equiv 0$, corresponding to their characteristic of having a fixed number of photons.

For the number state we find

$$g^{(2)}(\mathbf{x}t, \mathbf{x}t+\tau; \mathbf{x}t+\tau, \mathbf{x}t) = 1 - \frac{1}{n}. \tag{2.37}$$

Intuitively this means that measuring first a photon at time t reduces the probability to detect another photon some time later. For $\tau \to 0$ this phenomenon is called antibunching. Antibunching is impossible for classical states of radiation and for that reason number states are sometimes called nonclassical states. To see that antibunching cannot occur for classical fields, we note that for a classical light field

$$g^{(2)}(0,0) = \frac{\langle I^2\rangle}{\langle I\rangle^2}, \tag{2.38}$$

so that

$$g^{(2)}(0,0) - 1 = \frac{\langle(\hat{I} - \langle\hat{I}\rangle)^2}{\langle\hat{I}\rangle^2}, \tag{2.39}$$

where we only write the time arguments. Classically, the expectation values on the right hand side of this equation are calculated with a probability distribution $P(I)$ for the different values I of the intensity to occur, i.e.

$$g^{(2)}(0,0) - 1 = \frac{1}{\langle\hat{I}\rangle^2}\int dI P(I)(I - \langle I\rangle)^2. \tag{2.40}$$

Because the right hand side is manifestly positive, $g^{(2)}$ cannot be smaller than one.

Thermal fields

Thermal or chaotic fields cannot be described with a state vector. Rather they are given in terms of their density matrix $\hat{\rho}$. In general, the density matrix of a system in thermal equilibrium is given by [72, 57]

$$\hat{\rho} = Z^{-1}e^{-\beta\hat{H}}, \tag{2.41}$$

where $\hat{H}$ is the system's Hamiltonian, $\beta = 1/k_\mathrm{B}T$ with k_B the Boltzmann constant and T the temperature and $Z = \mathrm{tr}e^{-\beta\hat{H}}$ is the partition function.

[5] There are notable exceptions to this, one of the better known being the collapse and revival of the atomic population oscillations in the Jaynes-Cummings model if the light field is in a coherent state, that persist for arbitrarily large amplitude of the field.

Consider first the case of a single mode light field with creation and annihilation operator $\hat{a}$ and $\hat{a}^\dagger$ and with frequency ω. It's Hamiltonian is given by [89]

$$\hat{H} = \hbar\omega\hat{a}^\dagger\hat{a}, \tag{2.42}$$

so that the density operator becomes

$$\hat{\rho} = Z^{-1}e^{-\hbar\omega\hat{a}^\dagger\hat{a}/k_BT} = (1 - e^{-\beta\hbar\omega})\sum_n |n\rangle\langle n|e^{-\beta\hbar\omega n}. \tag{2.43}$$

Using the density operator we easily find

$$g^{(1)}(\mathbf{x}t;\mathbf{x}'t') = 1 \tag{2.44}$$

and

$$g^{(2)}(\mathbf{x}t,\mathbf{x}t+\tau;\mathbf{x}t+\tau,\mathbf{x}t) = 2, \tag{2.45}$$

i.e. the field is first order coherent but not second order coherent.

The single mode light field in a thermal state is the quantum mechanical analog of a perfectly monochromatic classical light source. In the classical theory, coherence is often associated with monochromaticity and this connection is reflected by $g^{(1)}$ remaining equal to 1 for arbitrarily large separations in space and time. According to the discussion of the classical coherence theory above, this means maximum visibility of interference fringes. We see however, that even the perfectly monochromatic field, which is considered perfectly coherent in the classical theory, does not posses coherence beyond the first order. In this context it is also interesting to note that the quantum mechanical thermal light field does not have a well defined intensity, as can be seen from the density operator Eq. (2.43).

$g^{(2)}$ being greater than one means that it becomes more likely to detect another photon after a first photon has been detected already. This effect is called photon bunching.

In reality, thermal light sources are not perfectly monochromatic but have a finite bandwidth. This can be described quantum mechanically by the multimode Hamiltonian

$$\hat{H} = \sum \hbar\omega_k\hat{a}_k^\dagger\hat{a}_k, \tag{2.46}$$

where $\hat{a}_k$ and $\hat{a}_k^\dagger$ are the annihilation and creation operators for mode $\mathcal{E}_k(\mathbf{x})$ and ω_k are the corresponding eigenfrequencies. With this Hamiltonian the positive frequency part of the field operator takes exactly the form of Eq. (2.13). Inserting in $g^{(1)}$ we find

$$g^{(1)}(\mathbf{x},t+\tau;\mathbf{x},t) = \frac{\sum_k e^{i\omega_k\tau}|\mathcal{E}_k(\mathbf{x})|^2\langle\hat{a}_k^\dagger\hat{a}_k\rangle}{\sum_k |\mathcal{E}_k(\mathbf{x})|^2\langle\hat{a}_k^\dagger\hat{a}_k\rangle}. \tag{2.47}$$

If the frequencies present in the multimode field extend over a frequency interval of width $\Delta\omega$, all the phase factors in the numerator are essentially the same for time delays $\tau \ll 1/\Delta\omega$, meaning that high contrast interference fringes can be observed. For longer times the phase factors get increasingly out of phase with each other and for $t \gg 1/\Delta\omega$ they average to zero, i.e. no interference fringes can be observed. Therefore $1/\Delta\omega$ is called the coherence time of the field. Note however that it only characterizes the first order coherence of the field. For instance for zero time delay we find

$$g^{(2)}(\mathbf{x},t;\mathbf{x},t) = 2 + \frac{\sum_k |\mathcal{E}_k(\mathbf{x}|^4 \left(\langle \hat{a}_k^\dagger \hat{a}_k^\dagger \hat{a}_k \hat{a}_k \rangle - \langle \hat{a}_k^\dagger \hat{a}_k \rangle^2\right)}{\left(\sum_k |\mathcal{E}_k(\mathbf{x}|^2 \langle \hat{a}_k^\dagger \hat{a}_k \rangle\right)^2}. \tag{2.48}$$

The second term goes to zero like $\frac{1}{\text{number of modes}}$ for a large number of modes. Thus we see that, even for times much shorter than the coherence time, the thermal field is not second order coherent. This was of course anticipated by the discussion of the perfectly monochromatic single mode thermal field above, which has an infinite coherence time.

2.3 Independent radiatiors and chaotic light

Light originating from an ensemble of N independent and identical radiators is a model of great importance because of its generality. With very few assumptions all statistical and correlation properties of such light can be calculated. Light from independent radiators is also often called chaotic light. Chaotic light provides a fairly good model for the light coming from thermal sources discussed in the previous section.

To be specific we consider the total field at position $\mathbf{r}$ that is the superposition of the N light fields radiated by N identical atoms,

$$E(t) = \sum_j E_j(t), \tag{2.49}$$

where here and below we supress the position dependence. The field amplitudes E_j are classical fields but, in a sense that we will make more precise below, subject to stochastic fluctuations. For simplicity we will assume that all the fields E_j have the same amplitude, so that

$$E(t) = E_0 \sum_j e^{i\phi_j(t)}. \tag{2.50}$$

The key ingredient of the model is the statistical independence of the phases ϕ_j for different radiators. Depending on the specific system that the atoms represent

the phases will take different forms. For some light sources all the atoms radiate at the same frequency $\omega_j^{(0)} = \omega_0$ but suffer random phase shifts $\phi_j^{(0)}$ on average in a time interval of duration τ_c, i.e.

$$\phi_j(t) = \omega_0 t + \phi_j^{(0)} \tag{2.51}$$

with the $\phi_j^{(0)}$ being independent random variables, evenly distributed over $[0, 2\pi]$. This is a good model for predominantly collision broadened light sources. For a purely inhomogeneously broadened system on the other hand the phases $\phi_j^{(0)}$ are fixed and the frequencies $\omega_j^{(0)}$ are distributed over a frequency interval τ_c^{-1}.

The first order correlation function is

$$\begin{aligned} G^{(1)}(\tau) = \langle E^*(\tau)E(0)\rangle &= |E_0|^2 \sum_{j,j'} e^{i(\phi_j(t)-\phi_{j'}(t))} && (2.52)\\ &= N\langle E_j^*(\tau)E_j(0)\rangle, && (2.53)\end{aligned}$$

where we have used that the crossterms in the sum average to zero and that the atoms are identical. The remaining correlation functions for light radiated by a single atom can be calculated using more details of the radiation process. In a purely collision broadened light field the first-order correlation function decays from one to zero with a Lorentzian line shape and for a purely Doppler broadened light field the correlation function decays with a Gaussian line shape[6], in both cases on a time scale of the decoherence time τ_c. Here our main interest is in general features of a *many atom* model and for more details on the *single atom* emission we refer the reader to the many books on the subject, e.g. [83].

Similarly to the first order correlation function we can calculate the second order correlation function

$$\begin{aligned} g^{(2)}(\tau) &= \frac{\langle E^*(0)E^*(\tau)E(\tau)E(0)\rangle}{\langle E^*(0)E^*(\tau)E(\tau)E(0)\rangle} && (2.54)\\ &= \frac{\sum_{ij}\langle E_i^*(0)E_i(0)\rangle\langle E_j^*(\tau)E_j(\tau)\rangle + \sum_{ij}\langle E_i^*(\tau)E_i(0)\rangle\langle E_j^*(0)E_j(\tau)\rangle}{\langle E^*(0)E^*(\tau)E(\tau)E(0)\rangle} && (2.55)\\ &= 1 + \frac{|g^{(1)}(\tau)|^2}{g^{(1)}(0)}. && (2.56)\end{aligned}$$

Just like the first order correlation function decays from one to zero, the second order correlation function decays from 2 at zero time delay to one.

The mean intensity is found from $G^{(1)}$ by setting $\tau = 0$ as

$$\langle I\rangle = NI_j, \tag{2.57}$$

[6] The Doppler broadened chaotic light can be thought of as a classical model for the multimode thermal field of the previous section.

where I_j is the intensity radiated by a single atom. Higher moments of the intensity can be calculated fairly easily. For instance the second moment is

$$\begin{aligned}\langle I^2\rangle &= \left(\frac{1}{2}c\varepsilon_0\right)^2 \langle E^*(0)E^*(0)E(0)E(0)\rangle &(2.58)\\ &= \left(\frac{1}{2}c\varepsilon_0\right)^2 \left(\sum_j \langle e^{i(\phi_j(t)+\phi_j(t)-\phi_j(t)-\phi_j(t))}\rangle \right.\\ &\quad \left. + \sum_{j\neq j'} \langle e^{i(\phi_j(t)+\phi_{j'}(t)-\phi_j(t)-\phi_{j'}(t))}\rangle + \langle e^{i(\phi_j(t)+\phi_{j'}(t)-\phi_{j'}(t)-\phi_j(t))}\rangle\right) &(2.59)\\ &= \left(2-\frac{1}{N}\right)\langle I\rangle^2 \approx 2\langle I\rangle^2. &(2.60)\end{aligned}$$

In general, in the rth moment of the intensity there will be $r!$ possibilities for the phases in the exponents to cancel each other and therefore we have

$$\langle I^r\rangle = r!\langle I\rangle^r. \tag{2.61}$$

2.4 Counting statistics

Another useful way to characterize the correlations and coherence properties of a mode of a quantum field is by means of the counting or number statistics associated with that mode. The counting statistics P_n of a mode is the probability to find n quanta in the mode,

$$P_n = \mathrm{tr}\hat{\rho}|n\rangle\langle n|. \tag{2.62}$$

Using the counting statistics we can calculate all moments of the number operator

$$\langle \hat{n}^m\rangle = \sum_n n^m P_n. \tag{2.63}$$

Thus the counting statistics provide a complete characterization of all intensity correlations (at equal time).

The counting statistics for the examples of subsection 2.2.3 are readily calculated. Fig. 2.2 shows the result for a coherent state. The number statistics of a coherent state is the well known Poissonian probability distribution,

$$P_{n,\mathrm{coh.}} = e^{-|\alpha|^2}\frac{\alpha^{2n}}{n!}, \tag{2.64}$$

with mean photon number $\langle n\rangle = |\alpha|^2$.

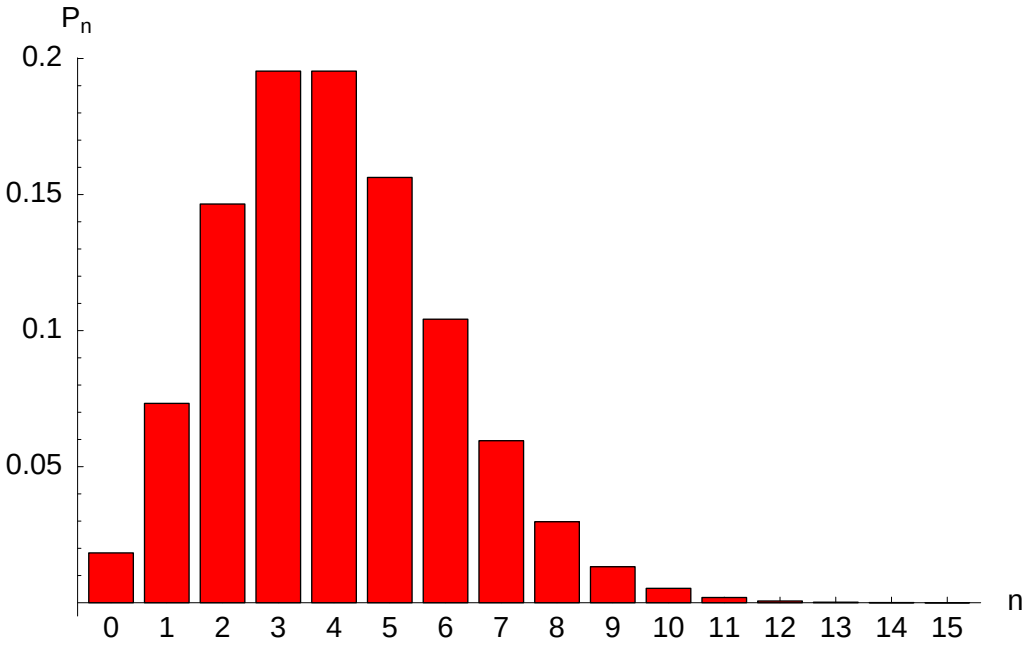

Fig. 2.2: Number statistics of a coherent state with $\alpha = 2$ and consequently $\langle n \rangle = 4$.

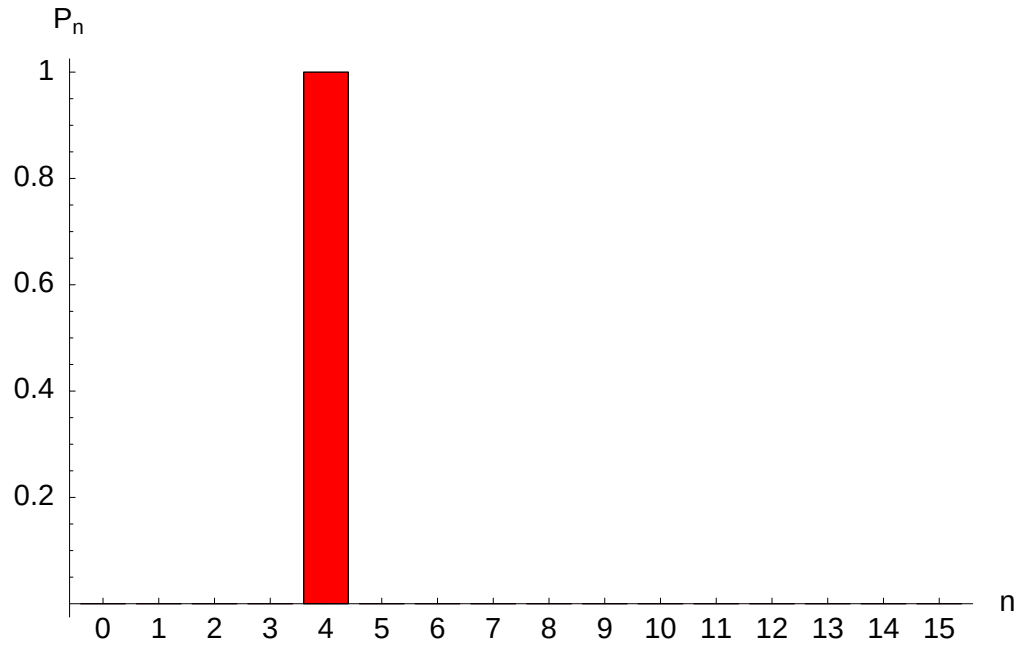

Fig. 2.3: Number statistics of a number state $|n\rangle$ with $n = 4$.

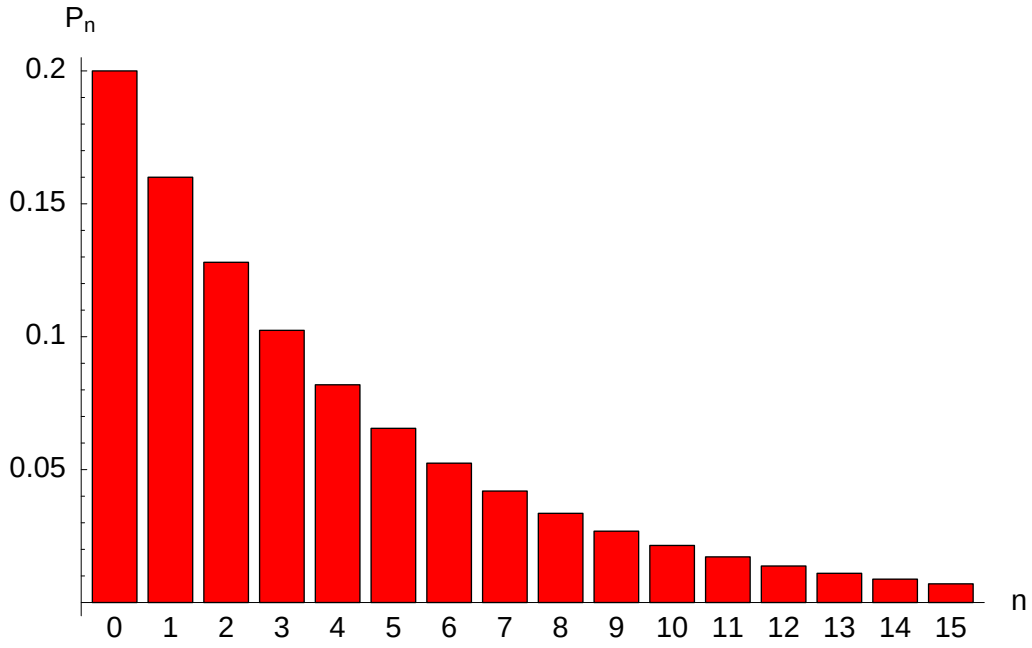

Fig. 2.4: Number statistics of a thermal state where the temperature has been chosen such that $\langle n \rangle = 4$.

For a number state $|n\rangle$ the counting statistics is of course

$$P_{n'} = \delta_{n,n'}, \tag{2.65}$$

see Fig. 2.3.

Finally, for a single mode thermal state the number statistics is shown in Fig. 2.4. The mean photon number is again 4.

These examples for the number statistics of various states with the same mean number of photons make it very clear that a description of quantum fields merely in terms of that mean is inadequate. Achieving a characterization of quantum fields in terms of observables is one of the main objectives of coherence theory.

3. ULTRA-COLD ATOMS AND MOLECULES

A number of excellent review articles exist on the subject of ultra-cold atoms and molecules [66, 74, 109, 37]. Therefore the purpose of this chapter is not to repeat what has already been said in those articles but to rather present a theoretical framework for the description of ultra-cold atoms and molecules that is custom made for the calculation and analysis of their coherence properties. Our approach has a top-down flavor to it: We assume that the quantum state describing the system under consideration has been determined by some physical mechanism and our focus is on the coherence properties of this state rather than on what physics gave rise to this state. In stressing the coherence properties, our approach is not ideal for dealing with certain other aspects of the problem, such as how the underlying microscopic physics can lead to a specific manybody state. However, as we will see, our framework is flexible enough to capture the salient features of the systems that we will consider. For the other aspects of the problem we refer the reader to the review articles cited above and the references therein.

In section 3.1 we show how a BEC and its fluctuations can be described. Our approach is based on the criterion of Penrose and Onsager for BEC and therefore it is extremely general. The fluctuations are treated in the Bogoliubov approximation. The treatment of the fluctuations has to be adapted to the spatially inhomogeneous situation typically encountered in trapped atomic gases. We will show how the local density approximation for the locally correlated fluctuations and a single mode description for the condensate can be combined to capture both condensate and fluctuations in a way that allows for the calculation of correlation functions in a simple way.

In section 3.2 we consider ultra-cold fermions. In subsection 3.2.1 we collect the properties of fermions in their normal state in a trapping potential. In subsection 3.2.2 we consider the superfluid case. We use the BCS mean field theory and show how it can be adapted to spatially inhomogenous situations in a trap.

Finally, section 3.3 gives the necessary background on Feshbach resonances and ultra-cold molecules. We briefly describe the two-body physics that gives rise to Feshbach resonances and we show how the molecules can be incorporated in an effective many-body theory.

3.1 Bose-Einstein condensates

According to Penrose and Onsager [94], Bose-Einstein condensation is characterized by off-diagonal long range order in the thermodynamic limit

$$V \to \infty, \quad N \to \infty, \quad \frac{N}{V} \to const., \tag{3.1}$$

where V is the volume occupied by the system and N is the particle number. Off-diagonal long range order means that

$$\lim_{|\Delta \mathbf{x}| \to \infty} \rho(\mathbf{x}, \mathbf{x} + \Delta \mathbf{x}) \neq 0, \tag{3.2}$$

where $\rho(\mathbf{x}, \mathbf{x}')$ is the density matrix of the system in the position representation. It can be shown [94] that this criterion is equivalent to the density matrix having a macroscopic eigenvalue. For simplicity we will restrict ourselves to the case where there is only one macroscopic eigenvalue, i.e. we consider a BEC without fractionization. In that case the density matrix can be written

$$\begin{aligned} \rho(\mathbf{x}, \mathbf{x}') &= \rho_0(\mathbf{x}, \mathbf{x}') + \delta\rho(\mathbf{x}, \mathbf{x}') && (3.3) \\ &\equiv \psi_0^*(\mathbf{x})\psi_0(\mathbf{x}') + \delta\rho(\mathbf{x}, \mathbf{x}'). && (3.4) \end{aligned}$$

ρ_0 describes the condensed fraction and can be factorized in terms of the condensate wave function ψ_0 and $\delta\rho$ describes the non-condensed density.

These definitions cannot be immediately applied to ultra-cold atoms in a trap because in such a system the particle number is finite and the atoms are constrained to a finite volume, hence the thermodynamic limit cannot be realized. Modifications of the thermodynamic limit to this setting are discussed e.g. in [74]. For practical purposes we can preserve the spirit of the Penrose and Onsager interpretation of BEC by assuming that the density operator still decomposes as in Eq. (3.4) into a large condensed part and a small fluctuations part. By "large" we mean that the number of particles N_0 occupying the condensate wave function is of the order of the total number of particles, i.e. macroscopic, while the number of particles occupying any other mode is at most of order unity.

The decomposition of the density operator of the system implies an analogous decomposition of the field operator as

$$\hat{\psi}(\mathbf{x}) = \hat{c}_0\psi_0(\mathbf{x}) + \delta\hat{\psi}(\mathbf{x}), \tag{3.5}$$

where $\hat{c}_0$ is the bosonic annihilation operator for an atom in the condensate and $\delta\hat{\psi}(\mathbf{x})$ describes the fluctuations. Because the density operator must be self adjoint the condensate wave function is orthogonal to the fluctuations and hence $\hat{c}_0$

commutes with $\delta\hat{\psi}$. Furthermore, the condensate wave function must be an energy eigenstate because the density operator commutes with the Hamiltonian for a thermal equilibrium state. $\hat{c}_0$ is time independent if we measure the energy from the energy eigenvalue of the condensate.

Using the decomposition of the field operator we can calculate normally ordered expectation values,

$$
\begin{aligned}
& G^{(n)}(1,\ldots,n;n+1,\ldots,2n) && (3.6)\\
&= \langle\hat{\psi}^\dagger(1)\cdots\hat{\psi}^\dagger(n)\hat{\psi}(n+1)\cdots\hat{\psi}(2n)\rangle && (3.7)\\
&= \langle\hat{\psi}_0^\dagger(1)\cdots\hat{\psi}_0^\dagger(n)\hat{\psi}_0(n+1)\cdots\hat{\psi}_0(2n)\rangle \\
&+ \sum_{\substack{i=1,\ldots,n\\ j=n+1,\ldots,2n}} \langle\hat{\psi}_0^\dagger(1)\cdots\delta\hat{\psi}^\dagger(i)\cdots\hat{\psi}_0^\dagger(n)\hat{\psi}_0(n+1)\cdots\delta\hat{\psi}(j)\cdots\hat{\psi}_0^\dagger(2n)\rangle \\
&+ \cdots && (3.8)\\
&= \frac{N_0!}{(N_0-n)!}\left(\psi_0^*(1)\cdots\psi_0^*(n)\psi_0(n+1)\cdots\psi_0(2n)+O(N_0^{-1})\right), && (3.9)
\end{aligned}
$$

where we have used the short-hand notation $1 = \mathbf{x}_1, t_1$ etc. for the space-time points. The sums in the second expression contain an increasing even number of fluctuation operators. Terms with an odd number of fluctuation operators vanish because in thermal equilibrium no correlations can exist between the condensate and the excitations. The corresponding decreasing number of condensate operators means that the terms with $m < n$ condensate operators are of order $O(N^m)$ because the occupation of the fluctuation modes is always microscopic.

3.1.1 Mean field approximation

If the condensate is very pure, i.e. almost all the atoms are in the condensate, the so called mean-field approximation can be made. It consists of two parts. First, fluctuations are neglected because their contributions to expectation value are of relative order N_0^{-1} compared to the contribution from the condensate alone, as e.g. in Eq. (3.9). This also means that we do not distinguish between the number of condensed atoms N_0 and the total number of atoms N. Second, the prefactor in Eq. (3.9) can be set equal to N_0^n since for all practical purposes $n \ll N_0$. Thus the normally ordered correlation functions factorize in the mean field approximation into products of complex valued functions and accordingly we can say, that in the mean field approximation the condensate is in a coherent state.

It is customary to introduce the condensate wave function,

$$\Psi_0(\mathbf{x}) = \sqrt{N}\psi_0(\mathbf{x}), \tag{3.10}$$

in terms of which

$$G^{(n)}_{\mathrm{MF}}(1,\ldots,n;n+1,\ldots,2n) = \Psi_0^*(1)\cdots\Psi_0^*(n)\Psi_0(n+1)\cdots\Psi_0(2n). \tag{3.11}$$

We see that at this level of approximation the condensate behaves like a classical stable field. At the formal level, the mean field approximation amounts to replacing all field operators by the condensate wave function.

Like every complex function the condensate wave function can be decomposed into an amplitude and a phase,

$$\Psi_0(\mathbf{x}) = \sqrt{\rho(\mathbf{x})}e^{i\phi(\mathbf{x})}. \tag{3.12}$$

From

$$\langle\hat{\psi}^\dagger(\mathbf{x})\hat{\psi}(\mathbf{x})\rangle \overset{\text{MF}}{=} \rho(\mathbf{x}) \tag{3.13}$$

we see that $\rho(\mathbf{x})$ describes the average density. Similarly,

$$\langle\mathbf{v}\rangle \equiv \left\langle\left(\frac{-i\hbar}{2M}(\nabla_\rightarrow - \nabla_\leftarrow)\right)\right\rangle \tag{3.14}$$

$$\overset{\text{MF}}{=} \frac{\hbar}{M}\int d^3x\rho(\mathbf{x})\nabla\phi(\mathbf{x}), \tag{3.15}$$

where M is the mass of the atoms and $\nabla_{\overset{\rightarrow}{\leftarrow}}$ is the gradient acting to the left and right respectively, shows that the gradient of ϕ characterizes the velocity of atoms in the condensate.

To find the wave equation that governs the condensate wave function we start from the Hamiltonian for an interacting Bose gas in a trap in second quantization,

$$\hat{H} = \int d^3x\hat{\psi}^\dagger(\mathbf{x})\left(\frac{\hbar^2}{2M}\nabla^2 + V(\mathbf{x}) + \frac{4\pi\hbar^2 a}{M}\hat{\psi}^\dagger(\mathbf{x})\hat{\psi}(\mathbf{x})\right)\hat{\psi}(\mathbf{x}). \tag{3.16}$$

The first term describes the atoms' kinetic energy, the second one is the trapping potential and the last one describes colissions. Because of the low temperatures we have assumed that the atoms interact only via *s*-wave interactions with each other, so that their interactions can be described by the two-body pseudo potential

$$U(\mathbf{x}-\mathbf{x}') = U_0\delta(\mathbf{x}-\mathbf{x}') \equiv \frac{4\pi\hbar^2 a}{M}\delta(\mathbf{x}-\mathbf{x}'), \tag{3.17}$$

where a is the *s*-wave scattering length. In most experiments the trapping potential $V(\mathbf{x})$ is to a very good approximation harmonic,

$$V(\mathbf{x}) = \frac{1}{2}\hbar\sum_{i=x,y,z}\omega_{\text{osc},i}\left(\frac{x_i}{a_{\text{osc},i}}\right)^2. \tag{3.18}$$

$\omega_{\text{osc},i}$ are the trap frequencies in direction $i = x,y,z$ and $a_{\text{osc},i} = \sqrt{\frac{\hbar}{M\omega_{\text{osc},i}}}$ are the corresponding oscillator lengths. Throughout this dissertation we will only

consider the case of trapping potentials with spherical symmetry, $\omega_{\mathrm{osc},x} = \omega_{\mathrm{osc},y} = \omega_{\mathrm{osc},z} = \omega_{\mathrm{osc}}$.

We can evaluate the expectation value of the energy $\langle \hat{H} \rangle$ in the mean field approximation which, according to the remark above, is accomplished by simply replacing the field operators in the Hamiltonian by the condensate wave function. The equation for the condensate wave function is then found by minimizing the energy functional subject to the constraint that the condensate wave function be normalized to the total number of atoms

$$\frac{\delta}{\delta \Psi_0^*} \left(\langle \hat{H} \rangle - \mu \int d^3x \Psi_0^*(\mathbf{x}) \Psi_0(\mathbf{x}) \right) = 0. \tag{3.19}$$

Carrying out the variation we find the so-called Gross-Pitaevski equation for the condensate wave function

$$\left(-\frac{\hbar^2}{2M} \nabla^2 + V(\mathbf{x}) + \frac{4\pi\hbar^2 a}{M} \Psi_0^*(\mathbf{x}) \Psi_0(\mathbf{x}) \right) \Psi_0(\mathbf{x}) = \mu \Psi_0(\mathbf{x}). \tag{3.20}$$

The eigenvalue μ is the chemical potential in the mean field approximation.

3.1.2 The Thomas-Fermi approximation

Solutions to the Gross-Pitaevski equation can rather easily be found numerically. E.g. for spherically symmetric problems one can seperate angles and the radial coordinate and one only has to solve the boundary value problem for the radial part.

In many cases of practical interest the so called Thomas-Fermi approximation, which consists in neglecting the kinetic energy and admits an analytic solution, provides a very good approximation to the exact ground state solution. The Thomas-Fermi approximation can be applied in cases where the interactions are repulsive and dominate over the kinetic energies. To explain what this means we make the following dimensional argument. The kinetic energies scale as $E_{\mathrm{kin}} \sim \hbar^2 R^{-2}/M$ and the interaction energie as $U \sim (4\pi\hbar^2 a/M) N/R^3$ where R is the radius of the condensate wave function, so that $U/E_{\mathrm{kin}} \sim Na/R$. Thus the Thomas-Fermi approximation can be applied if

$$\frac{Na}{R} \gg 1. \tag{3.21}$$

As we will see below R scales only very weakly with Na so that very often Na/a_{osc} can be used instead of Na/R as a dimensionless number characterizing the strength of the interaction.

Making the Thomas-Fermi approximation we find from the Gross-Pitaevski equation

$$\Psi_0(\mathbf{x}) = \sqrt{\frac{\mu - V(\mathbf{x})}{4\pi\hbar^2 a/M}}, \tag{3.22}$$

where we have chosen Ψ_0 to be real [1] and the wavefunction is set to zero for $V(\mathbf{x}) > \mu$. The chemical potential can be found from the normalization of the condensate wave function. Inserting the specific form of the trapping potential Eq. (3.18) we find

$$\Psi_0(\mathbf{x}) = \sqrt{\frac{15}{8\pi R_{\mathrm{TF}}^3}} \sqrt{1 - \frac{x^2}{R_{\mathrm{TF}}^2}}, \tag{3.23}$$

where

$$R_{\mathrm{TF}} = (15Na/a_{\mathrm{osc}})^{(1/5)} a_{\mathrm{osc}} \tag{3.24}$$

is the size of the condensate in the Thomas-Fermi approximation.

3.1.3 Bogoliubov approximation

In some cases it is necessary to consider corrections to the mean field description due to fluctuations caused by interactions or thermal excitations. Such an improved solution also allows one to check if the mean field approximation is applicable by calculating the depletion of the condensate.

One method to obtain corrections to the mean field state is by means of the so called Bogoliubov-de-Gennes equations [30]. These equations allow one to calculate the wave functions for the excitations taking the inhomogeneity due to the trap fully into account. Solutions to these equations can in most cases only be found numerically.

Since we are only interested in the qualitative changes that fluctuations bring about as far as the coherence of the atoms are concerned we will use a simpler method. We have adapted the commonly known Bogoliubov approximation for a homogeneous system to the situation of cold bosons in a trap by making use of the local density approximation. Our approach has several advantages. First of all, the necessary assumptions are mild and fairly natural for cold atoms in a trap so that the results are normally rather precise. Second, it allows us to write down very transparent and intuitively clear expressions for the fluctuations that lead to compact analytic solutions. Finally, the method can be easily adapted to the case of superfluid fermions, see subsection 3.2.2 below.

[1] The phase of the ground state condensate wave function has to be constant across the condensate since phase gradients would lead to a positive kinetic energy. The overall phase is arbitrary.

The method works if the correlation length of the fluctuations, ξ, is much smaller than the size of the condensate R,

$$\xi \ll R \tag{3.25}$$

In the context of superfluid systems ξ is often referred to as the healing length. It is the wavelength of excitations for which kinetic energy $\hbar^2/(2M\xi^2)$ and mean field energy $n4\pi\hbar^2 a/M$ are equal, i.e

$$\xi = (8\pi n a)^{-1/2}. \tag{3.26}$$

If condition Eq. 3.25 is met we can break up the system into cells that are larger than the correlation length, yet still much smaller than the condensate. Then we can assume that, first, the fluctuations in neighbouring cells are uncorrelated and, second, that the condensate wave function is a constant in every cell. These two assumptions allow us to calculate the fluctuations in every cell using the standard Bogoliubov approximation for homogeneous systems.

Since the Bogoliubov approximation plays such an important role in this method we first review it for the homogeneous case before we give more details on how to adapt it to the inhomogeneous case in the local density approximation.

Homogeneous system

In a homogeneous system there is no potential term in the Hamiltonian Eq. (3.16). It is advantageous to go over to the Fourier transformed field operators

$$\hat{c}_{\mathbf{q}} = \frac{1}{\sqrt{V}} \int_V d^3x e^{-i\mathbf{q}\mathbf{x}} \hat{\psi}(\mathbf{x}), \tag{3.27}$$

where V is the quantization volume. In terms of these Fourier transformed field operators the Hamiltonian becomes

$$\hat{H} = \sum_q \frac{\hbar^2 q^2}{2M} \hat{c}_q^\dagger \hat{c}_q + \frac{4\pi\hbar^2 a}{MV} \sum_{\mathbf{q},\mathbf{q_1},\mathbf{q_2}} \hat{c}^\dagger_{\mathbf{q}+\frac{\mathbf{q_2}}{2}} \hat{c}^\dagger_{\mathbf{q}-\frac{\mathbf{q_2}}{2}} \hat{c}_{\mathbf{q}-\frac{\mathbf{q_1}}{2}} \hat{c}_{\mathbf{q}+\frac{\mathbf{q_1}}{2}}. \tag{3.28}$$

The first part of the Bogoliubov approximation consists in making the mean field approximation for the condensed part, i.e. replacing the field operator for the condensate by the number of particles in the condensate. A homogeneous system condenses in the zero momentum mode so that we have

$$\hat{c}_0 \rightarrow \sqrt{N_0}. \tag{3.29}$$

Introducing the macroscopic number of particles in the condensate leads to a classification of the terms in the Hamiltonian Eq. (3.27) according to the power of $\sqrt{N_0}$ they contain. The higher the power in N_0 the more important is a term.

The second part of the Bogoliubov approximation consists in retaining only terms at least of order N_0 in the Hamiltonian. In this approximation we find

$$\begin{aligned}\hat{H}_{\text{Bogoliubov}} - H_0 &= \sum_{\mathbf{q}} \left(\frac{\hbar^2 q^2}{2M} \hat{c}^\dagger_{\mathbf{q}} \hat{c}_{\mathbf{q}} + 2n_0 U_0 \hat{c}^\dagger_{\mathbf{q}} \hat{c}_{\mathbf{q}} + n_0 U_0 \left(\hat{c}^\dagger_{-\mathbf{q}} \hat{c}^\dagger + \hat{c}_{\mathbf{q}} \hat{c}_{-\mathbf{q}} \right) \right) \\ &= \sum_{\mathbf{q} \geq 0} \left(\xi_{\mathbf{q}} (\hat{c}^\dagger_{\mathbf{q}} \hat{c}_{\mathbf{q}} + \hat{c}^\dagger_{-\mathbf{q}} \hat{c}_{-\mathbf{q}}) + 2n_0 U_0 (\hat{c}^\dagger_{-\mathbf{q}} \hat{c}^\dagger_{\mathbf{q}} + \hat{c}_{\mathbf{q}} \hat{c}_{-\mathbf{q}}) \right) \end{aligned} \quad (3.30)$$

where

$$H_0 = \frac{N_0^2 U_0}{V} \quad (3.31)$$

is the mean field energy of the condensate. The sum in the second line runs over momenta with a positive x-component and we have introduced the condensate density $n_0 = N_0/V$ and

$$\xi_{\mathbf{q}} = \frac{\hbar^2 q^2}{2M} + 2n_0 U_0. \quad (3.32)$$

The effective Hamiltonian Eq. (3.30) can be diagonalized by making a canonical transformation from the operators $\hat{c}_{\mathbf{q}}$ and $\hat{c}^\dagger_{-\mathbf{q}}$ to new bosonic creation and annihilation operators $\hat{a}_{\mathbf{q}}$ and $\hat{b}^\dagger_{\mathbf{q}}$. The most general such transformation can be written as

$$\begin{pmatrix} \hat{a}_{\mathbf{q}} \\ \hat{b}^\dagger_{\mathbf{q}} \end{pmatrix} = \begin{pmatrix} \alpha_{\mathbf{q}} & \alpha_{-\mathbf{q}} \\ \beta_{\mathbf{q}} & \beta_{-\mathbf{q}} \end{pmatrix} \begin{pmatrix} \hat{c}_{\mathbf{q}} \\ \hat{c}^\dagger_{-\mathbf{q}} \end{pmatrix} \quad (3.33)$$

For this transformation to be canonical we must have

$$[\hat{a}_{\mathbf{q}}, \hat{a}^\dagger_{\mathbf{q}}] = 1, \quad (3.34)$$

$$[\hat{b}_{\mathbf{q}}, \hat{b}^\dagger_{\mathbf{q}}] = 1, \quad (3.35)$$

$$[\hat{a}_{\mathbf{q}}, \hat{b}_{\mathbf{q}}] = 0, \quad (3.36)$$

from which it follows that

$$|\alpha_{\mathbf{a}}|^2 - |\alpha_{-\mathbf{q}}|^2 = 1, \quad (3.37)$$

$$|\beta_{\mathbf{a}}|^2 - |\beta_{-\mathbf{q}}|^2 = 1, \quad (3.38)$$

$$\alpha_{\mathbf{q}} \beta^*_{\mathbf{q}} - \alpha_{-\mathbf{q}} \beta^*_{-\mathbf{q}} = 0. \quad (3.39)$$

These conditions can be satisfied with

$$\alpha_{\mathbf{q}} = u_{\mathbf{q}} \quad , \quad \alpha_{-\mathbf{q}} = v_{\mathbf{q}} \quad (3.40)$$

$$\beta_{\mathbf{q}} = v_{\mathbf{q}} \quad , \quad \beta_{-\mathbf{q}} = u_{\mathbf{q}} \quad (3.41)$$

where $u_{\mathbf{q}}$ and $v_{\mathbf{q}}$ can be chosen real and satisfy $u^2_{\mathbf{q}} - v^2_{\mathbf{q}} = 1$. Inverting the transformation Eq. (3.33) and inserting in the simplified Hamiltonian Eq. (3.30) we find

diagonal terms proportional to $\hat{a}^\dagger\hat{a}$ and $\hat{b}^\dagger\hat{b}$ and off-diagonal terms proportional to $\hat{a}^\dagger\hat{b}^\dagger$ etc. The off-diagonal terms can be eliminated by chosing

$$u_{\mathbf{q}}^2 = \frac{1}{2}\left(\frac{\xi_{\mathbf{q}}}{E_{\mathbf{q}}} + 1\right) \tag{3.42}$$

$$v_{\mathbf{q}}^2 = \frac{1}{2}\left(\frac{\xi_{\mathbf{q}}}{E_{\mathbf{q}}} - 1\right), \tag{3.43}$$

where

$$E_{\mathbf{q}} = \sqrt{\left(\frac{\hbar^2 q^2}{2M}\right)^2 + 4n_0 U_0 \frac{\hbar^2 q^2}{2M}}, \tag{3.44}$$

so that the Hamiltonian becomes (up to an additive constant)

$$\hat{H}_{\text{Bogoliubov}} = \sum_{\mathbf{q}\geq 0} E_{\mathbf{q}}\left(\hat{a}_{\mathbf{q}}^\dagger\hat{a}_{\mathbf{q}} + \hat{b}_{\mathbf{q}}^\dagger\hat{b}_{\mathbf{q}}\right). \tag{3.45}$$

This means that the transformation Eq. (3.33) with Eq. (3.41) takes the fluctuations into noninteracting bosons with dispersion relation $E_{\mathbf{q}}$. In thermal equilibrium, the occupation of the quasiparticle modes is then given by the Gibbs distribution

$$\langle\hat{a}_{\mathbf{q}}^\dagger\hat{a}_{\mathbf{q}}\rangle = \langle\hat{b}_{\mathbf{q}}^\dagger\hat{b}_{\mathbf{q}}\rangle = Z^{-1}e^{-E_{\mathbf{q}}/k_{\text{B}}T} \tag{3.46}$$

with k_{B} the Boltzmann constant, Z the partition function and T the temperature. This allows us to calculate the occupation numbers of the physical fluctuations according to

$$\langle\hat{c}_{\mathbf{q}}^\dagger\hat{c}_{\mathbf{q}}\rangle = v_q^2 + (u_q^2 + v_q^2)Z^{-1}e^{-E_{\mathbf{q}}/k_{\text{B}}T}. \tag{3.47}$$

The first term that is even present at $T = 0$ is solely due to interactions and is sometimes referred to as quantum depletion. The second term describes thermal fluctuations.

Local density approximation for inhomogeneous systems

For an inhomogeneous system, as outlined above, we would like to make use of the Bogoliubov solution for homogeneous systems. To achieve this we partition the quantization volume V into smaller cubes V_j with edges of length $L \gg \xi$ and $L \ll a_{\text{osc}}$, see Fig. 3.1. The corresponding characteristic functions $A_j(\mathbf{x})$, which are equal to one inside of V_j and zero everywhere else, represent a partition of unity,

$$\sum_j A_j(\mathbf{x}) = 1. \tag{3.48}$$

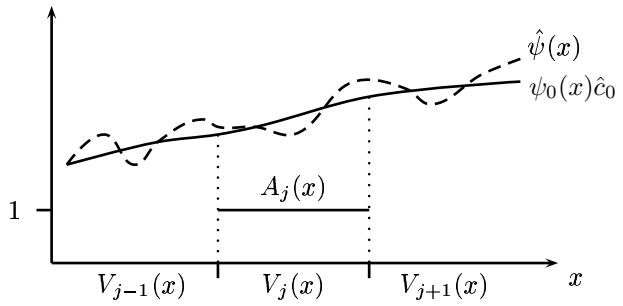

Fig. 3.1: Illustration of the partitioning of the quantization volume and the atomic field operator. Also indicated is the function $A_j(\mathbf{x})$.

Partitioning the atomic field operator accordingly, we get

$$\hat{\psi}(\mathbf{x}) = \sum_j A_j(\mathbf{x})\chi_0(\mathbf{x})\hat{c}_0 + \sum_j A_j(\mathbf{x})\delta\hat{\psi}(\mathbf{x}) \tag{3.49}$$

$$\equiv \psi_0(\mathbf{x})\hat{c}_0 + \sum_j \delta\hat{\psi}^{(j)}_{\rm loc}(\mathbf{x}) \tag{3.50}$$

where $\delta\hat{\psi}^{(j)}_{\rm loc}(x) = A_j(x)\delta\hat{\psi}(x)$. The partitioning of the field operator is also illustrated in Fig. 3.1.

The fluctuations have a typical correlation length of order ξ. Because the cubes V_j are assumed to be much larger than ξ fluctuations in neighbouring cells are only correlated with each other in a thin layer near the boundaries, while fluctuations in non-neighbouring cells are entirely uncorrelated. Neglecting this surface effect we can approximate the fluctuations in different cells as being uncorrelated. Mathematically this is expressed by

$$\langle\delta\hat{\psi}^{(j)\dagger}_{\rm loc}(\mathbf{x})\delta\hat{\psi}^{(i)}_{\rm loc}(\mathbf{x}')\rangle = \delta_{i,j}\langle\delta\hat{\psi}^{(j)\dagger}_{\rm loc}(\mathbf{x})\delta\hat{\psi}^{(i)}_{\rm loc}(\mathbf{x}')\rangle \tag{3.51}$$

and similarly for higher order correlations.

We will make use of this decomposition and the local density approximation for the fluctuations in chapter 7 to calculate concrete correlation functions.

3.2 Ultra-cold fermions

3.2.1 Normal Fermi gases

In this section we collect some of the ground state properties of trapped fermions in the normal state that will be used later.

In a homogeneous system with density n, neglecting interactions, the ground state of a system of fermions of one species is given by a Fermi sea in which the atoms occupy all states with energy below the Fermi energy

$$E_F = \frac{\hbar^2}{2M}(6\pi^2 n)^{2/3}. \tag{3.52}$$

In a trapped system in equilibrium the total energy for adding a particle anywhere in the system must be equal to the chemical potential. The total energy at a certain point in space in the local density approximation is given by the sum of the Fermi energy corresponding to the local density and the trapping potential so that we find

$$\frac{\hbar^2}{2M}(6\pi^2 n(\mathbf{x}))^{2/3} + V(\mathbf{x}) = \mu. \tag{3.53}$$

The density is found from this equation by solving for n (and setting n equal to zero where the solutions are negative). The chemical potential is then determined from the total number of particles by integrating the density over space,

$$\mu = (48N)^{1/3}\frac{1}{2}\hbar\omega_{\mathrm{osc}}, \tag{3.54}$$

so that we eventually find for the density

$$n(\mathbf{x}) = \frac{8N}{\pi^2 R^3}\left(1 - \left(\frac{\mathbf{x}}{R_{\mathrm{TF}}}\right)^2\right), \tag{3.55}$$

where

$$R_{\mathrm{TF}} = (48N)^{1/6} a_{\mathrm{osc}} \tag{3.56}$$

is the Thomas Fermi radius for noninteracting fermions in a spherical trap. Similarly to the bosonic case, the radius of the cloud scales only very weakly with the number of particles.

Repulsive interactions do not lead to any qualitative changes of the properties of cold fermions [73, 1]. They lead to excitations of particles just below the Fermi surface into states slightly above the Fermi surface. Particles deeply below the Fermi surface are not affected. Thus interactions lead to a slightly diminished hight in the drop in occupation number across the Fermi surface, but the occupation still changes discontinously. In general the effects of repulsive interactions are very similar to thermal excitations which also lead to the creation of particle hole pairs near the Fermi surface. Both effects do not have any significant consequences as far as the coherence properties of ultracold fermions are concerned and therefore we will neglect them for the most part.

3.2.2 BCS superfluidity

In contrast to repulsive interactions, attractive interactions change the properties of ultra cold fermions dramatically: They give rise to superfluidity. Fermionic superfluid systems have been known for a very long time. For example the electrons in a metal can exhibit superfluidity at low temperatures and as a consequence the metal becomes a superconductor, i.e. it carries current with virtually no resistance. Another traditional example is superfluidity of fermionic ^{3}He. In the last few years superfluidity of fermions has been realized in cold gases of neutral atoms [99, 117, 9].

The reason for the superfluid behaviour was a mystery for a long time. The suggestion of Fritz London in 1935 that the electrons in a superconductor occupy a macroscopic wave function [82, 80] and the resulting electromagnetic equations [81] could explain several properties of superconductors such as the Meissner effect. But the theory was still very incomplete and many aspects could not be explained, one of the chief problems being that the Pauli exclusion principle prohibits the electrons from occupying a single state.

A completely different route was taken by Landau and Ginzburg who, starting from Landau's theory of second order phase transitions, developed an effective theory for the superfluid order parameter that has to emerge at the superfluid phase transition [44, 43, 50]. The resulting theory could explain effects such as e.g. persistent currents and the Meissner effect but, being a purely effective theory, gave no insight into the microscopic mechanism leading to superfluidity.

A real breakthrough in the understanding of superfluid fermionic systems and superconductors was achieved with the theory of Bardeen, Cooper and Schrieffer (BCS)[8]. Their explanation of superfluidity is based on the observation that even a very small attractive interaction gives rise to the so-called Cooper instability [26]: Due to the large number of nearly degenerate particles near the Fermi surface the many body system can lower its total energy by forming superpositions of pairs of particles known as Cooper pairs. These pairs can condense in the zero total momentum state and this "condensate of Cooper pairs" is responsible for superfluidity. The "condensate wave function" of the Cooper pairs can be thought of as the microscopic version of Londons superfluid wave function and Ginzburg and Landau's order parameter.

The BCS theory is a weak coupling theory, since it is based on taking the interactions into account through perturbation theory. In this work we will use it exclusively for the study of superfluid fermionic systems and thus we are limiting ourselves to weak interactions. As was the case for BECs previously discussed, we need to adapt the BCS theory, which was first developed for homogeneous systems, to the inhomogeneous situation found in a trap. Similarly to the bosonic case, we will do so by making use of the local density approximation. Before

demonstrating how this can be done, we first review the BCS theory for a homogeneous system, mainly to introduce our notation and to set the stage.

In their original treatment Bardeen, Cooper and Schrieffer calculated the ground state of a Fermi gas with attractive interactions using a variational calculation. For our purposes it is more convenient to use the method based on a canonical transformation proposed at about the same time as the original BCS theory by Bogoliubov [12]. In this way the calculations become very similar to the BEC calculations above so that it is easier to draw analogies.

Homogeneous system

Because fermions of one species cannot interact with each other at low temperatures we need to consider at least two species, labeled $\uparrow$ and $\downarrow$. In the context of ultracold atoms these could be provided e.g. by the same kind of atoms in different hyperfine states. The manybody Hamiltonian describing this system reads in the momentum representation

$$\hat{H} = \sum_{\mathbf{q},\sigma} \xi_{\mathbf{q}} \hat{c}^\dagger_{\mathbf{q}\sigma} \hat{c}_{\mathbf{q}\sigma} + \frac{U_0}{V} \sum_{\mathbf{q},\mathbf{q}_1,\mathbf{q}_2} \hat{c}^\dagger_{\mathbf{q}+\frac{\mathbf{q}_1}{2}\uparrow} \hat{c}^\dagger_{\mathbf{q}-\frac{\mathbf{q}_1}{2}\downarrow} \hat{c}_{\mathbf{q}+\frac{\mathbf{q}_2}{2}\downarrow} \hat{c}_{\mathbf{q}-\frac{\mathbf{q}_2}{2}\uparrow}. \tag{3.57}$$

$\xi_q = \hbar^2 q^2/2/M - \mu$ is the kinetic energy of an atom of momentum $\hbar\mathbf{q}$ measured from the chemical potential μ. U_0 is now supposed to be negative, i.e. the scattering length a is negative. $\hat{c}_{\mathbf{q}\sigma}$ and $\hat{c}^\dagger_{\mathbf{q}\sigma}$ with $\sigma = \uparrow, \downarrow$ are the annihilation and creation operators for an atom of momentum $\mathbf{q}$ and internal state σ. They satisfy the usual fermionic anticommutation relations,

$$\{\hat{c}_{\mathbf{q}\sigma}, \hat{c}_{\mathbf{q}'\sigma'}\} = \delta_{\mathbf{q},\mathbf{q}'} \delta_{\sigma,\sigma'}, \tag{3.58}$$

with all other anticommutators vanishing.

The key observation of BCS is that if individual atomic states are occupied completely independently the interaction energy will have about as many positive contributions as negative contributions due to the anticommutation of the Fermi field operators, and as a consequence the interactions cannot lower the total energy. If however the Hamiltonian Eq. (3.57) is only considered in the subspace in which pairs of atoms $\mathbf{q}\uparrow$ and $-\mathbf{q}\downarrow$ are either present or absent the interactions are always negative and can lead to a reduction of the total energy. From a variational point of view this should give a good approximation for the low energy properties of the system. The Hamiltonian restricted to the pair subspace

$$\hat{H}_{\mathrm{BCS}} = \sum_{\mathbf{q},\sigma} \xi_{\mathbf{q}} \hat{c}^\dagger_{\mathbf{q}\sigma} \hat{c}_{\mathbf{q}\sigma} + \frac{U_0}{V} \sum_{\mathbf{q}_1,\mathbf{q}_2} \hat{c}^\dagger_{\mathbf{q}_1\uparrow} \hat{c}^\dagger_{-\mathbf{q}_1\downarrow} \hat{c}_{-\mathbf{q}_2\downarrow} \hat{c}_{\mathbf{q}_2\uparrow} \tag{3.59}$$

is known as the BCS-reduced Hamiltonian. Note that in the interaction term only pairs of atoms with center of mass momentum $\mathbf{q} = 0$ interact with each other.

The Hartree-Fock energy due to the interactions does not give rise to qualitative modifications. In particular it does not affect the pairing mechanism and superfluidity. To simplify the discussion we neglect it for now. It can easily be included later and we show how this can be done in the discussion of the inhomogeneous case below.

The calculation of the low energy excitations of the Bose gas in the previous section was based on the Bogoliubov approximation in which the field operator for the condensate is replaced by the mean field wich is a *c*-number. Here we make an analogous approximation. But because fermions cannot condense in a single state we need to consider pairs of fermions and split them in a *c*-number part giving rise to the mean field and a fluctuations part according to

$$\hat{c}_{\mathbf{q}\uparrow}\hat{c}_{-\mathbf{q}\downarrow} = \langle\hat{c}_{\mathbf{q}\uparrow}\hat{c}_{-\mathbf{q}\downarrow}\rangle + (\hat{c}_{\mathbf{q}\uparrow}\hat{c}_{-\mathbf{q}\downarrow} - \langle\hat{c}_{\mathbf{q}\uparrow}\hat{c}_{-\mathbf{q}\downarrow}\rangle). \tag{3.60}$$

Inserting this expression in the BCS-reduced Hamiltonian and keeping only terms containing at most one fluctuation, just like in the bosonic case above, we find the Hamiltonian in the mean field approximation

$$\hat{H}_{\mathrm{BCS,MF}} = \sum_{\mathbf{q},\sigma} \xi_{\mathbf{q}}\hat{c}^{\dagger}_{\mathbf{q}\sigma}\hat{c}_{\mathbf{q}\sigma} + \Delta\sum_{\mathbf{q}} \hat{c}^{\dagger}_{\mathbf{q}\uparrow}\hat{c}^{\dagger}_{-\mathbf{q}\downarrow} + \Delta^{*}\sum_{\mathbf{q}} \hat{c}_{-\mathbf{q}\downarrow}\hat{c}_{\mathbf{q}\uparrow}. \tag{3.61}$$

where we have omitted an irrelevant additive constant and the Hartree-Fock exchange energy. The gap

$$\Delta = \frac{U_0}{V}\sum_{q}\langle\hat{c}_{\mathbf{q}\uparrow}\hat{c}_{-\mathbf{q}\downarrow}\rangle, \tag{3.62}$$

which can be chosen real, will be determined selfconsistently below.

We see that the mean field Hamiltonian has a very similar form to the bosonic mean field Hamiltonian with off diagonal terms of the form $\hat{c}_{\mathbf{q}\downarrow}\hat{c}_{-\mathbf{q}\uparrow}$ etc. Accordingly, we try to eliminate these off-diagonal terms using again a canonical transformation to quasiparticles. The transformation to the quasiparticles $\hat{a}_{\mathbf{q}}$ and $\hat{b}_{\mathbf{q}}$ is given by

$$\begin{pmatrix} \hat{a}_{\mathbf{q}} \\ \hat{b}^{\dagger}_{\mathbf{q}} \end{pmatrix} = \begin{pmatrix} \alpha_{\mathbf{q}} & \alpha_{-\mathbf{q}} \\ \beta_{\mathbf{q}} & \beta_{-\mathbf{q}} \end{pmatrix}\begin{pmatrix} \hat{c}_{\mathbf{q}\uparrow} \\ \hat{c}^{\dagger}_{-\mathbf{q}\downarrow} \end{pmatrix}. \tag{3.63}$$

The transformation coefficients can be chosen real since we chose the gap to be real. For the transformation to be canonical the new field operators must now satisfy the fermionic anticommutation relations Eq. (3.58), leading to the conditions

$$\alpha_q^2 + \alpha_{-\mathbf{q}}^2 = 1, \tag{3.64}$$

$$\beta_q^2 + \beta_{-\mathbf{q}}^2 = 1, \tag{3.65}$$

$$\alpha_{\mathbf{q}}\beta_{\mathbf{q}} + \alpha_{-\mathbf{q}}\beta_{-\mathbf{q}} = 0. \tag{3.66}$$

Thus the transformation is canonical if we set

$$\alpha_{\mathbf{q}} = u_{\mathbf{q}} \quad , \quad \alpha_{-\mathbf{q}} = v_{\mathbf{q}} \tag{3.67}$$

$$\beta_{\mathbf{q}} = v_{\mathbf{q}} \quad , \quad \beta_{-\mathbf{q}} = -u_{\mathbf{q}} \tag{3.68}$$

where $u_q^2 + v_q^2 = 1$.

Inserting in the mean field Hamiltonian we find off diagonal elements proportional to $\hat{a}_{\mathbf{q}}^\dagger \hat{b}_{-\mathbf{q}}^\dagger$ which can be eliminated by setting

$$u_{\mathbf{q}}^2 = \frac{1}{2}\left(1 - \frac{\xi_{\mathbf{q}}}{\sqrt{\Delta^2 + \xi_{\mathbf{q}}^2}}\right), \tag{3.69}$$

$$v_{\mathbf{q}}^2 = \frac{1}{2}\left(1 + \frac{\xi_{\mathbf{q}}}{\sqrt{\Delta^2 + \xi_{\mathbf{q}}^2}}\right), \tag{3.70}$$

upon which the Hamiltonian finally becomes

$$\hat{H}_{\mathrm{BCS,MF}} = \sum_{\mathbf{q}} E_{\mathbf{q}} (\hat{a}_{\mathbf{q}}^\dagger \hat{a}_{\mathbf{q}} + \hat{b}_{\mathbf{q}}^\dagger \hat{b}_{\mathbf{q}}). \tag{3.71}$$

This means that the system is transformed into independent fermions with a dispersion relation given by

$$E_{\mathbf{q}} = \sqrt{\Delta^2 + \xi_{\mathbf{q}}^2}. \tag{3.72}$$

The ground state of this system has to be the vacuum state of the quasi particles. Up to a normalization constant, it can be written in the form

$$|BCS\rangle = \prod_{\mathbf{q}} \hat{a}_{\mathbf{q}} \hat{b}_{-\mathbf{q}} |0\rangle \tag{3.73}$$

$$= \prod_{\mathbf{q}} v_{\mathbf{q}} (u_{\mathbf{q}} + v_{\mathbf{q}} \hat{c}_{-\mathbf{q}\downarrow}^\dagger \hat{c}_{\mathbf{q}\uparrow}^\dagger) |0\rangle \tag{3.74}$$

where $|0\rangle$ is the vacuum of the real particles. That the state Eq. (3.74) is the vacuum of the quasiparticles is easily verified by noting that acting on it with a quasiparticle operator gives a square of a fermionic annihilation operator, which must vanish. The properly normalized ground state is obtained from Eq. (3.74) by omitting the factors of $v_{\mathbf{q}}$.

It remains to determine the gap Δ. To this end we need to evaluate the expectation value that appears in the definition of Δ in the properly normalized BCS ground state to find the so called gap equation

$$\Delta = \frac{U_0}{2} \sum_{\mathbf{q}} \frac{\Delta}{\sqrt{\Delta^2 + \xi_{\mathbf{q}}}}. \tag{3.75}$$

The sum in this equation diverges in the ultra-violet. The reason is that we have used the bare interaction which is assumed to be delta function like. This is a good approximation for the low momenta occurring in cold collisions of the fermions but it is violated for the high momenta occuring in the sum in Eq. (3.75).

In typical condensed matter systems this problem is solved by introducing a momentum cut-off, which is naturally provided by the Debye frequency ν_D [2]: The interactions between electrons become very weak once their relative momentum exceeds the Debye momentum and accordingly the interactions can be assumed to be pointlike for relative momenta below the Debye momentum and zero for larger momenta. This works well in condensed matter systems because $\hbar\nu_D$ is only a very small fraction of the Fermi energy.

In cold atoms systems this method is not applicable because the atomic interactions are still strong for momenta far exceeding the Fermi momentum. Therefore, one has to eliminate the bare interaction in favor of the effective interaction given by the zero energy value of the T-matrix. The T-matrix accurately captures the effect of all the high momentum components which are being integrated out. More details on this procedure can be found e.g. in chapter 14 of [95]. Going over to the effective interaction, which we again denote by U_0, we find the regularized gap equation

$$1 = \frac{U_0}{2}\sum_{\mathbf{q}}\left(\frac{1}{\sqrt{\Delta^2+\xi_{\mathbf{q}}}} - \frac{1}{\xi_{\mathbf{q}}}\right). \tag{3.76}$$

Inhomogeneous systems

In this section we closely follow the approach of Houbiers et. al. [56]. We assume that the spherically symmetric trapping potential is sufficiently slowly varying that the gas can be treated in the local density approximation. More quantitatively, the local density approximation is valid if the size of the Cooper pairs, given by the correlation length

$$\lambda(r) = \hbar v_F(r)/\pi\Delta(r),$$

is much smaller than the oscillator length of the trap. Here, $v_F(r)$ is the velocity of the atoms at the Fermi surface and $\Delta(r)$ is the pairing field at a distance r from the origin, which we take at the center of the trap.

We assume that, locally at each $\mathbf{x}$, the wave function can be approximated by the BCS wave function for a homogenous gas,

$$|BCS(\mathbf{x})\rangle = \prod_{\mathbf{k}}(u_{\mathbf{k}}(\mathbf{x}) + v_{\mathbf{k}}(\mathbf{x})\hat{c}^\dagger_{-\mathbf{k},\uparrow}\hat{c}^\dagger_{\mathbf{k},\downarrow})|0\rangle, \tag{3.77}$$

[2] The Debye frequency ν_D is the highest phonon frequency in a crystal. The Debye momentum is the momentum of an electron with kinetic energy equal to $\hbar\nu_D$.

with local Bogoliubov amplitudes $u_{\mathbf{k}}(\mathbf{x})$ and $v_{\mathbf{k}}(\mathbf{x})$ which have the same form as in the homogeneous case but with spatially varying gap $\Delta(\mathbf{x})$ and with $\xi_{\mathbf{k}}(r) = \epsilon_{\mathbf{k}} - \mu_{\mathrm{loc}}(r)$, where

$$\mu_{loc}(r) = \mu_0 - U(r) - U_0 n(r) \tag{3.78}$$

is the local chemical potential. In contrast to the normal Fermi gas, we have included the Hartree-Fock mean-field energy in the local chemical potential. For ultra-cold atom experiments it can usually not be neglected since in those systems fermionic superfluidity can typically only be observed for rather strong interactions. The equation for the local gap follows from Eq. (3.76),

$$\frac{-\pi}{2k_F(0)a} = \mu_0 k_F^{-3}(0) \int_0^\infty dk k^2 \left(\frac{1}{\sqrt{\xi_{\mathbf{k}}^2(\mathbf{x}) + \Delta^2(\mathbf{x})}} - \frac{1}{\xi_{\mathbf{k}}(\mathbf{x})} \right), \tag{3.79}$$

where $k_F(0)$ is the local Fermi momentum at the center of the trap.

In principle, equations (3.78) and (3.79) are two coupled implicit equations from which the total chemical potential μ_0 and the local gap $\Delta(\mathbf{x})$ have to be determined self consistently. However, to an excellent approximation, $\mu_{loc}(\mathbf{x}) = E_F(\mathbf{x})$ and the Fermi momentum is related to the local density by means of Eq. (3.52) so that Eq. (3.78) can be used by itself to determine μ_0 from the requirement that the density adds up to the total number of atoms N, $\int d^3x n(\mathbf{x}) = N$. Then the density profile $n(\mathbf{x})$ is known and we can solve the gap equation numerically for $\Delta(\mathbf{x})$.

3.3 Feshbach-resonances and ultra-cold molecules

3.3.1 Two body physics

In this dissertation we are mostly using an effective description of Feshbach resonances and ultra cold molecules. In this subsection we present the underlying two body physics.

For Feshbach resonances to occur in binary collisions the colliding particles must have at least two distinct internal states which we designate by M and P. These states could e.g. correspond to different hyperfine states or different electronic states. If we neglect the coupling between these two states we can consider the potential for the particles as a function of their separation for each internal state. These potential curves are shown in Fig. 3.2. The potential curves for the two different internal states are in general different. In particular the asymptotic energy of colission partners with vanishing kinetic energy at infinite seperation will in general be different and we assume that M is the state with the higher asymptotic energy E_M. For instance in the case where M and P correspond to different hyperfine states the different asymptotic energies correspond to the different

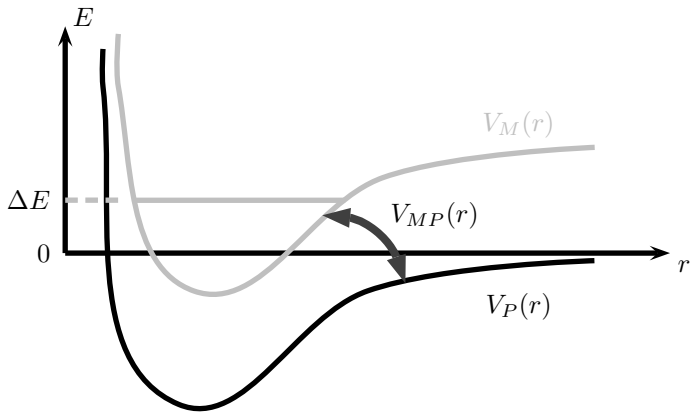

Fig. 3.2: Schematic of the interatomic potential for a Feshbach resonance for atoms in the open channel P and the closed channel M and the coupling between the two channels V_{MF}. Also shown is the molecular bound state in the closed channel detuned by ΔE form the open channel asymptote.

Zeeman shifts the atoms experience in an external magnetic field. In that case P corresponds to atoms in the triplet state with both spins parallel or antiparallel to the external magnetic field, depending on the sign of the Landé-g factor. We measure energies relative to the zero kinetic energy asymptote of channel P. Also we assume that M supports bound states, but we only take into account the state with binding energy ΔE closest to zero, i.e. nearest to the P channel asymptote[3].

In general there will be a coupling $V_{MP}(r)$ between the two internal states. The coupling has a range that is typically of the same order as the interatomic potential. In ultracold atoms, the coupling is given by the spin-orbit coupling or it can be generated with lasers driving the transition to a different electronic state. We assume that the incoming atoms are in the P state and that their energy is smaller than E_M. The interactions can then induce transitions to the M channel. Due to energy conservation the atoms cannot escape to infinity in the M state, i.e. M is a closed channel in the language of scattering physics. In contrast, P is an open channel. If the binding energy in the closed channel is close to 0, i.e. on resonance with the incoming atoms in the open channel, the scattering is very strongly affected by the presence of the bound state. This situation is called a Feshbach resonance.

Let us now turn to a more detailed discussion. If we write the wave function as

[3] In realistic atoms several bound states both of M and P channel need to be taken into account to describe the two body scattering quantitatively. In this sense Feshbach resonance physics in ultracold atoms often deviates from the universal picture that one obtains from including only one resonant state.

a spinor with the upper component the closed channel and the lower component the open channel, $|\varphi\rangle = (|\varphi_M\rangle, |\varphi_P\rangle)^T$, we can write the Hamiltonian as

$$\hat{H} = \begin{pmatrix} \hat{H}_M & \hat{V}_{MP} \\ \hat{V}_{PM} & \hat{H}_P \end{pmatrix}, \tag{3.80}$$

where $\hat{H}_M$ and $\hat{H}_P$ are the Hamiltonians for atoms in the closed and open channel, respectively. The Schrödinger equation is explicitly written as

$$\hat{H}_M|\varphi_M\rangle + \hat{V}_{MP}|\varphi_P\rangle = E|\varphi_M\rangle \tag{3.81}$$
$$\hat{H}_P|\varphi_P\rangle + \hat{V}_{PM}|\varphi_M\rangle = E|\varphi_P\rangle. \tag{3.82}$$

Since we are ultimately interested in outgoing scattering states we solve the second of these equations for $|\varphi_P\rangle$ using the propagator for outgoing atoms in the open channel,

$$|\varphi_P\rangle = |\varphi_P^{(+)}\rangle + \hat{g}^{(+)}(E)\hat{V}_{PM}|\varphi_M\rangle \equiv |\varphi_P^{(+)}\rangle + (E - \hat{H}_P + i\epsilon)^{-1}\hat{V}_{PM}|\varphi_M\rangle. \tag{3.83}$$

Here, $|\varphi_P^{(+)}\rangle$ is the scattering state for energy E in the absence of coupling to the closed channel, $\hat{V}_{MP} = 0$. Because we are studying low energy scattering, only the s-wave component of $|\varphi_P^{(+)}\rangle$ is of interest to us. We call the regular solution to the unperturbed Schrödinger equation for the s-wave component $u(r)$. As the separation r between the atoms becomes infinite, it can be written as a sum of an incoming and outgoing spherical waves and this way we can relate it to the scattering state,

$$\langle \mathbf{r}|\varphi_P^{(+)}\rangle = \frac{e^{-ikr}}{r} - e^{2i\delta_0}\frac{e^{ikr}}{r} = -2ike^{i\delta_0}u(r), \qquad (r \to \infty) \tag{3.84}$$

where

$$\delta_0 = -ka, \tag{3.85}$$

is the s-wave scattering phase, a is the scattering length and $k = \sqrt{ME/\hbar^2}$. Alternatively, the scattering wave function can be written in terms of an incoming plane wave and an outgoing spherical wave,

$$\langle \mathbf{r}|\varphi_P^{(+)}\rangle = e^{i\mathbf{kr}} + f\frac{e^{ikr}}{r}, \qquad (r \to \infty) \tag{3.86}$$

where

$$f = \frac{e^{2i\delta_0} - 1}{2ik} \tag{3.87}$$

is the scattering amplitude.

Inserting $|\varphi_P\rangle$ into the Schrödinger equation for the closed channel Eq. (3.81) we find

$$(E - \hat{H}_M)|\varphi_M\rangle = \hat{V}_{MP}|\varphi_P^{(+)}\rangle + \hat{V}_{MP}\hat{g}^{(+)}(E)\hat{V}_{PM}|\varphi_M\rangle. \tag{3.88}$$

Solving for the bound state,

$$|\varphi_M\rangle = \frac{1}{E - \hat{H}_M - \hat{V}_{MP}\hat{g}^{(+)}(E)\hat{V}_{PM}}\hat{V}_{MP}|\varphi_P^{(+)}\rangle, \tag{3.89}$$

and inserting in Eq. (3.83) we find the resonant scattering state in terms of the unperturbed scattering state,

$$|\varphi_P\rangle = |\varphi_P^{(+)}\rangle + \hat{g}^{(+)}(E)\hat{V}_{PM}\frac{1}{E - \hat{H}_M - \hat{V}_{MP}\hat{g}^{(+)}(E)\hat{V}_{PM}}\hat{V}_{MP}|\varphi_P^{(+)}\rangle. \tag{3.90}$$

In the spirit of perturbation theory we can replace

$$\frac{1}{E - \hat{H}_M - \hat{V}_{MP}\hat{g}^{(+)}(E)\hat{V}_{PM}} \rightarrow |\phi_M^{(0)}\rangle\frac{1}{E - E_m + i\Gamma_M/2}\langle\phi_M^{(0)}|, \tag{3.91}$$

where $|\phi_M^{(0)}\rangle$ is the unperturbed closed channel bound state and the resonance energy is

$$E_m = \mathrm{Re}\langle\phi_M^{(0)}|\hat{H}_M - \hat{V}_{MP}\hat{g}^{(+)}(E)\hat{V}_{PM}|\phi_M^{(0)}\rangle \tag{3.92}$$

and the resonance width is

$$\Gamma_m/2 = -\mathrm{Im}\langle\phi_M^{(0)}|\hat{V}_{MP}\hat{g}^{(+)}(E)\hat{V}_{PM}|\phi_M^{(0)}\rangle. \tag{3.93}$$

In neglecting the other bound states in the expansion Eq. (3.91) we assume that the resonance is narrow compared to the the level separation, $\Gamma_M \ll |E_m^{(0)} - E_n^{(0)}|$, with $E_m^{(0)}$ the unperturbed energy of $|\phi_M^{(0)}\rangle$ and $E_n^{(0)}$ the energies of all the other levels, and in neglecting the continuum states the resonance has to be narrow compared to the binding energy of the closed channel molecule, $\Gamma_M \ll E_M - \Delta E$.

For low energy scattering the general form of the resonance width can easily be studied. The eigenstates of the propagator $g^{(+)}(E)$ are the outgoing scattering states $|k\rangle$. Inserting this complete basis between $\hat{V}_{MP}$ and $g^{(+)}(E)$ in Eq. (3.93) we find

$$\Gamma_m/2 = -\mathrm{Im}\sum_k |\langle\phi_M^{(0)}|\hat{V}_{MP}|k\rangle|^2\frac{1}{E - E_k + i\delta} \tag{3.94}$$

$$= \pi\sum_k |\langle\phi_M^{(0)}|\hat{V}_{MP}|k\rangle|^2\delta(E - E_k). \tag{3.95}$$

At low energy all partial waves except the *s*-wave are zero within the range of $\hat{V}_{MP}$ so that only the *s*-wave component of $\langle r|k\rangle$ enters the matrix element in Eq.

(3.95). At low energies this wave function is essentially energy independent so that we can replace the matrix element by a constant,

$$\alpha = \lim_{|k|\to 0} \langle \phi_M^{(0)} | \hat{V}_{MP} | k \rangle, \tag{3.96}$$

so that we finally obtain

$$\Gamma_m = \pi \alpha^2 D(E) = 2\gamma k, \tag{3.97}$$

where

$$D(E) = \frac{\sqrt{M}^3}{\sqrt{2}\pi^2\hbar^3} \sqrt{E} \tag{3.98}$$

is the density of states for the atom pairs with relative kinetic energy E in the open channel and $\gamma = \frac{\alpha^2 M}{4\pi\hbar^2}$. $D(E)$ is proportional to the momentum of the outgoing atoms, i.e. proportional to $\sqrt{E}$. This dependence of the resonance width on the square root of the resonance energy is known as the Wigner threshold law.

The expression Eq. (3.90) for the scattering wave function including coupling to the closed channel allows us to calculate the modified S-matrix. To this end we need to inspect the asymptotic behavior of the scattering wave function $\langle r|\varphi_P\rangle$ in the limit $r \to \infty$. In that limit we have

$$\langle r | g^{(+)}(E) \hat{V}_{PM} | \phi_m^{(0)} \rangle = -\left(\frac{M}{4\pi\hbar^2}\right) \frac{e^{ikr}}{r} e^{i\delta_0} \alpha, \tag{3.99}$$

where we have used the asymptotic form of the s-wave component of the propagator,

$$\lim_{r\to\infty} \langle r | g^{(+)}(E) | r' \rangle = -\left(\frac{M}{4\pi\hbar^2}\right) \frac{e^{ikr}}{r} e^{i\delta_0} u(r'). \tag{3.100}$$

Using this matrix element we find the asymptotic form of the scattering state,

$$\lim_{r\to\infty} \langle r|\varphi_P\rangle \;=\; \frac{e^{-ikr}}{r} - \left(1 - \frac{i\Gamma_m}{E - E_m + i\Gamma_m/2}\right) e^{2i\delta_0} \frac{e^{ikr}}{r}. \tag{3.101}$$

The coefficient of the outgoing spherical wave is the sought S-matrix element. It has unit magnitude, as it must due to unitarity, and hence can be written

$$\frac{E - E_m - i\Gamma_m/2}{E - E_m + i\Gamma_m/2} e^{2i\delta_0} \equiv e^{2i\delta} \tag{3.102}$$

From δ we find the s-wave scattering length through $\delta = -ka$ and expanding for low scattering energies we find

$$a = a_0 - \frac{\gamma}{\Delta E}. \tag{3.103}$$

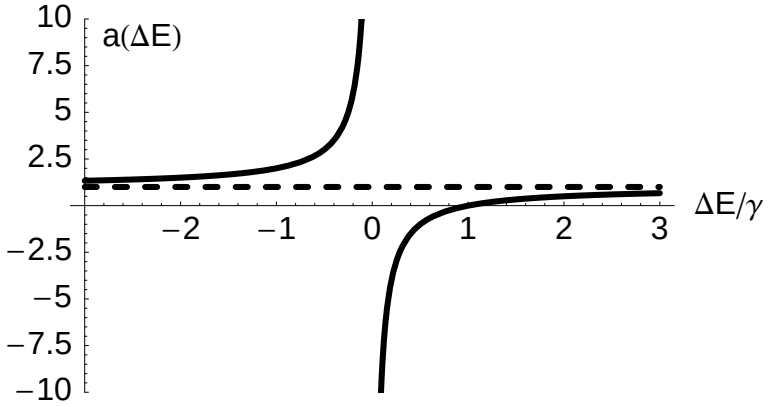

Fig. 3.3: Scattering length in the vicinity of a Feshbach resonance. Energy is measured in units of the width of the resonance and the scattering length in units of the background scattering length. The dashed line shows the background scattering length.

An example for this resonant behavior of the scattering length is shown in Fig. 3.3. For large detunings the scattering length approaches the background scattering length. Approaching the resonance from below the scattering length becomes very large and positive, i.e. the interactions are strongly repulsive. At the resonance the scattering length goes through infinity and becomes very large and negative just above the resonance, i.e. the interactions are very strongly attractive. At $\Delta E = \gamma$ the scattering length vanishes, i.e. the atoms are effectively noninteracting.

In magnetic Feshbach resonances the energy difference between the resonant state and the open channel is given by the Zeeman shift between the two different spin states in an external magnetic field. Thus the energy difference ΔE and consequently the strength of the interactions can be controlled through the external magnetic field. Similarly, for optically induced Feshbach resonances the scattering strength can be controlled through the two-photon detuning from the energy difference between open channel atom pairs and closed channel molecular state.

We should note that for many Feshbach resonances occuring in ultra cold atomic systems the simple universal picture presented here is valid only in a narrow region around the resonance. A complete quantitative understanding of the experiments oftentimes requires the inclusion of more than just one bound state, both in the closed and the open channel [70].

3.3.2 Effective many-body theory

There are mainly two natural ways to include the resonant scattering physics in a many-body theory. The first consists in replacing the scattering length in the interaction part in the Hamiltonian for the atoms by the effective scattering length Eq. (3.103). This method works only for broad Feshbach resonances which have a very strong coupling between the open channel and the closed channel. For such resonances the bound state Eq. (3.89) has very little closed channel admixture and therefore any manybody effect due to its presence can be neglected.

If however the coupling between open and closed channel is not very strong the resonant state has to be explicitly included. Loosely speaking, colliding atoms spend a substantial time in the closed channel and could e.g. condense, which will obviously change the qualitative properties of the many particle system. The basis for explicitly including the closed channel molecules is to introduce a field operator $\hat{\varphi}(\mathbf{x})$ for them. If the atoms pairing up to form a molecule are both bosons or both fermions the resulting molecule is a boson and if one of the constituent atoms obeys fermi statistics and the other bose statistics the molecule is a fermion [78].

The formation of molecules with an *s*-wave symmetry is not possible for identical fermions, but fermions in different internal states can form such molecules. *p*-wave molecules could in principle be formed out of identical fermions and indeed *p*-wave resonances have been seen in recent experiments [115][4]. But here we will restrict ourselves to *s*-symmetrical molecules.

Regarding the statistics of the molecules the following question may arise: If for example two fermions are bound very tightly in a molecular state the spatial structure of which is not resolved it has to be considered bosonic. If on the other hand the atoms are very loosely bound and the atoms are far away from each other, the system is better described as two independent fermions. Somehow there has to be a transition between these two extremes and it is interesting to find the criterion that allows us to treat the composite particle as a boson. To this end we have to check the commutation relations between the molecular field operators and between molecular field operators and atoms. We explicitly write the molecular field operator in terms of its constituent fermions as[5]

$$\hat{\varphi}(\mathbf{R}) = \int d^3x \varphi_m(\mathbf{x}) \hat{\psi}_\uparrow(\mathbf{R} + \mathbf{x}/2) \hat{\psi}_\downarrow(\mathbf{R} - \mathbf{x}/2). \tag{3.104}$$

It is easy to see that the commutators between molecular creation operators and

[4] Even d-wave resonances between bosons have been seen [16, 38].

[5] In general, the molecular wave function involves different internal states of the atoms and φ_m should be thought of as a spatially dependent tensor of rank (1,1) in the atomic spin space. We suppress the internal states, except for $\uparrow$ and $\downarrow$, for clarity because the calculation is essentially the same.

between molecular annihilation operators vanish. Let us then turn to the commutator between annihilation and creation operator. Using $[\hat{A},\hat{B}\hat{C}] = \{\hat{A},\hat{B}\}\hat{C} - \hat{B}\{\hat{A},\hat{C}\}$ one finds

$$\begin{aligned}[\hat{\varphi}(\mathbf{R}),\hat{\varphi}^\dagger(\mathbf{R}')] &= \delta(\mathbf{R}-\mathbf{R}') \\ &- \int d^3x \varphi_m(\mathbf{x})\varphi_m^*(\mathbf{x}+2(\mathbf{R}'-\mathbf{R}))\hat{\psi}_\uparrow^\dagger(2\mathbf{R}'-\mathbf{R}+\mathbf{x}/2)\hat{\psi}_\uparrow(\mathbf{R}+\mathbf{x}/2) \\ &- \int d^3x \varphi_m(\mathbf{x})\varphi_m^*(\mathbf{x}-2(\mathbf{R}'-\mathbf{R}))\hat{\psi}_\downarrow^\dagger(2\mathbf{R}'-\mathbf{R}-\mathbf{x}/2)\hat{\psi}_\downarrow(\mathbf{R}-\mathbf{x}/2). \quad (3.105)\end{aligned}$$

To obtain the δ-function in the first line we have used the fact that the molecular wave function is normalized to unity. The δ-function by itself means that the molecular field describes bosons but the other two terms proportional to the atomic density spoil the commutation relation. To understand the density terms we recall that the commutator is a distribution and therefore we consider what happens if e.g. the first density term is integrated against a test function $f(\mathbf{R})$,

$$\begin{aligned}\int d^3R d^3x f(\mathbf{R}) f(\mathbf{R})\varphi_m(\mathbf{x})\varphi_m^*(\mathbf{x}+2(\mathbf{R}'-\mathbf{R}))\hat{\psi}_\uparrow^\dagger(2\mathbf{R}'-\mathbf{R}+\mathbf{x}/2)\hat{\psi}_\uparrow(\mathbf{R}+\mathbf{x}/2) \\ \approx f(\mathbf{R}')\hat{\psi}_\uparrow^\dagger(\mathbf{R}')\hat{\psi}_\uparrow(\mathbf{R}')V_{\mathrm{mol}}. \quad (3.106)\end{aligned}$$

Here we have used that the molecules are tiny compared to the length scales occuring in the effective manibody theory, i.e. compared to the distances over which the atomic field operators and the test function change. V_{mol} is of the order of the volume occupied by the molecule so that f is being multiplied by the number of atoms of type $\uparrow$ within the molecule. The second density term gives the same result for the $\downarrow$-atoms. The remaining commutators between molecules and atoms lead to similar results. Thus we find that the field introduced by means of Eq. (3.104) is a proper bosonic field as long as the size of the molecules is much smaller than the mean interatomic separation,

$$V_{\mathrm{mol}} n \ll 1, \quad (3.107)$$

where n is the density of the atoms [6]. The case of molecules formed from bosonic atoms and the case of fermionic molecules made from a boson and a fermion are very similar.

For bosonic molecules formed from two fermions the coupling Hamiltonian $\hat{V}_{MP} + \hat{V}_{PM}$ can be written in second quantization as

$$\hat{V} = \hbar g \int d^3x \hat{\varphi}^\dagger(\mathbf{x})\hat{\psi}_\uparrow(\mathbf{x})\hat{\psi}_\downarrow(\mathbf{x}) + H.C. \quad (3.108)$$

[6] Incidentally, this result also explains why one cannot think of Cooper pairs as molecules: For Cooper pairs the pair wave function plays the role of the molecular wave function and typically there are a great number of fermions within the correlation volume of the Cooper pair.

$\hbar g = \gamma/\sqrt{2}$ is the coupling strength between the open and closed channel molecules. The explicitly written term describes molecule association and its hermitian conjugate describes molecule dissociation. For bosonic atoms the fermionic operators are simply replaced by bosonic operators and the spin indices can be dropped.

In addition to the coupling Hamiltonian a kinetic energy term and a trapping term have to be added for the molecules. Furthermore there can be scattering between molecules and between atoms and molecules. In this dissertation we will however mostly consider situations where the density of molecules is very low, so that these extra collision terms can be neglected.

For two species of fermionic atoms the total Hamiltonian describing the coupled atom-molecule maniparticle system is then

$$\begin{aligned}\hat{H} = \int d^3x \sum_{\sigma=\uparrow,\downarrow} \hat{\psi}^\dagger_\sigma(\mathbf{x})\left(\frac{\hbar^2}{2M}\nabla^2 + V(\mathbf{x})\right)\hat{\psi}_\sigma(\mathbf{x}) \\ + \frac{4\pi\hbar^2 a}{M}\int d^3x \hat{\psi}^\dagger_\uparrow(\mathbf{x})\hat{\psi}^\dagger_\downarrow(\mathbf{x})\hat{\psi}_\downarrow(\mathbf{x})\hat{\psi}_\uparrow(\mathbf{x}) \\ + \int d^3x \hat{\varphi}^\dagger(\mathbf{x})\left(\frac{\hbar^2}{M}\nabla^2 + V_{\mathrm{m}}(\mathbf{x}) + \Delta E\right)\hat{\varphi}(\mathbf{x}) \\ + \hbar g \int d^3x \hat{\varphi}^\dagger(\mathbf{x})\hat{\psi}_\uparrow(\mathbf{x})\hat{\psi}_\downarrow(\mathbf{x}) + H.C. \quad (3.109)\end{aligned}$$

The atomic parameters are the same as in section 3.1, and we have used that the molecules have twice the mass of the atoms. V_{m} is the trapping potential for the molecules.

3.3.3 Single mode approximation

The full manybody problem of coupled ultra cold atoms and molecules is much too complicated to be solved directly. The main difficulty is the large number of degrees of freedom of the quantized fields involved and the nonlinear coupling between them [7]. Several approximation schemes are commonly employed to obtain computationally tractable models.

One class of approximation schemes introduces expectation values of correlation functions of the atomic and molecular fields. The equations of motion for these correlation functions can be derived using the Hamiltonian. Lower order correlation functions couple to higher orders because of the nonlinearity of the Hamiltonian. This hirarchy has to be truncated at some point because of the increasing numerical complexity with increasing order of the correlation functions. The truncation schemes can sometimes be physically motivated but in most cases

[7] In principle, the number of degrees of freedom is of course infi nite.

they introduce uncontrolled errors and these can give rise to mathematical difficulties, especially due to the nonlinearities[8]. The main advantage of methods of this class is that fairly detailed, spatially resolved information can be obtained for the correlation orders that are actually taken into account. The main drawback is, besides the uncontrolled errors due to the truncation already mentioned, that no information on higher order correlations can be obtained. We will use a method of this kind in chapter 7 to study the first order correlations of a molecular gas coupled to different atomic states and for more details on this method we refer the reader to that chapter.

In this section we discuss the principles of a second method, the so called single or few mode approximation, that is based on taking into account only a minimal number of degrees of freedom for each quantum field. The resulting effective models are ideally so much simpler that they can be solved exactly. Thus one gains access to correlation functions of all orders. Furthermore the approximate models are still governed by a Schrödinger equation and therefore they are mathematically well behaved. Another advantage of few mode approximations is that the resulting effective models can often be connected to models well known in other areas of physics, e.g. in quantum optics. The identification of ultracold atoms systems with quantum optical systems allows one to understand qualitative properties from a quantum optics perspective and this has served as a guide for large parts of the work presented in this dissertation. In making the single mode approximation one looses of course all spatial resolution for the correlation functions.

Here we only discuss the few mode approximation for the coupling between atoms and molecules. Few mode descriptions of other aspects of the problem, such as e.g. the atomic kinetic energies, are discussed in chapter 5.

Bosons

The essence of the single mode approximation can most easily be seen for bosonic atoms. We split the atomic field operator into a condensed part and fluctuations as in Eq. (3.5) and we neglect the fluctuations. Similarly, the molecular field is split into an "important" component with wave function φ and annihilation operator $\hat{a}$ and another part $\hat{\varphi}_\perp$ that we will neglect,

$$\hat{\varphi}(\mathbf{x}) = \varphi(\mathbf{x})\hat{a} + \hat{\varphi}_\perp(\mathbf{x}) \equiv \varphi(\mathbf{x})\hat{a} + \sum_n \varphi_n(\mathbf{x})\hat{a}_n. \tag{3.110}$$

[8] For instance one may be forced to include non-Gaussian fluctuations and these can give rise to negative probabilities in the course of a numerical simulation.

All the mode functions φ_n have to be orthogonal to φ,

$$\int d^3x \varphi^*(x)\varphi_n(\mathbf{x}) = 0, \tag{3.111}$$

in order for the commutation relations to be canonical.

There are two natural choices for $\varphi(\mathbf{x})$ depending on what aspect of the molecular dynamics is dominant. If the coupling to the atoms is dominant and all other molecular energies such as e.g. their kinetic and trapping energies can be neglected, it is natural to choose $\varphi(\mathbf{x}) \propto \psi_0^2(\mathbf{x})$. It is easy to see that for this choice there is no coupling of the atoms to any other molecular modes. If on the other hand the molecular energies are much larger than the coupling it is a better approximation to take the molecular ground state for φ, i.e. to assume that the molecules are in a condensate, and coupling of the atoms to non-condensed modes is neglected.

Inserting the ansatz for the molecular field Eq. (3.110) into the bosonic version of the coupling Hamiltonian Eq. (3.108) we find

$$\hat{V}_{\text{singlem.}} = \hbar\tilde{g}\hat{a}^\dagger\hat{c}^2 + H.C., \tag{3.112}$$

where

$$\tilde{g} = g\int d^3x \varphi^*(\mathbf{x})\psi_0^2(\mathbf{x}) \tag{3.113}$$

is the effective coupling constant.

Fermions

For fermions one is forced to take into account many modes due to the Pauli Exclusion Principle. Under suitable approximations, it is still possible to introduce a single collective degree of freedom. This is explained in detail in chapter 5. Here we keep the many fermionic modes while we make the single mode approximation for the molecular field.

The momentum distribution of the molecular mode $\varphi(\mathbf{x})$ is in most cases much smaller than the typical spread in momenta of the fermions. In particular, in the local density approximation the fermions are described by plane waves, i.e. they are momentum eigenstates, and the molecular wave function can be considered constant. Then the overlap integrals analogous to Eq. (3.113) that give the coupling constants of atoms with momenta $\hbar\mathbf{k}'$ and $\hbar\mathbf{k}$ to molecules become

$$g\int \frac{d^3x}{V}\varphi^*(\mathbf{x})e^{i(\mathbf{k}+\mathbf{k}')\mathbf{x}} = \tilde{g}\delta_{\mathbf{k},-\mathbf{k}'}, \tag{3.114}$$

i.e. only atom pairs that are at rest with respect to the molecular state can be converted into molecules.

The atom molecule coupling Hamiltonian then simplifies to

$$\hat{V} = \hbar\tilde{g}\hat{a}^{\dagger}\sum_{\mathbf{k}}\hat{c}_{-\mathbf{k},\uparrow}\hat{c}_{\mathbf{k},\downarrow} + H.C. \tag{3.115}$$

4. COHERENCE THEORY OF ATOMIC FIELDS

4.1 Experiments

The long range phase coherence of the matter wave field describing ultra cold atoms below the BEC transition temperature is one of the most striking features of BEC. This coherence can be indirectly seen already in the sharply peaked momentum distributions that where used to identify the condensation in the very first experiments [3, 27, 15]: Because the momentum is canonically conjugate to the atom's position, a wavefunction that is narrow in momentum space must be wide in position space. Another early experiment that impressively demonstrates the long range coherence of atomic matter waves is the analog of Young's double slit experiment [4]. In that experiment, Andrews et. al. coherently split a condensate into two components and separated these in space. Subsequently the two components where released from the trap and allowed to overlap. Measurements of the density of the atomic cloud then reveiled interference fringes.

Many more studies of coherence were made in the context of atom lasers [10], the matter wave analog of optical lasers. In ref. [11] Bloch et. al. studied the coherence length of an atom laser by retroreflecting the atomic beam and observing the fringe contrast of the resulting standing wave. In Ref. [69] interference fringes between two atom lasers were observed.

The phase fluctuations of a condensate have been used to study the transition to a 1d quasi condensate and ultimately a Tonks-Girardeau gas in traps with tight radial confinement [45, 40, 36, 54, 42, 101]. It is well known that in a homogeneous one dimensional system condensation is not possible because of quantum fluctuations. In the finite volume systems studied with cold atoms in a trap this manifests itself in a finite phase coherence length along the atomic cloud. Furthermore, bosons in one dimension can behave very similarly to fermions if the interactions between the atoms are sufficiently strong. This "fermionization" in the strongly correlated regime leads to another change of the coherence properties as the gas is tuned from weakly interacting to strongly interacting. In the above experiments the phase fluctuations were studied through their connection to the

momentum distribution of the gas, see chapter 3.

Coherence properties of atoms in an optical lattice were used to study the superfluid to Mott insulator transition of atoms in an optical lattice [52, 53]. In the superfluid phase atoms can move rather unrestrictedly from one well to another by means of tunneling. In this way the atoms can establish phase coherence between different wells and upon release from the optical lattice potential the matter wave fields from different wells interfere with each other. If the on-site interactions between the atoms become very strong, the atoms become localized at the lattice sites and hopping is inhibited. Matter wave fields from different wells have random phases and, upon release from the trap, one sees the incoherent mixture of the fields from each site.

Another focus of research has been the coherent splitting and recombination of matter waves in matter wave interferometers [17]. Matter wave interferometers have been demonstrated with thermal atoms [65]. These interferometers are promising for rotation sensing and accelerometers [75]. They are potentially more sensitive than optical interferometers because the wavelength of the matter waves is smaller so that the acquired phaseshifts due to e.g. rotation are larger. Interferometers using condensates offer several advantages over interferometers with thermal atoms. First, they should yield stronger signals than thermal atoms because the atomic fluxes are so much higher. Second, the translational degrees of freedom can be manipulated easily e.g. using lasers or magnetic fields. Finally, nonlinear effects due to the interactions of the atoms can in principle be used enhance the sensitivity of the interferometer, although they can also be very detrimental if the phase shifts they give rise to are not controlled.

The majority of experimental studies of the coherence of matter wave fields to date have been concerned with first order coherence. These experiments require density measurements, the analog of intensities in optics. The main obstacle for measuring higher order atomic correlation functions is that atomic detectors of the same quality as optical detectors are not available.

Still, several experiments have also considered higher order correlations in atomic fields. In Ref. [18] Burt et. al. have studied three body losses in a BEC and from the loss rates they were able to infer the third order correlation function $g^{(3)}$ at equal time and equal position. For a perfectly coherent condensate this should be close to one and for non degenerate thermal atoms one expects a value of $6 = 3!$, and this ratio was confirmed in the experiment of Burt et. al.

Several experiments in the group of D. Jin have studied noise correlations in the density of expanding atomic clouds [51], see also [2]. These noise correlations contain information about the second order correlations in the gas that were used in the aforementioned experiments to detect superfluidity in fermionic systems.

Fairly recently, a series of experiments in the group of T. Esslinger have studied higher order correlations of atom lasers using single atom detection in a high

finesse optical cavity [14, 93]. In these experiments $g^{(2)}$ for a fixed position and variable delay, as well as the full counting statistics of the atom laser have been measured. Both an atom laser and a thermal matter wave field were considered.

4.2 Theory

For bosonic matter wave fields one might think that a coherence theory very similar to the quantum optical coherence theory of chapter 2 can be developped. One major obstacle is however that the atoms must obey particle conservation, at least for the nonrelativistic energies we are concerned with. In our discussion of Glauber's theory of the photodetector we used in a crucial way that in the photodetector a photon can be annihilated when the detector atom is promoted to a different internal state. For atoms on the other hand only transformations of the state of the atom are allowed and thus a more careful analysis is necessary. Inspired by Glauber's operational approach to coherence, Meystre and his coworkers have analyzed several versions of atom detectors and the signals they deliver [48, 49, 97, 98, 104]. Based upon the form of these detector signals, they have introduced three different notions of coherence which we will review briefly.

In the first detector scheme, the atomic field that is to be analyzed is irradiated by a classical near resonant laser field of frequency ω_L. Through the optical dipole interaction this field can lead to transitions of the atoms from their ground state $|g\rangle$ to an excited state state $|e\rangle$ and to scattering of photons into modes that are initially in vacuum. The scattered light serves as the detector signal. The scattered light is, up to retardation and propagation effects, given by the atomic dipole density,

$$E^{(+)}(\mathbf{r},t) \propto \hat{\Sigma}_+(\mathbf{r},t) \equiv \hat{\psi}_g^\dagger(\mathbf{r},t)\hat{\psi}_e(\mathbf{r},t), \tag{4.1}$$

where $\hat{\psi}_{g,e}$ are the bosonic field operators for atoms in the ground and excited state. Thus the correlation functions of the scattered light are sensitive to correlations of the dipole density with all the $\Sigma_- = (\Sigma_+)^\dagger$ are to the right of all the Σ_+. For instance for the fluorescence spectrum one finds

$$S(\omega) \propto \int d\tau e^{-i(\omega-\omega_L)\tau}\langle\hat{\Sigma}_+(\mathbf{r},\tau)\hat{\Sigma}_-(\mathbf{r},0)\rangle, \tag{4.2}$$

where we have assumed stationarity of the scattered light. Thus an atomic field for which expectation values of the dipole density factorize as

$$\begin{aligned}\langle\hat{\Sigma}_+(\mathbf{r_1},t_1)\cdots\hat{\Sigma}_+(\mathbf{r_n},t_n)\hat{\Sigma}_-(\mathbf{r_{n+1}},t_{n+1})\cdots\hat{\Sigma}_+(\mathbf{r_{2n}},t_{2n})\rangle = \\ \langle\hat{\Sigma}_+(\mathbf{r_1},t_1)\rangle\cdots\langle\hat{\Sigma}_+(\mathbf{r_n},t_n)\rangle\langle\hat{\Sigma}_-(\mathbf{r_{n+1}},t_{n+1})\rangle\cdots\langle\hat{\Sigma}_+(\mathbf{r_{2n}},t_{2n})\rangle\end{aligned} \tag{4.3}$$

will appear coherent to this kind of atom detector similar to the factorization condition introduced by Glauber for the *n*-th order coherent optical field. This type of coherence is called *electronic coherence* [104].

A second detector scheme [48, 49, 98, 97] is obtained by assuming that the laser light is far detuned from the atomic transition frequency so that the excited state can be adiabatically eliminated. Then the scattered light, which plays again the role of the detector signal, is proportional to the atomic ground state density, $\hat{n}(\mathbf{r},t) = \hat{\psi}_g^\dagger(\mathbf{r},t)\hat{\psi}_g(\mathbf{r},t)$. Thus, correlation functions of the scattered light will now be proportional to expectation values of products of atomic densities and accordingly factorization properties of the type

$$\langle \hat{n}(\mathbf{r_1},t_1)\cdots n(\mathbf{r_n},t_n)\rangle = \langle \hat{n}(\mathbf{r_1},t_1)\rangle \cdots \langle n(\mathbf{r_n},t_n)\rangle \tag{4.4}$$

lead to the notion of *density coherence* [48, 49]. The density correlations of a trapped Bose gas have been studied in detail by Naraschweski and Glauber [91].

These two measurement schemes are only able to characterize bilinear products of atomic operators. The cause for this lies in the light field only coupling to bilinear combinations of matter due to the particle number conservation mentioned above. These limitations can be overcome if another atomic field is used as a detector signal, as is done e.g. in photoionization experiments. If we assume that a classical laser field is driving transitions of atoms in the internal state 0 that is to be analyzed to some final state j with strength V_{j0}, the interaction can be written as

$$\hat{V}_{p.i.} = \sum_j \int d^3x V_{j0}(\mathbf{x})\hat{\psi}_j^\dagger(\mathbf{x})\hat{\psi}(\mathbf{x}) + H.C. \tag{4.5}$$

From this expression we see that, in contrast to the previous two cases, the final "detector states" j couple to the field operator directly, and not to bilinear combination of them. Thus, detecting the final states yields correlation functions of the atomic field operator and the resulting notion of *field coherence* is the one that is closed to coherence in the quantum optical.

The considerations that will lead us to use molecules to study higher order correlations of atomic fields in chapter 7 are generalizations of this idea of analyzing atomic fields by converting them to some other internal state. As we will discuss in more detail in that chapter, atom *pairs* are nonlinearly converted into a new molecular state and these molecules will then serve as the signal.

The way these notions of coherence have been developed is rather general and can be applied to atomic fields obeying either Bose or Fermi statistics. For Fermions however, the concept of coherence is fairly problematic and to a certain degree still an open question. The difficulties with fermions mostly stem from the Pauli exclusion principle and the closely property that the wavefunctions for multiple fermions have to be antisymmetric under particle exchange. The Pauli

exclusion principle restricts the occuption number of every atomic mode to at most one so that any coherence theory for fermions that considers correlations beyond the first order must necessarily be a multimode coherence theory.

Fermionic analogs of coherent states have been studied by K. E. Cahill and R. J. Glauber [22] using Grassmann variables. These results have however not found widespread application mainly because, in contrast to the bosonic case, the coherent states that one finds don't lend themselves to an easy physical interpretation.

5. CORRESPONDENCES BETWEEN ULTRA-COLD ATOMS AND QUANTUM OPTICAL SYSTEMS

Throughout this dissertation we make use of the numerous analogies between ultra-cold atoms and quantum optical systems. Formally, these analogies are expressed through mathematical mappings between operators of one system onto operators of its analog. There are many benefits in this precise mathematical formulation of the correspondences: They allow one to transfer methods from quantum optics to ultra-cold atoms and the differences and equivalences between the two become apparent. Furthermore, our intuitive understanding shaped in well studied problems of quantum optics can be used as a valuable guide when we study new aspects of the atoms. The new problems that may arise in the cold atoms' context that have no analog also shed new light on old problems in quantum optics.

In this chapter we systematically discuss the various mappings between atomic and molecular and quantum optical systems.

5.1 Non-degenerate atoms

It is well known that matter also possesses wave character [29]. The wavelength λ_{dB} of these matter waves is inversely proportional to the velocity of the atoms. Through the mean velocity of atoms at a certain temperature we can establish a relation between the wavelength of the atoms and the temperature,

$$\lambda_{\mathrm{dB}} = \sqrt{\frac{2\pi\hbar^2}{m k_{\mathrm{B}} T}}. \tag{5.1}$$

From this relation we see that the wave nature becomes more important at low temperatures. In the high temperature limit the wavelength of the atoms becomes very small and they can be described as particles. This corresponds to the limit of ray optics.

The atoms are non-degenerate, if the phase space density is much smaller than one, or in other words the probability for a certain quantum state to be occupied is much smaller than one. Roughly speaking, the wave-packets that represent each atom do not overlap, i.e. the thermal de Broglie wavelength is larger than the interatomic separation $n_0^{-1/3}$ with n_0 the atomic density.

An ensemble of atoms with different kinetic energies corresponds to the light field generated by an inhomogeneously broadened light source. Each atom by itself also has a spread in kinetic energies and this corresponds to homogeneous broadening.

In the non-degenerate case, each atom's center of mass motion is described by a single particle Schrödinger equation and therefore their dispersion relation is quadratic. Thus the wavepacket of an atom will spread over time, even in vacuum. This is different from photons in vacuum that are described by Maxwell's equations and have a linear dispersion relation. Because of the linear dispersion relation photons propagate in vacuum without spreading[1].

By making the slowly varying envelop approximation the wave equation for light takes on a form that is very similar to the Schrödinger equation. A medium can give rise to dispersion and the quadratic dispersion term is formally the same as the kinetic energy term in the Schrödinger equation, with the dispersion coefficient being inversely proportional to the mass of the atoms. The potential energy terms in the Schrödinger equation correspond to a refractive index. Note however that it is not uncommon for the potential energy to take on very large positive or negative values compared to the kinetic energy. Refractive index contrasts on the other hand are usually small and in particular large negative refractive indices are very difficult to obtain, at least in the optical frequency range.

Another difference between the two is that atoms typically have a large number of distinct internal states. The two polarization states of a photon can be viewed as different internal states, but atoms with more than two internal states have no direct analog.

5.2 BEC

The many-body wave function of bosons has to be symmetric under particle exchange. This symmetry becomes relevant when the atoms enter the degenerate regime, i.e. when the phase space density becomes larger than one or when their de Broglie waves start to overlap $\lambda_{\mathrm{dB}} \sim n_0^{-1/3}$. A BEC is the extreme situation where many atoms are in the exact same state. This is analogous to a laser in

[1] This is of course only true, if the photons have a very large extend in the transverse direction and no phase curvature, so that diffraction effects can be neglected. In this case the photons can be approximated as plane waves.

which many photons occupy the same mode of the electromagnetic field. Photons are of course bosons themselves.

A pure BEC corresponds to a purely homogeneously broadened laser. At the mean field level one can derive the Gross-Pitaevski equation for the condensate wave function, see section 3.1. The Gross-Pitaevski equation is formally equivalent to the non-linear Schrödinger equation commonly used to describe the propagation of a light pulse in a non-linear medium. As mentioned above, the kinetic energy of the atoms corresponds to dispersion. The *s*-wave colissions between atoms correspond to a $\chi^{(3)}$-nonlinearity. For atoms, the nonlinearities can be much larger than in the optical case. Furthermore they can be controlled over a wide range using Feshbach resonances.

Especially the analogy between BECs in the mean-field approximation and non-linear optics has lead to a rapid understanding of the dynamics of BECs and has suggested many experiments such as four-wave-mixing, parametric amplification and experiments with solitons.

5.3 Ultra-cold fermions

Every quantum mechanical state can be approximated by at most one fermion due to the Pauli-exclusion principle. While this prevents us from constructing a mean field theory as in the previous section it opens up the possibility for a different analogy. Every mode has exactly two states. It can be occupied or unoccupied. This suggests that one should be able to map these modes onto an ensemble of two level atoms. This is however not directly possible because the many-body wave function of the fermions must change sign under particle exchange.

The mapping onto an ensemble of two level atoms still works, if the modes can be arranged in distinct pairs on which the fermionic field operators always act at the same time. Then the two sign changes the wave-function undergoes under particle exchange cancel each other.

An example is provided by momentum states of fermions with two internal states coupled to each other without change of momentum, described by the coupling Hamiltonian

$$\hat{V} = \sum_{\mathbf{k}} \hbar\Omega_{\mathbf{k}} \hat{c}^{\dagger}_{\mathbf{k}\uparrow} \hat{c}_{\mathbf{k}\downarrow} + H.C. \tag{5.2}$$

The system is mapped onto spins or, which is equivalent, onto two-level atoms by means of the transformation

$$\hat{\sigma}^{x}_{\mathbf{k}} = \hat{\sigma}^{+}_{\mathbf{k}} + \hat{\sigma}^{-}_{\mathbf{k}}, \quad \hat{\sigma}^{y}_{\mathbf{k}} = \frac{1}{i}(\hat{\sigma}^{+}_{\mathbf{k}} - \hat{\sigma}^{-}_{\mathbf{k}}), \quad \hat{\sigma}^{z}_{\mathbf{k}} = \hat{c}^{\dagger}_{\mathbf{k}\uparrow}\hat{c}_{\mathbf{k}\uparrow} - \hat{c}^{\dagger}_{\mathbf{k}\downarrow}\hat{c}_{\mathbf{k}\downarrow}, \tag{5.3}$$

where

$$\hat{\sigma}^{+}_{\mathbf{k}} = (\hat{\sigma}^{-}_{\mathbf{k}})^{\dagger} = \hat{c}^{\dagger}_{\mathbf{k}\uparrow}\hat{c}_{\mathbf{k}\downarrow}. \tag{5.4}$$

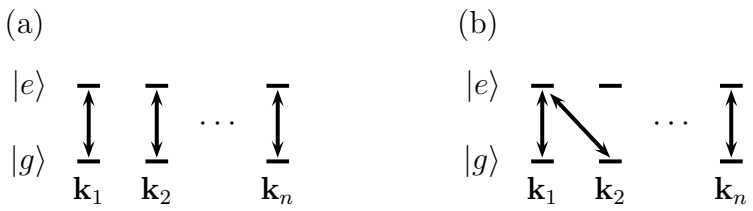

Fig. 5.1: Schematic of the fermions with two distinct internal states $|e\rangle$ and $|g\rangle$ and different momentum states. In situation (a) the atoms in each mode couple exclusively to each other and hence they can be mapped onto two level atoms by means of Eq. (5.3). In (b) however the atom in the excited state in mode $\mathbf{k_1}$ couples to $\mathbf{k_1}$ and $\mathbf{k_2}$ and hence a mapping to independent two level atoms is impossible.

It is easy to check that these operators realize a SU(2) algebra,

$$[\hat{\sigma}^l_{\mathbf{k}}, \hat{\sigma}^m_{\mathbf{k}'}] = 2i\epsilon_{lmn}\delta_{\mathbf{k},\mathbf{k}'}\sigma^n_{\mathbf{k}}, \qquad l,m,n \in \{x,y,z\} \tag{5.5}$$

with ϵ_{lmn} the Levi-Chevita-Symbol.

This example may seem almost trivial but it shows, that fermionic two level atoms behave like conventional two level atoms even when cooled to degeneracy. Furthermore it is worth noting that this mapping breaks down if a fermion in one state can couple to several other modes, e.g. by means of $(\hat{c}^\dagger_{\mathbf{k}\uparrow} + \hat{c}^\dagger_{\mathbf{k}'\uparrow})\hat{c}_{\mathbf{k}\downarrow} + H.C.$ In that case the spin operators for different modes do no longer commute. This is illustrated in Fig. 5.1.

Another situation in which fermions can be replaced by two-level atoms arises when atoms are created and annihilated in distinct pairs. As an example we consider the case where pairs of atoms with opposite momentum and spin are created and annihilated. This is the case for the BCS-reduced Hamiltonian (3.59) where it is pairs of atoms with zero center of mass momentum that scatter and for the coherent molecule formation if the center of mass momentum of the molecules is neglected, see Eq. (5.10). The two states of the fictious two-level atom representing a pair of modes are then the state with both modes occupied and the state with both modes empty,

$$|e_{\mathbf{k}}\rangle = \hat{c}^\dagger_{\mathbf{k}\uparrow}\hat{c}^\dagger_{-\mathbf{k}\downarrow}|0\rangle, \tag{5.6}$$

$$|g_{\mathbf{k}}\rangle = |0\rangle, \tag{5.7}$$

where $|0\rangle$ is the vacuum state of the two modes. The mapping to two-level atoms is accomplished by the transformation

$$\hat{\sigma}^z_{\mathbf{k}} = \hat{c}^\dagger_{\mathbf{k}\uparrow}\hat{c}_{\mathbf{k}\uparrow} + \hat{c}^\dagger_{-\mathbf{k}\downarrow}\hat{c}_{-\mathbf{k}\downarrow} - 1, \tag{5.8}$$

$$\hat{\sigma}^+_{\mathbf{k}} = (\hat{\sigma}^-_{\mathbf{k}})^\dagger = \hat{c}^\dagger_{\mathbf{k}\uparrow}\hat{c}^\dagger_{-\mathbf{k}\downarrow}. \tag{5.9}$$

Again it is crucial that an atom cannot be created or annihilated together with an atom from several other modes. Furthermore, states in which a pair is only partly occupied, e.g. $|\mathbf{k}\uparrow\rangle$ occupied and $|\mathbf{k}\downarrow\rangle$ unoccupied, cannot be described.

5.4 Molecules

The formation of ultra-cold molecules can be mapped on different quantum optical systems depending on the atoms' statistics.

5.4.1 Molecules out of bosons

The molecule formation out of bosonic atoms is described by the coupling hamiltonian Eq. (3.112) and is analogous to optical three-wave mixing: Up-conversion corresponds to molecule association and down-conversion corresponds to molecule dissociation. The analogy is illustrated in Fig. 5.2(a).

Energy conservation in the molecule formation process corresponds to phase matching. For molecules it can be achieved in a variety of ways. If the open and closed channel are different hyperfine states and the detuning between them is controlled with an external magnetic field, the most common method is to apply a sweep of the magnetic field. Efficient molecule formation has also been demonstrated by modulating the external field at a frequency corresponding to the binding energy [108]. This is similar to quasi phase matching in e.g. periodically poled lithium niobate in optical sum frequency generation. If the open and closed channel are different electronic states and the coupling between them is furnished by two lasers in Raman configuration, energy conservation is easily met by choosing the detuning between the two lasers appropriately.

5.4.2 Molecules out of fermions

In this case we can use the mapping of the previous section of pairs of fermionic modes to two-level atoms. In the process of molecule formation the pairs of modes decay from the excited states $|e_{\mathbf{k}}\rangle$ of the effective two-level atom to the ground states $|g_{\mathbf{k}}\rangle$, as illustrated in Fig. 5.2(b).

This analogy only works if the molecular wavefunction changes little over the extend of the wavefunctions of the atoms out of which the molecule is being formed. Then the molecules can be considered to have a well defined momentum and all the atom pairs become distinct. If however molecules with different momenta can be formed or if each molecule by itself has a large momentum spread an atom can belong to different pairs of modes and the analogy breaks down.

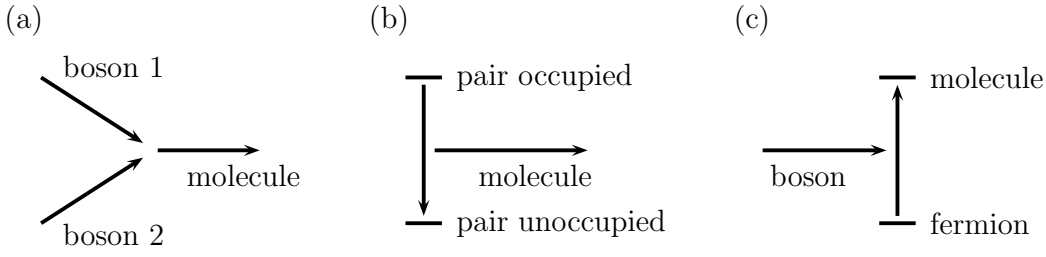

Fig. 5.2: Illustration of the analogies for the coherent molecule formation from atoms with various statistics. In (a) two bosons are combined into a molecule similar to optical sum frequency generation. In (b) an effective two-level atom decays from the excited state, representing a pair of fermionic atomic modes being occupied, to the ground state, representing the atomic modes being empty, under "emission" of a molecule. In (c) an incoming bosonic atom is "absorbed" by a fermionic atom to form a different fermionic state, the molecule.

In case the molecules have a well defined momentum in this sense the molecule formation is conventionally described by the coupling Eq. (3.115). Including the kinetic energies $E_{\mathbf{k}} = \hbar^2 k^2/(2M)$ of the atoms and the detuning of the molecular state ν and applying the mapping Eq. (5.8) and (5.9) to the fermionic field operators the Hamiltonian describing the system takes the form [60, 7]

$$\hat{H} = \sum_k E_k \hat{\sigma}^z_{\mathbf{k}} + \hbar\nu\hat{a}^\dagger\hat{a} + \hbar g\left(\hat{a}^\dagger \sum_k \hat{\sigma}^-_{\mathbf{k}} + H.C.\right). \tag{5.10}$$

This Hamiltonian is formally equivalent to the well studied Tavis-Cummings model of quantum optics, which describes the coupling of an ensemble of two-level atoms to a single quantized mode of the electromagnetic field [107]. The kinetic energies correspond to inhomogeneous broadening of the atomic transition.

In the homogeneously broadened or degenerate limit all the kinetic energies are assumed to be identical,

$$E_{\mathbf{k}} \equiv E,$$

and can be absorbed in the detuning ν. The conditions under which this degenerate approximation is valid has been studied in more detail in the context of ultra-cold atoms and molecules in [90]. In the degenerate approximation the system can be described in terms of collectiv spin operators

$$\Sigma^z = \frac{1}{2}\sum_{\mathbf{k}} \sigma^z_{\mathbf{k}}, \qquad \Sigma^+ = (\Sigma^-)^\dagger = \sum_{\mathbf{k}} \sigma^+_{\mathbf{k}}. \tag{5.11}$$

The system can then be described in the eigenbasis $|S, m\rangle$ of the operators Σ^z and $\Sigma^2 = \Sigma^{x^2} + \Sigma^{y^2} + \Sigma^{z^2}$ with $\Sigma^x = \frac{1}{2}(\Sigma^+ + \Sigma^-)$ and $\Sigma^y = \frac{1}{2i}(\Sigma^+ - \Sigma^-)$. In the context of light-matter interaction these states are sometimes referred to as Dicke states and the system can exhibit Dicke-superradiance.

From a computational point of view the mapping to the collective degree of freedom $\mathbf{\Sigma}$ has profound consequences: If the system starts in a subspace with a specific S it will remain in that subspace for all times and hence can be described in a $(2S + 1)$-dimensional Hilbertspace. For instance the state with initially N atom pairs and no molecules corresponds to the state $|N, N\rangle$ and the dimension of the Hilbert space is $N + 1$. It scales linearly with the number of atoms which is a tremendous improvement over the exponential scaling with the number of atoms in the general non-degenerate case.

Another analogy that can be drawn in the homogeneously broadened limit is based on the Schwinger mapping from an angular momentum in the subspace $\{|S, m\rangle, \ m = -S, \ldots, S\}$ to two bosonic modes with field operators $\hat{d}_1$ and $\hat{d}_2$,

$$\Sigma^z \to \frac{1}{2}(\hat{d}_1^\dagger \hat{d}_1 - \hat{d}_2^\dagger \hat{d}_2), \quad \Sigma^+ \to \hat{d}_1^\dagger \hat{d}_2, \quad \Sigma^- \to \hat{d}_2^\dagger \hat{d}_1, \tag{5.12}$$

confined to the subspace $\{|\psi\rangle, \ \frac{1}{2}(\hat{d}_1^\dagger \hat{d}_1 + \hat{d}_2^\dagger \hat{d}_2)|\psi\rangle = S|\psi\rangle\}$. This mapping shows that, from a mathematical point of view, the molecule production from fermionic pairs corresponds to optical down-conversion. The operators $\hat{d}_1$ and $\hat{d}_2$ have however no obvious physical interpretation.

In general, the kinetic energies cannot be neglected and they destroy the collective behavior of the system much like dephasing does for two-level atoms interacting with a cavity mode.

5.4.3 Molecules out of a fermion and a boson

Molecules formed from a fermion and a boson are fermions. Therefore the molecule formation can be viewed as the conversion of one fermionic state, the atom, into a different fermionic state, the molecule, under absorption of a bosonic atom. This process is illustrated in Fig. 5.2(c). The same caveat as in the molecule formation from fermions applies: This analogy only works, if all the bosons have the same sharp momentum.

6. RECONSTRUCTION OF THE PHASE OF MATTER WAVES USING MOMENTUM RESOLVED CROSS CORRELATIONS

As we have seen in chapter 3 atomic BECs can often be well characterized by their condensate wavefunction. The amplitude of this complex wave function corresponds to the atomic density and can rather easily be measured using for example absorption or phase contrast imaging [113, 112, 96, 66].

The phase of the wave function, on the other hand, is relatively hard to measure directly. Still, knowledge of the phase is in many cases very essential for the characterization of quantum-degenerate atomic systems, such as rotating BECs with vortices [86] on which we will focus here. Good methods for phase measurements should also be very valuable in studies of systems where the phase coherence is destroyed due to quantum fluctuations such as for ultracold atoms in a highly elongated trap, where the atoms can enter the Tonks-Girardeau regime [45, 77, 76, 40, 42].

Most schemes that have been used for measurements of the phase of the condensate wavefunction so far rely on the relation between phase gradients and the velocity distribution established in chapter 3. The velocity distribtion of the atoms can in principle be measured spectroscopically. The idea is to resolve the Doppler shift that the atomic transition lines suffer as the atoms move relative to the probing laser beams. Using e.g. Raman spectroscopy several researchers have succeeded in measuring the velocity distribution of atoms, see [101, 36, 54, 103] and references therein.

Even though these spectroscopic measurements can give some information about the phase gradients in a BEC, this information is still very incomplete. They yield the probability to find a certain phase gradient and this is obviously still very far from knowing what the phase is at any given point in space. Furhtermore these experiments are very cumbersome because the measurements are destructive: For every momentum for which one wishes to determine the probability a new condensate has to be made. On top of being very time consuming this method also introduces new uncertainties in the results because each data point is obtained from a different atomic sample and BECs typically have large shot to shot vari-

ations. Finally, the momentum distribution can only be obtained in the direction along the probing laser beams and for a reconstruction of the full three dimensional velocity distribution several laser beams are necessary. Other schemes for measuring the phase of an atomic field have been implemented, e.g. [86] but these very heavily rely on the specific conditions of the experiment at hand and cannot be applied in general.

A situation that is in many ways similar is encountered in the context of ultrashort laser pulses of a few optical cycles duration. The characterization of these pulses, which are of considerable interest in both fundamental science and applications, requires likewise the knowledge of both amplitude and phase. Already for the simplest pulses a characterization merely in terms of the envelop $|\psi(z,t)|$ can be insufficient, e.g. if very precise control of the peak intensity is required: Without knowledge of the phase we cannot tell whether the field has a node or antinode at the peak of the envelop. For a Fourier limited Gaussian pulse of a few optical cycles duration this can lead to a difference in the peak intensity of about one percent. Furthermore, in recent years researchers in the field of coherent control have managed to taylor pulses that drive chemical reactions in selected reaction channels with high efficiency. These pulses have typically a very complicated temporal structure and require exquisite control of the phase. Without a reliable and accurate method for the phase measurement these experiments would hardly be possible.

The problem of the measurement of the time-dependent phase of ultrashort laser pulses has found a solution that is in many respects optimal in the so-called Frequency-Resolved Optical Gating (FROG) methods [23, 62, 31, 111]. These methods, which can be adapted to many different situations, offer very high resolution and precision, are stable against noise, and can even compensate for or detect some sources of systematic errors. Single-shot measurements are possible [63], and measurements of fields with less than one photon per pulse on average have also been successfully demonstrated. Almost every aspect of the FROG methods has been studied in depth. The high level of maturity of the FROG methods that has been reached in ultra short laser physics, sometimes to the point where these methods are employed in industrial products, provides us with substantial motivation to try to adapt these methods for the phase measurement problem for matter waves. Good starting points for accessing the wealth of research literature on that subject are the review article [102] and Ref. [110].

In essence, FROG methods consist of two parts. In the first part a so-called spectrogram of the unknown laser pulse is recorded, see Fig. 6.1. The spectrogram is the spectrum of parts of the pulse that have been "cut out" with a gate function for various delays. Because the laser pulses of interest are typically of sub pico second duration the only means to gate the pulse accurately and reliably is with another ultrashort laser pulse using nonlinear mixing between the two pulses. On

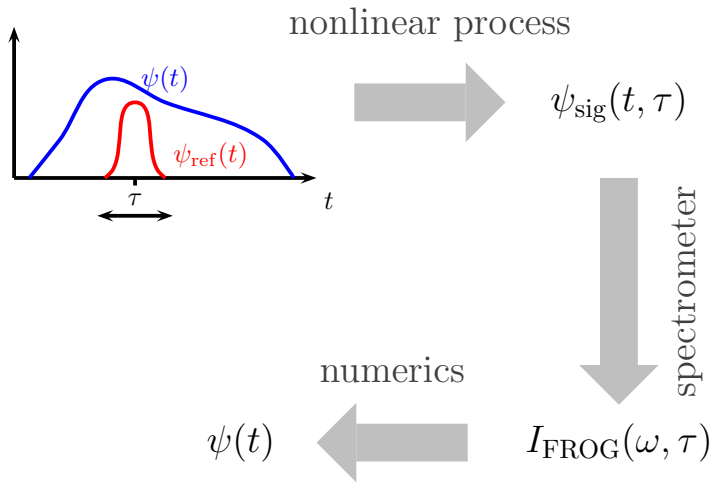

Fig. 6.1: Elements of pulse retrieval with FROG. A part of the pulse $\psi(t)$ that is to be analyzed is cut out with the reference pulse $\psi_{ref}(t)$ by means of nonlinear mixing for various delays τ to give the signal field $\psi_{sig}(t,\tau)$. The spectrum $I_{\rm FROG}(\omega,\tau)$ of $\psi_{sig}(t,\tau)$ is then used to numerically reconstruct the original field $\psi(t)$.

the experimental side, the robustness of FROG methods derives to a large degree from the measurement of the spectrogram being noninterferomentric. In the second part the pulse is numerically reconstructed. Various algorithms are employed for this step. The numerical part of the pulse reconstruction is also mostly very robust, as we will discuss in some more detail below. Many of the methods used have been studied very thoroughly, first in the context of image reconstruction for astronomical and military purposes and in recent years also very intenisively specifically for pulse reconstruction with FROG.

In this chapter we show how XFROG [79], a specific version of the general FROG scheme, can be adapted for the phase measurement problem for matter waves.

In the next section we first review the basics of the XFROG method. We go on by developing a concrete physical model that allows one to use the same method for the phase reconstruction problem for matter waves. As an example we study the resconstruction of a vortex state. We analyze the feasibility of the method by studying their sensitivity to noise and to a reduction in the number of measurements, both questions of considerable importance for practical applications.

6.1 Review of XFROG for ultrashort laser pulses

The basic experimental setup for the field reconstruction of an ultrashort laser pulse by means of the XFROG method is shown in Fig. 6.2. For simplicity we assume that only one direction of polarization of the electrical field needs to be considered. The unknown field $\psi(t)$ is mixed with a known reference field $\psi_{\mathrm{ref}}(t)$ in a nonlinear crystal with $\chi^{(2)}$ nonlinearity after a variable delay τ. The fields ψ_{ref} and ψ should be of roughly comparable duration, which means in practice that the pulse durations can differ by up to about an order of magnitude. The sum frequency signal is

$$\psi_{\mathrm{sig}}(t,\tau) \propto \psi(t)\psi_{\mathrm{ref}}(t-\tau). \tag{6.1}$$

The form of the signal field nicely illustrates how the reference pulse acts as a variably delayed gate. The signal ψ_{sig} is then spectrally analyzed. The resulting spectrum,

$$\begin{aligned} I_{\mathrm{XFROG}}(\omega,\tau) &\equiv \left| \int dt e^{-i\omega t} \psi_{\mathrm{sig}}(t,\tau) \right|^2 \\ &= \left| \int dt e^{-i\omega t} \psi(t)\psi_{\mathrm{ref}}(t-\tau) \right|^2 , \end{aligned} \tag{6.2}$$

is the key quantity for the XFROG method. It contains enough information to reconstruct amplitude and phase of the pulse $\psi(t)$.

Thus the rest of the problem consists in numerically finding $\psi(t)$ from I_{XFROG}. One of the most successful methods for this inversion is the method of generalized projections [41, 114, 34, 35]. The main benefits of this method are its versatility, robustness and accuracy. A drawback of the method may be its slow speed, especially in applications where very fast field recovery is necessary, such as in feedback applications. The slow speed is due to the iterative nature of the algorithm. For most applications however the recovery speed is tolerable, especially considering the computing power of todays personal computers. Therefore we will exclusively discuss this method for the field recovery.

To see how the field recovery with the generalized projections algorithm works in detail, we first note that it is sufficient to find $\psi_{\mathrm{sig}}(t,\tau)$ since $\psi(t)$ can then be obtained, up to a multiplicative constant that can be determined from the normalization of ψ, by simply integrating over τ [1]. This way the problem is cast in the form of a two-dimensional phase retrieval problem: We seek to find the complex valued function ψ_{sig} from the modulus of its Fourier transform. Problems of this

[1] Alternatively one could obtain ψ by dividing by $\psi_{\mathrm{ref}}(t-\tau)$. In practice this is mostly avoided since it requires a very precise knowledge of ψ_{ref}: Inaccuracies in ψ_{ref} contaminate the recovered fi eld. Furthermore ψ_{ref} typically falls off to zero in a time comparable to the pulse duration so that a division becomes problematic.

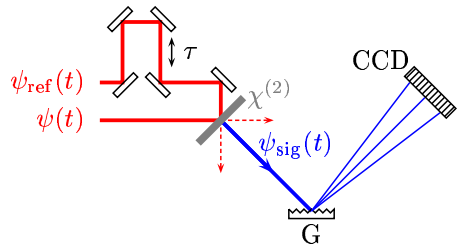

Fig. 6.2: Basic experimental setup for the XFROG method. The unknown field $\psi(t)$ is mixed in a nonlinear crystal with a known reference pulse $\psi_{ref}(t)$ after a variable delay. The sum frequency signal $\psi_{sig}(T)$ is spectrally analyzed with the diffraction grating G and the spectrum of the signal field is recorded with the CCD array.

type have been studied for decades in the context of image restoration, see e.g. [41, 114] and references therein.

From Eqs. (6.1) and (6.2) it is clear that ψ_{sig} must simultaneously belong to the two sets [2]

$$O = \{f(t,\tau) | f(t,\tau) = g(t)\psi_{\mathrm{ref}}(t-\tau) \text{ for some } g\} \tag{6.3}$$

and

$$F = \left\{ f(t,\tau) \left| \left| \int dt e^{-i\omega t} f(t,\tau) \right|^2 = I_{\mathrm{XFROG}}(\omega,\tau) \right. \right\}, \tag{6.4}$$

i.e.

$$\psi_{\mathrm{sig}}(t,\tau) \in O \cap F. \tag{6.5}$$

Figure 6.3a suggests that one can find the solution to this problem, called a feasibility problem in mathematics and especially in optimization theory, by iteratively projecting onto the two constraint sets O and F. This is the core of the method of generalized projections. For closed convex sets with exactly one point of intersection, this method always leads to a unique solution. In our case, though, the constraint set F is not convex [3] and the intersection of O and F consists

[2] Since we do not strive for the most mathematical generality possible all the fi elds considered in this chapter are taken from $C_0^\infty(\mathbb{R}^n, \mathbb{C})$, the set of smooth (complex valued) functions with compact support in $\mathbb{R}^n$ with n equal to one or two as appropriate.

[3] To see this take two functions f_1 and f_2 and $\alpha \in [0,1]$. Then

$$\left| \int dt e^{-i\omega t} (\alpha f_1(t,\tau) + (1-\alpha) f_2(t,\tau)) \right|^2 = (1-2\alpha) I_{\mathrm{XFROG}}(\omega,\tau) + 2\alpha(1-\alpha) Re\left[\tilde{f}_1^*(\omega,\tau) \tilde{f}_2(\omega,\tau) \right],$$

where the tilde denotes Fourier transformation with respect to t. This is in general clearly not equal

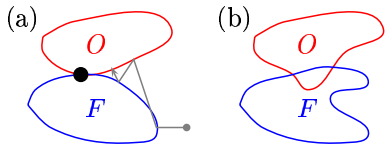

Fig. 6.3: Illustration of the constraint sets O and F (a) in the case where O and F are convex and their intersection contains exactly one element and (b) in the non-convex case with more than one element in the intersection. Fig. (a) also shows a typical trajectory of the generalized projections algorithm.

of more than one function [4]. This is illustrated in Fig. 6.3b. Hence, the algorithm of generalized projections is not guaranteed to converge for every initial guess and even if it does the solution is not unique. Still, in practice it converges for a vast majority of initial guesses and the ambiguity in the solution is physically reasonable. In particular, XFROG determines the field ψ_{sig} up to an overall phase. On those rare occasions when the algorithm does not converge for a particular initial guess, this non-convergence is revealed by a large distance of the fixed point from the constraint sets, in a sense that will be made precise below. Thus one knows for sure if the algorithm has succeeded in reconstructing the field or not. In case the reconstruction has failed one can simply restart the reconstruction algorithm with a different initial guess.

Specifically, ψ_{sig} is found from I_{XFROG} as follows:

1. Initialize $\tilde{\psi}^{(0)}_{\mathrm{sig}}(\omega,\tau)$ with random numbers for its real and imaginary part.

2. The projection onto the constraint set F is accomplished by setting

$$\psi^{(n)}_{\mathrm{sig}}(\omega,\tau) = \frac{\tilde{\psi}^{(n-1)}_{\mathrm{sig}}(\omega,\tau)}{|\tilde{\psi}^{(n-1)}_{\mathrm{sig}}(\omega,\tau)|} I^{1/2}_{\mathrm{FROG}}(\omega,\tau). \tag{6.6}$$

   The signal field now has the correct magnitude, which clearly guarantees that $\psi^{(n)}_{\mathrm{sig}}$ satisfies condition (6.4), but the phases may still be wrong.

3. Inverse Fourier transform $\psi^{(n)}_{\mathrm{sig}}(\omega,\tau)$ with respect to its first argument to find

$$\psi^{(n)}_{\mathrm{sig}}(t,\tau) = \int \frac{d\omega}{2\pi} e^{i\omega t} \psi^{(n)}_{\mathrm{sig}}(\omega,\tau). \tag{6.7}$$

to I_{XFROG} and hence F is not convex.

[4] The uniqueness is spoiled by the invariance of F under multiplication with an overall phase.

4. Determine $\psi^{(n)}(t)$ such that

$$Z = \int dtd\tau \left|\psi^{(n)}_{\text{sig}}(t,\tau) - \psi^{(n)}(t)\psi_{\text{ref}}(t-\tau)\right|^2 \tag{6.8}$$

becomes a minimum. With $\psi^{(n)}(t)$ determined this way form

$$\tilde{\psi}^{(n)}_{\text{sig}}(t,\tau) = \psi^{(n)}(t)\psi_{\text{ref}}(t-\tau), \tag{6.9}$$

which can be no further from the set O than $\psi^{(n)}_{\text{sig}}(t,\tau)$.

5. Use the Fourier transform

$$\tilde{\psi}^{(n)}_{\text{sig}}(\omega,\tau) = \int dt e^{-i\omega t}\tilde{\psi}^{(n)}_{\text{sig}}(t,\tau) \tag{6.10}$$

as a new input in step 2, and iterate until the error Z in Eq. (6.8) becomes sufficiently small.

Upon exit from the algorithm, $\psi^{(n)}$ is the retrieved field. The minimization of Z in step 4 is well behaved because the error functional is quadratic in the unknown field $\psi^{(n)}(t)$. We have found that in practice it is sufficient to perform a single one dimensional line minimization along the direction of the gradient $\delta Z/\delta\psi^{(n)}$[5].

An important characteristic of the XFROG method is its robustness, which mainy results from two reasons. First, the XFROG signal contains a high degree of redundancy: If I_{XFROG} is measured on a grid of size $N \times N$ the $2N$ unknowns of the field $\psi(t)$ – its real and imaginary parts – are retrieved from N^2 measured values. The XFROG algorithm makes use of this high degree of redundancy to yield a highly stable pulse retrieval. Second, the functional form of ψ_{sig} is very restrictive in the sense that a randomly generated ψ_{sig} will not normally correspond to any physical pulse ψ. Thus, if the XFROG signal has been grossly deteriorated by systematic errors the XFROG algorithm will not converge for any initial guess and one can conclude that the data is corrupted. Furthermore the redundancies contained in the XFROG trace allow for powerful consistency checks using the marginals of the trace and can thus help detecting systematic errors [33], and even correct corrupted XFROG traces. Thus the XFROG method does not only tell one if something is wrong with the data, it also gives valuable information as to where to look for errors and can correct errors ”after the act”. More details on the role of systematic errors and their corrections using FROG techniques can be found in references [106, 32, 33].

Another advantage of XFROG is the extremely high temporal resolution that is achieved by making use of the Fourier domain information. Instead of being determined by the length of the reference pulse, this resolution is essentially given by the response time of the non-linear medium.

[5] Naturally, the actual calculations are carried out on a grid and the functional derivative becomes a usual gradient with respect to the real and imaginary part of $\psi^{(n)}$ at every grid point.

6.2 Application of XFROG to ultra cold atoms

We now turn to the central point of this chapter, which is to adapt the XFROG method to the characterization of matter-wave fields. To this end we consider the case of atomic bosons with two internal states denoted by $\uparrow$ and $\downarrow$. The atoms are assumed to be initially in a pure Bose-Einstein condensate (BEC) at temperature $T = 0$, with all atoms in internal state $\downarrow$. Neglecting fluctuations, the atomic field operator can be written

$$\hat{\psi}(\mathbf{r}) = \hat{c}_{\downarrow}\psi_0(\mathbf{r}), \tag{6.11}$$

where $\psi_0(\mathbf{r})$ is the condensate wave function and $\hat{c}_{\downarrow}$ is the bosonic annihilation operator for an atom in the condensate.

The states $\uparrow$ and $\downarrow$ are coupled to each other by a spatially dependent interaction of the generic form

$$\hat{V}_J = \int d^3r V(\mathbf{r}-\mathbf{R})\hat{\psi}^{\dagger}_{\uparrow}(\mathbf{r})\hat{\psi}_{\downarrow}(\mathbf{r}) + H.C. \tag{6.12}$$

that is switched on at time $t = 0$. Potentials of this type have been used e.g. for coherent outcoupling of matter waves for atom lasers [10]. Various physical realizations are possible. One way is to use microwave induced hyperfine transitions. The coupling describing these transitions becomes spatially dependent because in a magneto optical trap the Zeeman splitting between the levels is position dependent. Another possibility is to use a two-photon Raman transition, with V then being proportional to the product of the mode functions of the two lasers driving the transition.

For short enough times the $\uparrow$-component of the atomic field can be calculated in perturbation theory and we find

$$\hat{\psi}_{\uparrow}(\mathbf{r}) \propto \tilde{V}(\mathbf{r}-\mathbf{R})\hat{\psi}_{\downarrow}(\mathbf{r}). \tag{6.13}$$

The resulting momentum distribution of the $\uparrow$-atoms is

$$\begin{aligned} n(\mathbf{q},\mathbf{R}) &\propto \int d^3r d^3r' e^{i\mathbf{q}\mathbf{r}} e^{-i\mathbf{q}\mathbf{r}'} \left\langle \hat{\psi}^{\dagger}_{\uparrow}(\mathbf{r})\hat{\psi}_{\uparrow}(\mathbf{r}')\right\rangle & (6.14)\\ &\propto \int d^3r d^3r' e^{i\mathbf{q}\mathbf{r}} e^{-i\mathbf{q}\mathbf{r}'} \\ &\quad \times \psi^*(\mathbf{r})V^*(\mathbf{r}-\mathbf{R})\psi(\mathbf{r}')V(\mathbf{r}'-\mathbf{R}) & (6.15)\\ &= \left| \int d^3r e^{-i\mathbf{q}\mathbf{r}}\psi(\mathbf{r})V(\mathbf{r}-\mathbf{R})\right|^2 . & (6.16) \end{aligned}$$

$n(\mathbf{q},\mathbf{R})$ can be measured using for example absorption imaging after free expansion, provided that the interactions between the atoms can be neglected, a situation

that can for example be realized by rapidly sweeping a magnetic field to the vicinity of a Feshbach resonance [58], were two-body interactions can effectively be switched off, see section 3.3. Other methods for measuring the momentum distribution include Bragg spectroscopy [105] and Raman spectroscopy [64]. Those two methods are however not very well suited for the problem at hand because they require a much larger number of measurements and furthermore they provide only information about the one dimensional momentum distribution along the direction of momentum transfer.

Equation (6.16) shows that, when measured as a function of the shift $\mathbf{R}$ between coupling and condensate, the momentum distribution of the $\uparrow$-atoms is an XFROG signal, with the role of the reference field being played by the space dependent coupling strength. Hence, the XFROG algorithm can be used to fully recover the field ψ.

Experimentally, the situation is in some sense simpler for the characterization of atomic fields than for ultrashort laser pulses. A difficulty for ultrashort laser pulses stems from the pulses being so extremely short that one has to rely on gating them with another optical pulse. Since this gating has to be coherent one has to use nonlinear mixing in a crystal between the two pulses. The signals obtained are therefore typically weak. For matter waves on the other hand many ways are known to provide a gate $V(\mathbf{r})$ of sufficient smallness in the position domain, as e.g. the two examples given above. In contrast to the optical case one does not have to rely on interactions between matter waves. Thus the gate can be provided by a very well controlled *external* field so that *linear* FROG schemes become possible.

A fully three-dimensional XFROG scheme as suggested by Eq. (6.16) is difficult to realize in practice. First, it requires a very large number of measurements. Ten different shifts in each direction correspond to a total of 1000 runs of the experiment. The large amount of data necessary for the fully three-dimensional scheme also poses serious challenges to the numerical reconstruction algorithm as far as computer memory and time are concerned. Second, in time-of-flight absorption imaging one typically measures the column-integrated density so that the three-dimensional momentum distribution is not directly accessible. It appears therefore preferable to limit the reconstruction to a two-dimensional scheme.

It can be easily verified that if the field ψ and the coupling strength can be factorized as

$$\psi(\mathbf{r}) = f(z)\psi(x,y), \quad V(\mathbf{r}) = h(z)V(x,y), \tag{6.17}$$

where z is the direction along which the imaging is done and f and h are two arbitrary functions, Eq. (6.16) remains valid if we interpret $\mathbf{r}$ and $\mathbf{R}$ as two-dimensional vectors in the plane perpendicular to z and $\mathbf{q}$ as a corresponding two-dimensional momentum, providing us with the two-dimensional XFROG scheme sought. Many fields of practical interest can at least approximately be written in

the form Eq. (6.17). For example, the two-photon Raman coupling mentioned earlier is of that type provided that the lasers are directed along z and the Rayleigh length is much longer than the extend of the atomic cloud in that direction.

6.3 Reconstruction of a vortex-field

As a concrete example we demonstrate in this section how the matter wave field of a rotating BEC with a single vortex [86] can be directly reconstructed using the XFROG method.

For a zero temperature pure condensate in the Thomas-Fermi approximation the structure of the vortex core is essentially the same as that of a vortex in a uniform BEC and its wave function can to a good approximation be written as [95]

$$\psi_0(r,\varphi,z) = f(z)\frac{r/R}{\sqrt{2(\xi/R)^2+(r/R)^2}}\sqrt{1-(r/R)^2}e^{i\varphi}, \tag{6.18}$$

where we have used cylindrical coordinates with the vortex core at the symmetry axis. As discussed above, the z-dependence of the wave-function is unimportant and we will not regard it any further. In the rest of this chapter we use $\xi/R = 0.1$, but none of our results depend strongly on this ratio as long as $\xi/R \ll 1$. The real part of the wave-function (6.18) is shown in Fig. 6.5(a).

As an interaction Hamiltonian, or 'reference field' in the language of XFROG, we use Eq. (6.12) with the Gaussian coupling potential

$$V(r) = e^{-(r/w)^2}, \tag{6.19}$$

the z-dependence being again irrelevant for our purposes. A potential of this shape would naturally be expected for Raman outcoupling with Gaussian laser pulses.

We have numerically simulated an XFROG signal on a grid of 64×64 points using ψ_0 of Eq. (6.18) and the reference field (6.19), and applied the XFROG algorithm to reconstruct the field. Since in this numerical example we know the input field ψ_0 we can monitor the success of the field reconstruction using the χ^2-error per degree of freedom [6]

$$\chi^2 = \frac{1}{2N^2}\sum_{i,j}|\psi^{(n)}(\mathbf{r}_{ij}) - \psi_0(\mathbf{r}_{ij})|^2, \quad i,j \text{ grid points.} \tag{6.20}$$

Here, N is the number of grid points in one direction. For the example consider here, as a rule of thumb, the algorithm has qualitatively recovered the original field as soon as the χ^2 error is smaller than 10^{-2}.

[6] For χ^2 of Eq. (6.20) to be useful as a measure of the error it is necessary to determine the arbitrary overall phase of $\psi^{(n)}$ such that χ^2 becomes a minimum.

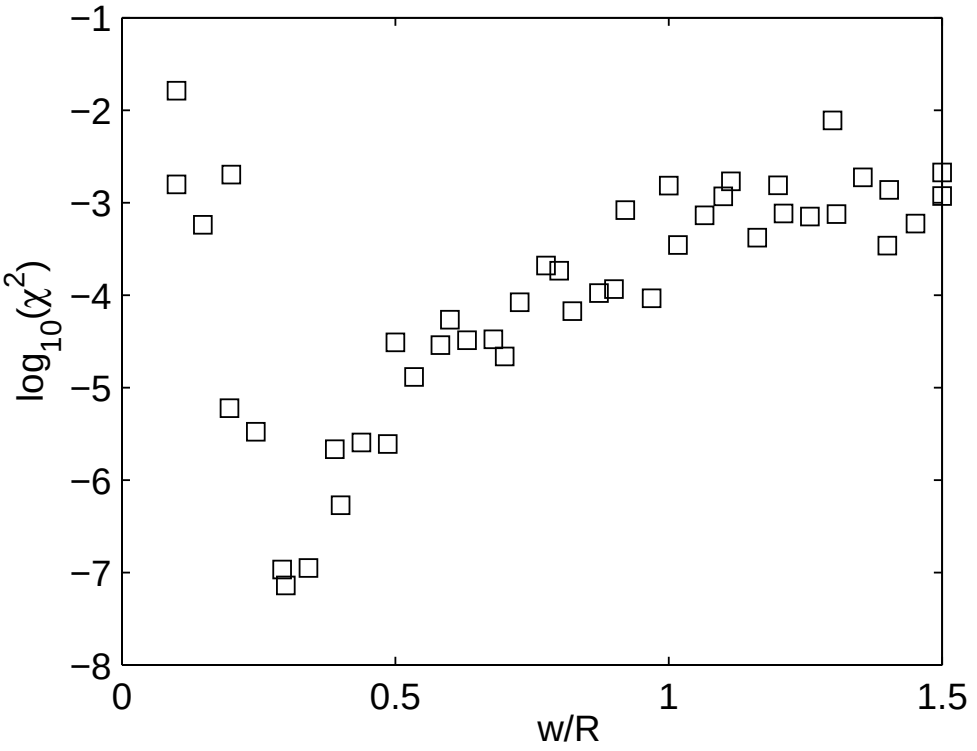

Fig. 6.4: χ^2 error of the reconstructed vortex field after 100 iterations as a function of the width w of V.

Our first task is to determine the optimal width w of V or, more generally, to understand how the field reconstruction depends on the choice of w. To this end we have numerically reconstructed the input field for various values of w and calculated χ^2 after 100 iterations of the generalized projections algorithm. The results of these simulations are summarized in Fig. 6.4. They show that the XFROG algorithm works rather well for a wide range of widths provided that they are comparable to the size of the condensate. The comparatively poor quality of the retrieved fields for larger widths is to some degree due to unphysical correlations across the boundaries of the simulation grid arising from the periodic boundary conditions that we are using. These effects can in principle be avoided by using a larger grid. The best results were obtained for widths of $w \approx 0.35R$ and in all that follows we will use that width. Larger widths tend to render the algorithm more stable, in the sense that it will converge to the correct solution for more initial guesses. Narrower reference fields on the other hand result in faster convergence, with the caveat that the algorithm sometimes gets stuck in a local minimum of Z and one has to start over with a new initial guess.

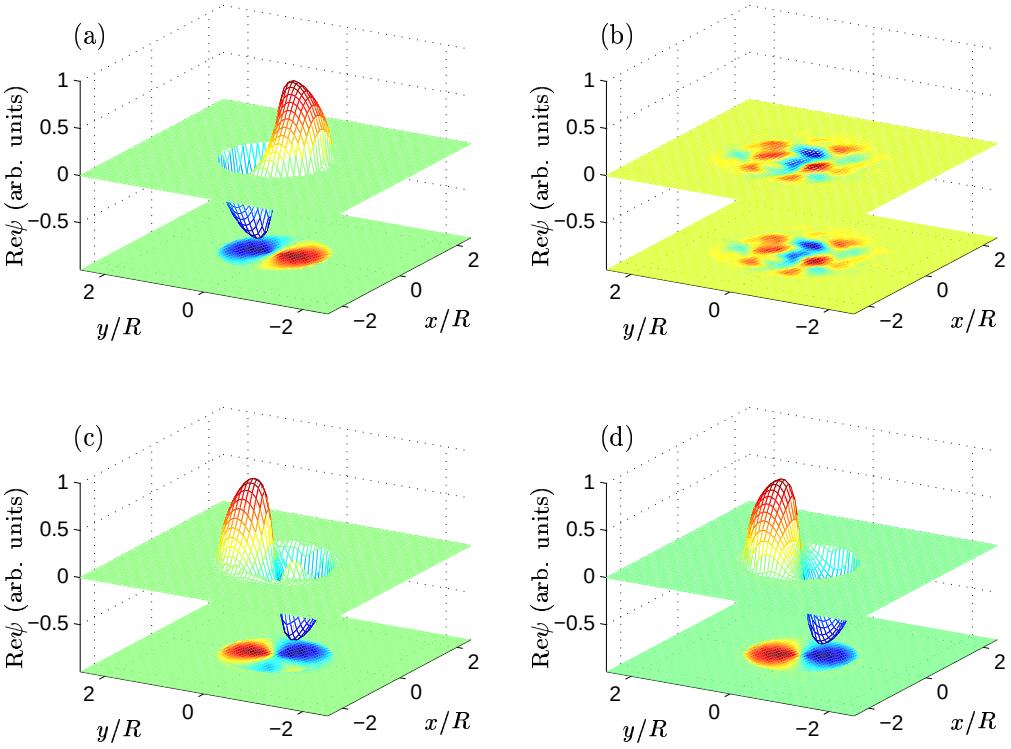

Fig. 6.5: Reconstruction of a vortex state on a grid of 64×64 points. Figure (a) shows the real part of the original state and figures (b)-(d) show the initial guess and the reconstructed state after 50 and 100 iterations, respectively.

Several stages of the reconstruction algorithm are shown in figures 6.5(b)-(d). The field reconstruction in this example takes about 30 minutes on a Pentium 4 CPU and uses approximately 400 MB of memory. We show only the real part of the field, as the imaginary part shows a similar degree of agreement. The XFROG error Z of Eq. (6.8) for the same simulation run is shown in Fig. 6.6 as a function of the number of iterations of the generalized projection algorithm. Also shown is the deviation from the reconstructed field from the original field χ^2. The figure shows that the algorithm converges exponentially after some initial stagnation. It also shows that, after the ambiguity in the total phase has been taken into account, the XFROG error Z is a good measure of the actual discrepancy between reconstructed and original field. This is important for real-life applications since in practice one does not know the original field so that χ^2 cannot be calculated and only the XFROG error is accessible.

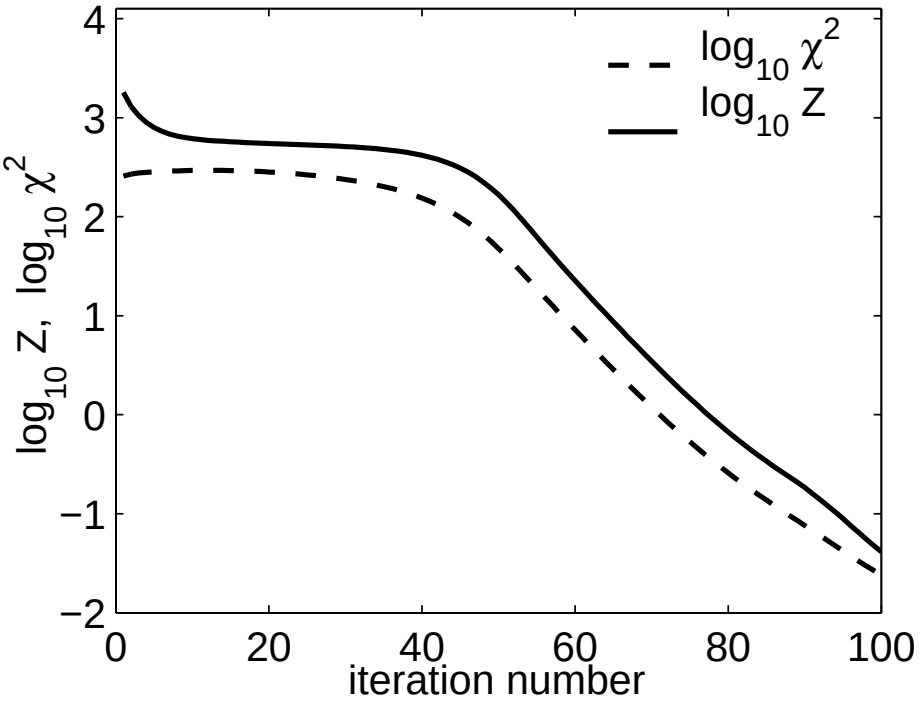

Fig. 6.6: XFROG error Z and field error χ^2 for the simulation run of Fig. 6.5.

6.3.1 Reduction of the number of measurements

Time of flight absorption imaging is a comparatively easy way to obtain many data points in the Fourier domain, but it is cumbersome to obtain the data sets for different shifts $\mathbf{R}$ because each such set requires a new run of the experiment. Therefore it is desirable to reduce the number of lateral shifts of the coupling potential for which a measurement is performed and we need to know how the field reconstruction is affected by that.

To answer this question we have calculated XFROG signals I_{XFROG} on grids of dimension $n \times n$, interpolated them onto a larger grid of dimension $N \times N$ using two dimensional cubic splines, and applied the XFROG algorithm to the resulting XFROG signals. Fig. 6.7 shows an example for $n = 10$. The recovered field shows good qualitative agreement with the original field, with differences in some details, e.g. near the maxima, resulting from the smoothing property of the interpolation with splines.

To quantitatively characterize the dependence of the success of the field recovery on the number of measurements we have evaluated χ^2 of the recovered field after 100 iterations as a function of n. The result is shown in Fig. 6.8. While the discrepancy between the recovered field and the original field grows as expected

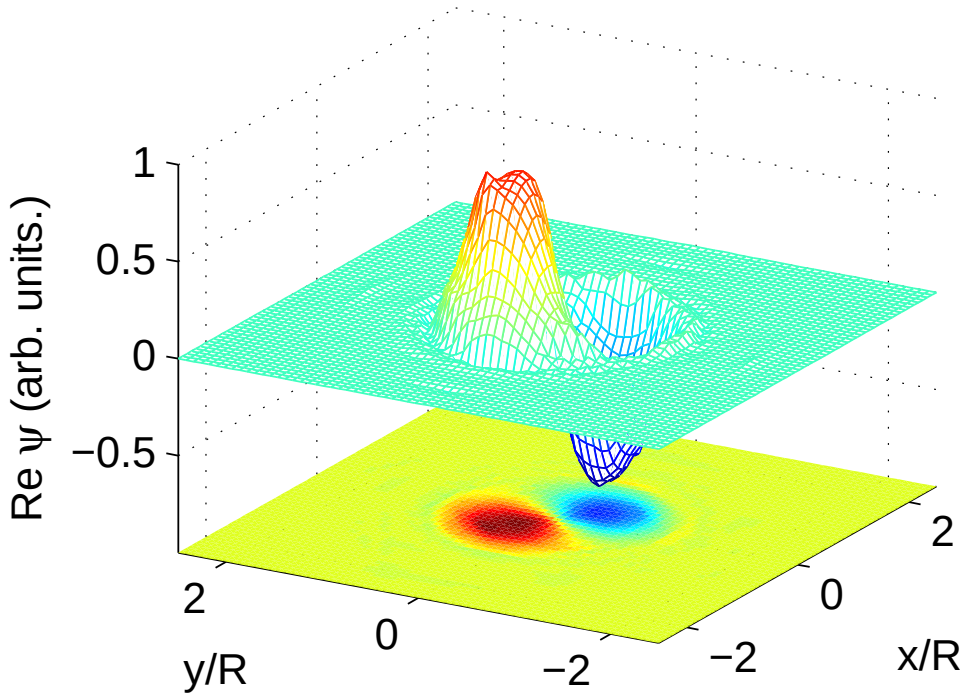

Fig. 6.7: Reconstruction of the field of Fig. 6.5 with the XFROG signal simulated on a grid of 10×10 and interpolated on a grid of 64×64 after 100 iterations.

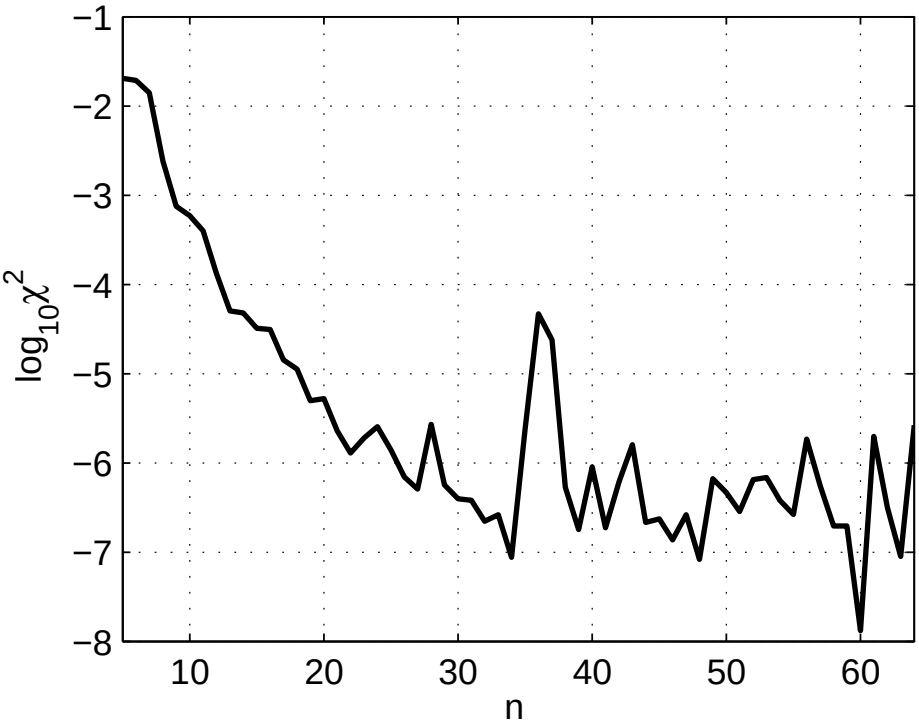

Fig. 6.8: χ^2 error of the recovered field after 100 iterations as a function of the number of measured data points n (same parameters as in figures 6.5 and 6.6).

as the number of measurements decreases, the field is qualitatively retrieved down to $n = 7$. For even smaller n the field reconstruction fails. In those cases the algorithm is honest enough to admit its failure by generating a large residual XFROG error. Nonetheless, the conclusion is that a rather limited number of measurements is sufficient to accurately measure the field.

We may remark that these considerations are actually rather pessimistic. In reality one often knows the size of the atomic cloud and the XFROG signal is clearly zero if there is no overlap between coupling V and atomic field ψ. Thus, many data points in the XFROG signal can be padded with zeros. Even those zeros contain useful information for the XFROG algorithm because they encode a support constraint for the recovered field. Support constraints, together with Fourier domain information, are widely used in image reconstruction for astronomic imagery and under certain circumstances they characterize an image completely. Furthermore, among the remaining non-zero measurements some will give excessively small signals. In practice one should try to avoid these measurements in favor of other displacements that give a stronger signal.

6.3.2 Robustness against noise

In an actual experiment the measurement of an XFROG signal will be subject to several sources of noise. In the case of noisy data the intersection of the sets O and F in Fig. 6.3 will in general be empty, and the XFROG algorithm determines a field that has the correct XFROG signal, i.e. belongs to the set F, and at the same time minimizes the distance to the set O as measured by Z.

The XFROG signal Eq. (6.8) is insensitive to fluctuations in the total phase of the atomic field ψ from one run of the experiment to the other, i.e. for different $\mathbf{R}$ — a consequence of the non-interferometric character of FROG methods in general. Hence it is sufficient to study the impact of uncertainties in the measurement of the displacements $\mathbf{R}$ themselves and in the total intensity of the XFROG signal from shot to shot. The latter can arise from variations of the number of atoms in the original condensate, from fluctuations in the coupling strength, and from fluctuations in the interaction times. We have simulated XFROG signals with Gaussian fluctuations in $\mathbf{R}$ and in shot-to-shot total intensity I with variances $\Delta\mathbf{R}$ and ΔI, respectively.

We have applied the XFROG algorithm to these contaminated signals and we have measured χ^2 after 100 iterations. To be more realistic, we have simulated the XFROG signals only on a grid of 10×10 and interpolated onto a grid of 64×64 as above. We have simulated the situation with errors in $\mathbf{R}$ only, errors in I only, and errors in both $\mathbf{R}$ and I. The results are summarized in Fig. 6.10. We were able to qualitatively reconstruct the atomic field up to relative errors as large as $\Delta R/R \approx 0.3$ and $\Delta I/I = 1$. The algorithm was found to be significantly less sensitive to uncertainties in the total intensity than to uncertainties in the displacements. Even XFROG signals with $\Delta I/I = 1$ yield recovered fields of surprisingly high quality[7]. In our simulations we observe that the XFROG algorithm becomes more stable and more exact if more data points are measured, i.e. if n is increased.

Figure 6.9 shows the retrieved field after 100 iterations for $\Delta R/R = 0.11$ and $\Delta I/I = 0.11$. The broad features of the original field are clearly reproduced and the noisy fine structure is almost exclusively due to the fluctuations in $\mathbf{R}$.

Thus, although the error in the retrieved field increases with increasing noise, we conclude that the algorithm is not very sensitive to noise and yields at least reliable qualitative information. In a sense, the field as recovered by the XFROG method contains less noise than the input data. This is reminiscent of the situation encountered in image reconstruction e.g. in astronomical applications. It was exactly for the purpose of removing noise from images by using a mixture of

[7] The relatively high residual errors for $\Delta I/I \approx 0.4$ and $\Delta I/I \approx 0.8$ come about because the XFROG algorithm did not find the global minimum of Z for the particular initial guess. Restarting the algorithm with a different initial guess (but with the exact same contaminated XFROG signal) lead to residual errors that nicely interpolate the the other data points.

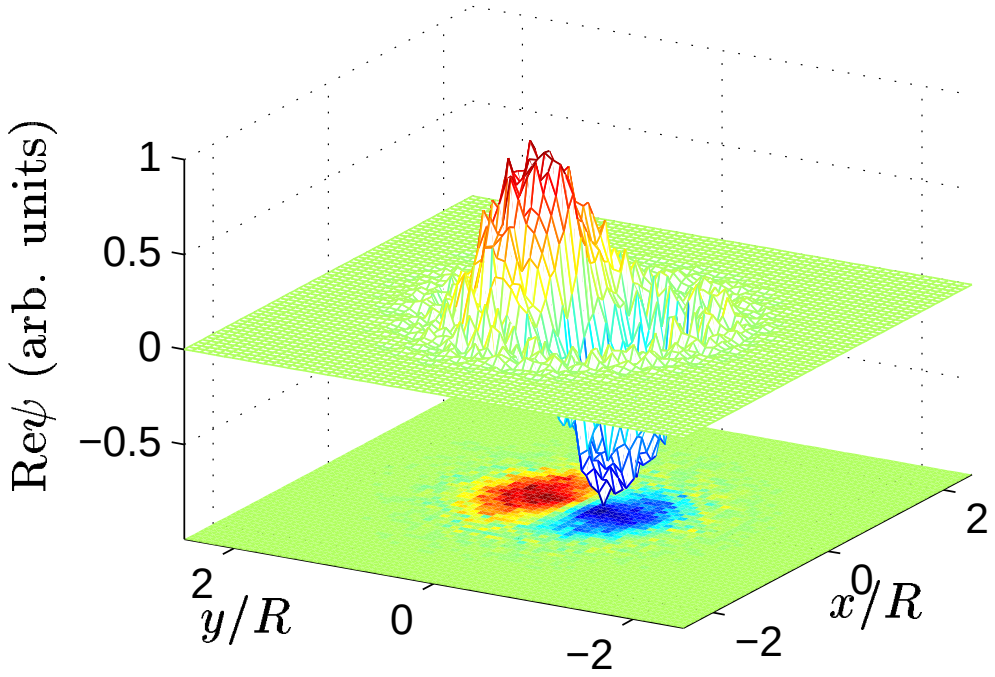

Fig. 6.9: Same as Fig. 6.7 but with simulated noise $\Delta R/R = 0.1$ and $\Delta I/I = 0.1$ in the XFROG signal.

position space and Fourier space information that some of the methods for the solution of the two-dimensional phase retrieval problem were first discussed.

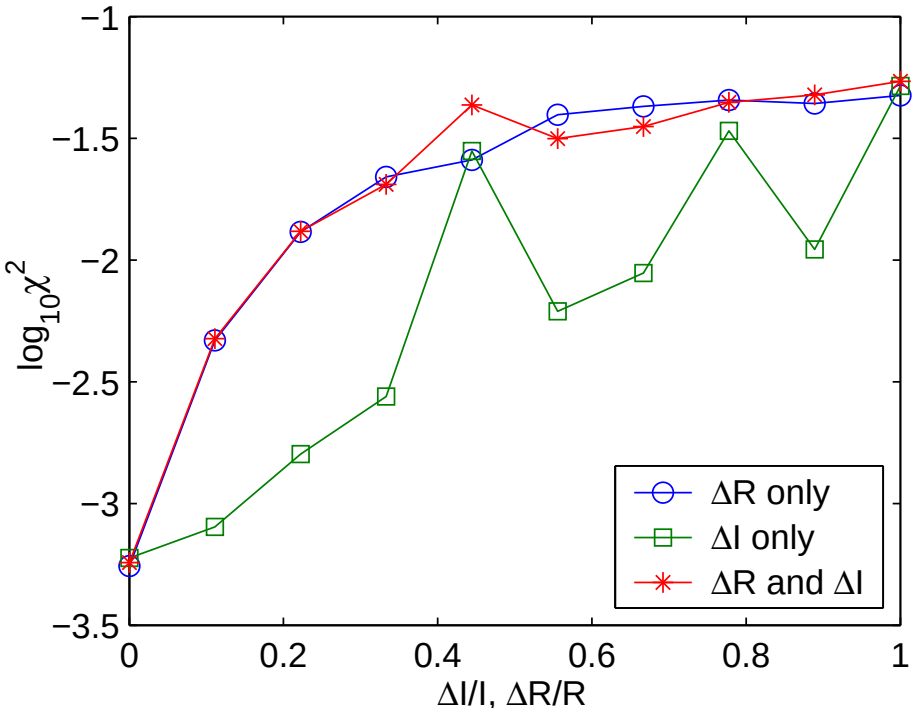

Fig. 6.10: χ^2 error of the recovered field after 100 iterations as a function of several noise sources.

7. MEASURING SECOND ORDER CORRELATIONS OF ULTRA COLD ATOMS USING MOLECULES

To date, many experiments concerned with the coherence properties of ultra cold atoms have studied first order correlation functions. The reason for this lies without question in the first order correlation functions being readily accessible through measurements of atomic densities. Densities can rather easily be measured using absorption or phase contrast imaging [66].

From the discussion of optical coherence in chapter 2 it is clear that a more detailed characterization of the coherence properties of a quantum or classical field is possible by means of higher order correlation functions. In fact some quantum states cannot be distinguished by analyzing just their first order correlations.

One such example is provided by superfluid fermionic systems, see 3.2.2. Recently, the newly available superfluid fermionic systems in the ultra cold atoms arena [100, 117] have attracted a lot of attention. The high degree of control over many system parameters possible with ultra cold atoms has enabled researchers to study these systems from new angles. For instance the possibility to tune interactions using Feshbach resonances has enabled controlled studies of the so called BEC-BCS crossover [92], a long standing problem of condensed matter physics.

A major difficulty in the studies of the BEC-BCS crossover and fermionic superfluidity in general with ultra cold atoms has been that, as far as their first order correlations are concerned, fermionic superfluids are very similar to their normal counter parts and hence first order correlations cannot be used to detect fermionic superfluidity. Several researchers have proposed and implemented schemes that allow one to measure higher order correlations [18, 55, 21, 2, 100, 6] but those methods are still very difficult to realize experimentally, see chapter 4 for more details.

Specifically as regards detection of superfluidity in the strongly interacting regime very close to the Feshbach resonance, evidence for fermionic superfluidity has been obtained by projecting the atom pairs onto a molecular state by a rapid sweep of the magnetic field through the resonance [100, 117]. More direct evidence of the gap in the excitation spectra due to pairing was obtained by rf

spectroscopy [24] and by measurements of the collective excitation frequencies [67, 9]. Very recently quantized vortices of the fermionic superfluid have been demonstrated [116].

As we have mentioned in chapter 2 there are also theoretical difficulties regarding the interpretation of fermionic superfluidity.

In this chapter we present a technique for measuring the second order correlation functions of an atomic gas that can overcome several of these difficulties. The idea is similar to the measurement of field correlations of matter waves by means of converting atoms to a different internal state and using these different states as detector signal as outlined in chapter 4. Here, instead of converting individual atoms, we would like to convert *pairs* of atoms into a signal field. A way to do just that is furnished by the coupling of atom pairs to molecules as described in chapter 3. This way, fermionic pairs are transformed into bosonic molecules for which a clear interpretation of coherence exists. On the experimental side this method has the advantage that, due to the nonlinear nature of the atom-molecule coupling, measurements of second order correlations of the atomic field can be avoided in favor of density measurements albeit of the molecules.

In this section we will first discuss some general aspects of the correlation measurement scheme and in doing so we will focus on the case of fermionic atoms since this will be the prime application. Then we will go on to discuss several specific cases that illustrate the usefulness of this scheme in characterizing fermionic superfluid systems. We consider the limiting cases of strong or weak atom-molecule coupling as compared to the relevant atomic energies. The molecule formation from a Bose-Einstein condensate (BEC) serves as a reference system. There we can rather easily study the contributions to the molecular signal from the condensed fraction as well as from thermal and quantum fluctuations above the condensate. The cases of a normal Fermi gas and a BCS superfluid Fermi system are then compared with it. We show that the molecules formed from a normal Fermi gas and from the unpaired fraction of atoms in a BCS state have very similar coherence properties to those of the molecules formed from the non-condensed atoms in the BEC case. The state of the molecular field formed from the pairing field in the BCS state on the other hand is similar to that resulting from the condensed fraction in the BEC case. The qualitative information gained from the analogies with the BEC case help us gain a physical understanding of the molecule formation in the BCS case where direct calculations are difficult and not nearly as transparent.

7.1 General considerations

We assume that some atomic state has been initially prepared in the absence of any molecules. At time $t = 0$ the coupling to the molecular field is switched on.

Experimentally, there are two alternatives how the preparation stage and the switching on of the interactions can be realized. First, in the case of magnetic Feshbach resonances one can prepare the atoms very far away from the resonance. Far away from the resonance the coupling between atoms and molecules is very ineffective because of the large detuning and there will be essentially no molecules at all. The switching on of the interactions can then be achieved by ramping the magnetic field close to the resonance. The second alternative is to use an optical Feshbach resonance. Then the coupling to the molecular field is realized by the two color Raman lasers and these lasers can be switched on at $t = 0$.

After the coupling has been switched on the molecular wavefunction changes due to the dressing with the atomic continuum. This happens on a rather fast two-body time scale that is typically of the order of tens of microseconds for magnetic Feshbach resonances. The two-body time scale can be substantially longer for optical Feshbach resonances. For the purpose of using the molecular field as a detector signal the strong admixture of open channel component is not desirable since it will lead to significant changes in the atomic state. This means that the interactions have to be switched on fast compared to the two body time scale and should also not be switched on for much longer than the two body time scale. For magnetic Feshbach resonances this is hard to realize. In all sweep experiments to date the two body state adiabatically follows the instantaneous magnetic field. For optical Feshbach resonances on the other hand there is a higher degree of control over the strength of the interactions through the laser intensities so that optical Feshbach resonances seem better suited for this scheme.

While the initial atomic state corresponds to a trapped gas, we assume that the molecules can be treated as free particles. This is justified if the atomic trapping potential does not affect the molecules or if the interaction time between the atoms and molecules is much less than the oscillation period in the trap or if the trap is switched off. Finally, the state of the molecular field is analyzed by standard techniques, e.g. time of flight measurements to find the momentum distribution of the molecules.

There are two different regimes as far as the strength of the Feshbach coupling compared to the atomic kinetic, interaction and potential energies are concerned. The Feshbach coupling can be much stronger, for which we will suggestively write $g\sqrt{N} \gg E_{\rm kin}$, or much weaker $g\sqrt{N} \ll E_{\rm kin}$ than the atomic kinetic and trap energies. $E_{\rm kin}$ denotes the characteristic kinetic energy of the atoms. It corresponds to zero point motion for condensate atoms, to the thermal energy $k_B T$ for non-condensed thermal bosons, and to the Fermi energy for a degenerate Fermi

gas. For brevity we will refer to the first case as the strong coupling regime and to the second case as the weak coupling regime.

Throughout this chapter we will assume that first order time dependent perturbation theory is applicable. This has slightly different implications for the strong and weak coupling regimes. In order to explain the most salient features of our scheme we will for now focus on the strong coupling regime since in that case the calculations are more transparent. We will point out the modifications that are to be expected in the weak coupling regime and these will also become very clear in the detailed discussion of the specific examples given below. Also at this point we will explicitly consider only the case of fermionic atoms.

Apart from making the system tractable by analytic methods there is also a deeper reason why the coupling should be such that perturbation theory is applicable: Since we ultimately wish to get information about the atomic state, it should not be modified too much by the measurement itself, i.e. the coupling to the molecular field. Furthermore, the molecular signal should be linearly connected to the atoms in as simple a way as possible. If the molecules were formed through very complicated nonlinear processes it would be very difficult to infer detailed information about the atoms from them. Thus our treatment follows the same spirit as Glauber's original theory of photon detection, where it is assumed that the light-matter coupling is weak enough so that the detector photo-current can be calculated using Fermi's Golden rule.

In the strong coupling regime the Heisenberg equations of motion for the molecular field can be from Eq. (3.108) as

$$i\hbar\frac{d}{dt}\hat{\varphi}(\mathbf{x}) = \hbar g\hat{\psi}_\uparrow(\mathbf{x})\hat{\psi}_\downarrow(\mathbf{x}), \tag{7.1}$$

where we have neglected the molecular kinetic energies. The energy non-conservation in molecule formation in the strong coupling limit is similar to the Raman-Nath regime of atom diffraction.

In first order perturbation theory the atomic operators are treated as constants so that we find

$$\hat{\varphi}(\mathbf{x}) = -igt\hat{\psi}_\uparrow(\mathbf{x})\hat{\psi}_\downarrow(\mathbf{x}). \tag{7.2}$$

This means that the molecular field directly couples to the pairing field of the atoms $\hat{\psi}_\uparrow(\mathbf{x})\hat{\psi}_\downarrow(\mathbf{x})$ which is exactly what one needs in order to detect fermionic superfluidity. Correlation functions of the molecular field then directly translate into correlation functions of the pairing field,

$$\begin{aligned}\langle\hat{\varphi}^\dagger(1)\cdots\hat{\varphi}^\dagger(n)\hat{\varphi}(n+1)\cdots\hat{\varphi}(2n)\rangle \propto \\ \langle\hat{\psi}_\downarrow(1)\hat{\psi}_\uparrow(1)\cdots\hat{\psi}_\downarrow(n)\hat{\psi}_\uparrow(n)\hat{\psi}_\uparrow(n+1)\hat{\psi}_\downarrow(n+1)\cdots\hat{\psi}_\uparrow(2n)\hat{\psi}_\downarrow(2n)\rangle,\end{aligned} \tag{7.3}$$

where we have used the same short hand notation for the space time points as in chapter 2. The molecular densities are of course the most important from an experimental point of view and according to Eq. (7.3) they are linked to four-point correlations of the atoms.

If we take into account the possibility to coherently split the atomic many-particle state into several components and to shift these against each other and to then probe them with the molecular field we see that by this method all even order correlation functions of the atomic field are accessible, at least in principle.

In the weak coupling regime molecule formation is only possible in such a way that the total energy is conserved. Therefore it is more convenient to analyze this case in the momentum representation. Qualitatively, the results are however similar to the strong coupling case with the added energy selectivity that leads to a more detailed detector signal. In this case the molecules can be thought of as a narrow band detector and in the strong coupling regime they are a broad band detector [20].

7.2 Model

We consider the three cases where the atoms are bosonic and initially in a BEC, or consist of two species of ultra-cold fermions, with or without superfluid component. In the following we describe explicitly the situation for fermions, the bosonic case being obtained from it by omitting the spin indices and by replacing the Fermi field operators by bosonic field operators.

Since we are primarily interested in how much can be learned about the second-order correlations of the initial atomic cloud from the final molecular state, we keep the physics of the atoms themselves as well as the coupling to the molecular field as simple as possible. We use the effective many-body theory described in subsection 3.3.2. The calculations are most conveniently done in the momentum representation. Introducing Fourier transformed field operators analogous to Eq. (3.27) the fermionic analog of Eq. (3.109) becomes [25, 109]

$$\begin{aligned}\hat{H} &= \sum_{\mathbf{k},\sigma} \epsilon_{\mathbf{k}} \hat{c}^{\dagger}_{\mathbf{k}\sigma}\hat{c}_{\mathbf{k}\sigma} + \sum_{\mathbf{k}} E_{\mathbf{k}} \hat{a}^{\dagger}_{\mathbf{k}}\hat{a}_{\mathbf{k}} + V^{-1/2}\sum_{\mathbf{k}_1,\mathbf{k}_2,\sigma} \tilde{U}_{\mathrm{tr}}(\mathbf{k}_2-\mathbf{k}_1)\hat{c}^{\dagger}_{\mathbf{k}_2\sigma}\hat{c}_{\mathbf{k}_1\sigma} \\ &+ \frac{U_0}{2V}\sum_{\mathbf{q},\mathbf{k}_1,\mathbf{k}_2} \hat{c}^{\dagger}_{\mathbf{k}_1+\mathbf{q}\uparrow}\hat{c}^{\dagger}_{\mathbf{k}_2-\mathbf{q}\downarrow}\hat{c}_{\mathbf{k}_2\downarrow}\hat{c}_{\mathbf{k}_1\uparrow} + \hbar g\left(\sum_{\mathbf{q},\mathbf{k}} \hat{a}^{\dagger}_{\mathbf{q}}\hat{c}_{\mathbf{q}/2+\mathbf{k}\downarrow}\hat{c}_{\mathbf{q}/2-\mathbf{k}\uparrow} + \mathrm{H.c.}\right) \quad (7.4)\end{aligned}$$

Here $\epsilon_{\mathbf{k}} = \hbar^2k^2/2M$ is the kinetic energy of an atom of mass M and momentum $\hbar\mathbf{k}$ and $E_{\mathbf{k}} = \epsilon_{\mathbf{k}}/2 + \hbar\nu$ is the energy of a molecule with momentum k and detuning parameter $\Delta E = \hbar\nu$. $\tilde{U}_{\mathrm{tr}}(\mathbf{k}) = V^{-1/2}\int_V d^3x e^{-i\mathbf{kx}}V(\mathbf{x})$ is the Fourier transform of the atoms' trapping potential. We assume that the trapping potential and background scattering are relevant only for the preparation of the initial state before

the coupling to the molecules is switched on at $t = 0$ and can be neglected in the calculation of the dynamics. This is justified if $\hbar g\sqrt{N} \gg U_0 n, \hbar\omega_i$ where n is the atomic density, N the number of atoms, and ω_i are the oscillator frequencies of the atoms in the harmonic trapping potential. In experiments, the interaction between the atoms can effectively be switched off by ramping the magnetic field to a position where the scattering length is zero, see section 3.3.

For first order time dependent perturbation theory to be applicable the state of the atoms must not change significantly and consequently, only a small fraction of the atoms are converted into molecules. It is reasonable to assume that this is true for short interaction times or weak enough coupling. The exact criteria for the applicability of perturbation theory will be considered for each specific case below.

The quantity we will primarily be interested in is the momentum distribution of the molecules[1],

$$n(\mathbf{p}, t) = \langle \hat{a}^\dagger_{\mathbf{p}}(t)\hat{a}_{\mathbf{p}}(t)\rangle. \tag{7.5}$$

The momentum distribution can be measured in experiments e.g. using absorption imaging of the molecular cloud after free expansion. As we have seen above, the first order correlations of the molecules are linked to the second order correlations of the atoms so that it should be possible to detect fermionic superfluidity.

7.3 BEC

We consider first the case where the initial atomic state is a BEC in a spherically symmetric harmonic trap. We note that all of our results can readily be extended to anisotropic traps by an appropriate rescaling of the coordinates in the direction of the trap axes. We assume that the temperature is well below the BEC transition temperature and that the interactions between the atoms are not too strong so that the Bogoliubov approximation can be used to describe the state of the atoms. Furthermore we will make the local density approximation leading to the Thomas-Fermi wavefunction Eq. (3.24) for the condensate and to uncorrelated fluctuations at positions further appart than the healing length ξ. In accordance with the assumption of low temperatures and weak interactions we do not distinguish between the total number of atoms and the number of atoms in the condensate.

[1] Note that due to our choice of a symmetrical normalization of the Fourier transform and its inverse with $V^{-1/2}$ each, the momentum distribution is a pure number representing the mean occupation number of each mode in the quantization volume V. Densities are obtained by multiplying by the density of states in V.

7.3.1 Strong coupling, $E_{\rm kin} \ll \hbar g\sqrt{N}$

The calculation of the molecular signal field in perturbation theory is very similar to the calculations that have been performed in the context of sum frequency generation in quantum optics [84, 71]: We expand $n(\mathbf{p},t)$ in a Taylor series around $t = 0$ and make use of the Heisenberg equations of motion for the molecular field operator analogous to Eq. (7.1),

$$i\frac{\partial \hat{a}_{\mathbf{p}}(t)}{\partial t} = g\sum_{\mathbf{k}} \hat{c}_{\mathbf{p}/2+\mathbf{k}}\hat{c}_{\mathbf{p}/2-\mathbf{k}}, \tag{7.6}$$

and similarly for $\hat{a}^\dagger_{\mathbf{p}}$, to express the time-derivatives in the Taylor expansion. In Eq. (7.6) we have neglected the kinetic energy term because we assume that we are in the strong coupling regime.

To lowest non-vanishing order in gt we find

$$n_{\rm BEC,s.c.}(\mathbf{p},t) = (gt)^2\sum_{\mathbf{k_1},\mathbf{k_2}}\left\langle \hat{c}^\dagger_{\mathbf{p}/2-\mathbf{k_1}}\hat{c}^\dagger_{\mathbf{p}/2+\mathbf{k_1}}\hat{c}_{\mathbf{p}/2+\mathbf{k_2}}\hat{c}_{\mathbf{p}/2-\mathbf{k_2}}\right\rangle + O((gt)^4), \tag{7.7}$$

where the atomic operators are the initial ($t = 0$) operators. This expression can be evaluated by making use of the decomposition of the atomic field operator Eq. (3.5) and the local density approximation for the part describing the fluctuations. In the momentum representation the decomposition Eq. (3.5) becomes

$$\hat{c}_{\mathbf{p}} = \tilde{\psi}_0(\mathbf{p})\hat{c}_0 + \sum_j \sqrt{\frac{V_j}{V}}\delta\hat{c}^{(j)}_{\mathbf{p}}, \tag{7.8}$$

where $\tilde{\psi}_0$ is the Fourier transform of the condensate mode and the local fluctuation operators $\delta\hat{c}^{(j)}_{\mathbf{p}} = \frac{1}{\sqrt{V_j}}\int_{V_j} d^3x e^{-i\mathbf{p}\mathbf{x}/\hbar}\delta\hat{\psi}^{(j)}(\mathbf{x})$ are the Fourier transforms of the local fluctuation operators $\delta\hat{\psi}^{(j)}(\mathbf{x})$[2].

The uncorrelatedness between fluctuations in different cells Eq. (3.51) becomes in the momentum representation

$$\langle \delta\hat{c}^{(i)\dagger}_{\mathbf{k}_1}\delta\hat{c}^{(j)}_{\mathbf{k}_2}\rangle \equiv \delta_{i,j}\delta_{\mathbf{k}_1,\mathbf{k}_2}\langle \delta\hat{c}^{(i)\dagger}_{\mathbf{k}_1}\delta\hat{c}^{(i)}_{\mathbf{k}_1}\rangle. \tag{7.9}$$

Inserting the decomposition of the field operator in eq. (7.7), keeping only first order terms in the fluctuations and making use of relation Eq. (7.9) we find

$$\begin{aligned} n_{\rm BEC,s.c.}(\mathbf{p},t) = (gt)^2N(N-1)\sum_{\mathbf{k}_1,\mathbf{k}_2}\tilde{\psi}^*_0(\mathbf{p}/2-\mathbf{k}_1)\tilde{\psi}^*_0(\mathbf{p}/2+\mathbf{k}_1)\tilde{\psi}_0(\mathbf{p}/2-\mathbf{k}_2)\tilde{\psi}_0(\mathbf{p}/2+\mathbf{k}_2) \\ + 4(gt)^2N\sum_{\mathbf{k},j}\frac{V_j}{V}|\tilde{\psi}_0(\mathbf{p}-\mathbf{k})|^2\langle \hat{c}^{(j)\dagger}_{\mathbf{k}}\hat{c}^{(j)}_{\mathbf{k}}\rangle. \end{aligned} \tag{7.10}$$

[2] Division of the momenta by $\hbar$ to obtain wavevectors is understood if momenta appearas the arguments of Fourier transformed functions.

The sum in the fully coherent term is readily shown to be

$$\sum_{\mathbf{k}_1,\mathbf{k}_2} \tilde{\psi}_0^*(\mathbf{p}/2-\mathbf{k}_1)\tilde{\psi}_0^*(\mathbf{p}/2+\mathbf{k}_1)\tilde{\psi}_0(\mathbf{p}/2-\mathbf{k}_2)\tilde{\psi}_0(\mathbf{p}/2+\mathbf{k}_2) = \left|\widetilde{\psi_0^2}(\mathbf{p})\right|^2. \quad (7.11)$$

In accordance with what has been said in section 3.3.3 the wavefunction of the coherently produced molecules is proportional to the square of the atomic wavefunction and their momentum distribution is just the Fourier transform of that[3].

Using the Thomas-Fermi wave function for the condensate, Eq. (3.23), we can calculate the condensate contribution in closed form as[4]

$$(gt)^2N(N-1)\left|\tilde{\psi}_0^2(\mathbf{p})\right|^2 = \frac{225N(N-1)(gt)^2}{4(pR_{TF}/\hbar)^6}\left(\frac{6\sin(pR_{TF}/\hbar)}{(pR_{TF}/\hbar)^2} - \frac{6\cos(pR_{TF}/\hbar)}{pR_{TF}/\hbar} - 2\sin(pR_{TF}/\hbar)\right)^2. \quad (7.12)$$

In the incoherent term we notice that $|\tilde{\psi}_0(\mathbf{p})|^2$ is a much narrower function than $\langle\hat{c}_{\mathbf{k}}^{(j)\dagger}\hat{c}_{\mathbf{k}}^{(j)}\rangle$, the former having a typical width of $\sim\hbar/R_{TF}$ while the latter has a typical width of $\sim\hbar/\xi$. Hence, to a good approximation, $\langle\hat{c}_{\mathbf{k}}^{(j)\dagger}\hat{c}_{\mathbf{k}}^{(j)}\rangle$ can be treated as a constant for the momentum range for which $|\tilde{\psi}_0(\mathbf{p})|^2$ is nonzero and we obtain

$$\begin{aligned}4(gt)^2N\sum_{\mathbf{k},j}\frac{V_j}{V}|\tilde{\psi}_0(\mathbf{p}-\mathbf{k})|^2\langle\hat{c}_{\mathbf{k}}^{(j)\dagger}\hat{c}_{\mathbf{k}}^{(j)}\rangle &\approx 4(gt)^2N\sum_j\frac{V_j}{V}\langle\hat{c}_{\mathbf{k}}^{(j)\dagger}\hat{c}_{\mathbf{k}}^{(j)}\rangle\sum_{\mathbf{k}}|\tilde{\psi}_0(\mathbf{p}-\mathbf{k})|^2 \\ &= 4(gt)^2N\sum_j\frac{V_j}{V}\langle\hat{c}_{\mathbf{k}}^{(j)\dagger}\hat{c}_{\mathbf{k}}^{(j)}\rangle, \quad (7.13)\end{aligned}$$

where we have made use of the normalization of $\tilde{\psi}_0(\mathbf{p})$ in the last step. Since $\xi \ll R_{TF}$ the volumes V_j can be made small and the sum can be approximated by a Rieman integral, leading us finally to

$$n_{\mathrm{BEC,s.c.}}(\mathbf{p},t) = (gt)^2N(N-1)V\left|\tilde{\psi}_0^2(\mathbf{p})\right|^2 + (gt)^2 4N\int\frac{d^3x}{V}\left\langle\delta\hat{c}_{\mathbf{p}}^\dagger(\mathbf{x})\delta\hat{c}_{\mathbf{p}}(\mathbf{x})\right\rangle. \quad (7.14)$$

The local occupation numbers of the fluctuations can be calculated using the Bogoliubov approximation with the local densities, see section 3.1.3 for details.

[3] Note that in Eq. (7.11) the square of the atomic wavefunction is taken first, and then the Fourier transform.

[4] Due to the symmetrical normalization of the Fourier transform with $V^{-1/2}$ the occupation numbers of the modes $\langle\hat{b}_{\mathbf{q}}^\dagger\hat{b}_{\mathbf{q}}\rangle$ are pure numbers. Densities are obtained from them using the density of states in the volume V with periodic boundary conditions.

From Eq. (7.14) we see that our approach is justified if $(\sqrt{N}gt)^2 \ll 1$ because for such times the initial atomic state can be assumed to remain undepleted.

The momentum distribution (7.14) is illustrated in Fig. 7.1. We chose to scale our momenta in units of $\hbar(3\pi^2 n_0)^{1/3}$ since this will allow an easier comparison with the fermionic cases considered below. The width of the coherent contribution being small on the scale of $\hbar(3\pi^2 n_0)^{1/3}$ indicates that the atoms are coherent over many interatomic distances. The contribution from the condensate is a collective effect, as indicated by its quadratic scaling with the atom number. It clearly dominates over the incoherent contribution from the fluctuations, which is proportional to the number of atoms.

Using the same approximation scheme we can calculate the second-order correlation

$$g^{(2)}(\mathbf{p}_1, t_1; \mathbf{p}_2, t_2) = \frac{\langle \hat{a}^\dagger_{\mathbf{p}_1}(t_1)\hat{a}^\dagger_{\mathbf{p}_2}(t_2)\hat{a}_{\mathbf{p}_2}(t_2)\hat{a}_{\mathbf{p}_1}(t_1)}{n(\mathbf{p}_1, t_1)n(\mathbf{p}_2, t_2)}. \tag{7.15}$$

If we neglect fluctuations we find

$$\begin{aligned} g^{(2)}_{\mathrm{BEC,b}}(\mathbf{p}_1, t_1; \mathbf{p}_2, t_2) &= \frac{(N-2)!^2}{(N-4)!N!} \\ &= 1 - \frac{6}{N} + O(N^{-2}). \end{aligned} \tag{7.16}$$

For $N \to \infty$ this is very close to 1, which is characteristic of a coherent state. The fluctuations lead to a larger value of $g^{(2)}$, making the molecular field partially coherent, but their effect is only of order $O(N^{-1})$. The physical reason why the resulting molecular field is almost coherent is of course that almost all the atoms are in the condensate and that the mean field approximation gives an excellent description for the atoms.

7.3.2 Weak coupling, $E_{\mathrm{kin}} \gg \hbar g\sqrt{N}$

For weak coupling, the typical kinetic energies associated with the atoms and molecules, E_{kin}, are much larger than the atom-molecule interaction energy. This implies that even for very short interaction times, $t \lesssim (g\sqrt{N})^{-1}$, the phase of the atoms and molecules can evolve significantly, $E_{\mathrm{kin}}t/\hbar \gg 1$. As a result, only transitions between atom pairs and molecules that conserve energy can occur. In this case, it is convenient to go over to the interaction representation

$$\hat{c}_{\mathbf{p}}(t) \to e^{-i\epsilon_{\mathbf{p}}t/\hbar}\hat{c}_{\mathbf{p}}(t), \quad \hat{a}_{\mathbf{p}}(t) \to e^{-iE_{\mathbf{p}}t/\hbar}\hat{a}_{\mathbf{p}}(t), \tag{7.17}$$

where we will denote the interaction picture operators by the same symbols as the Heisenberg operators used in the previous subsection.

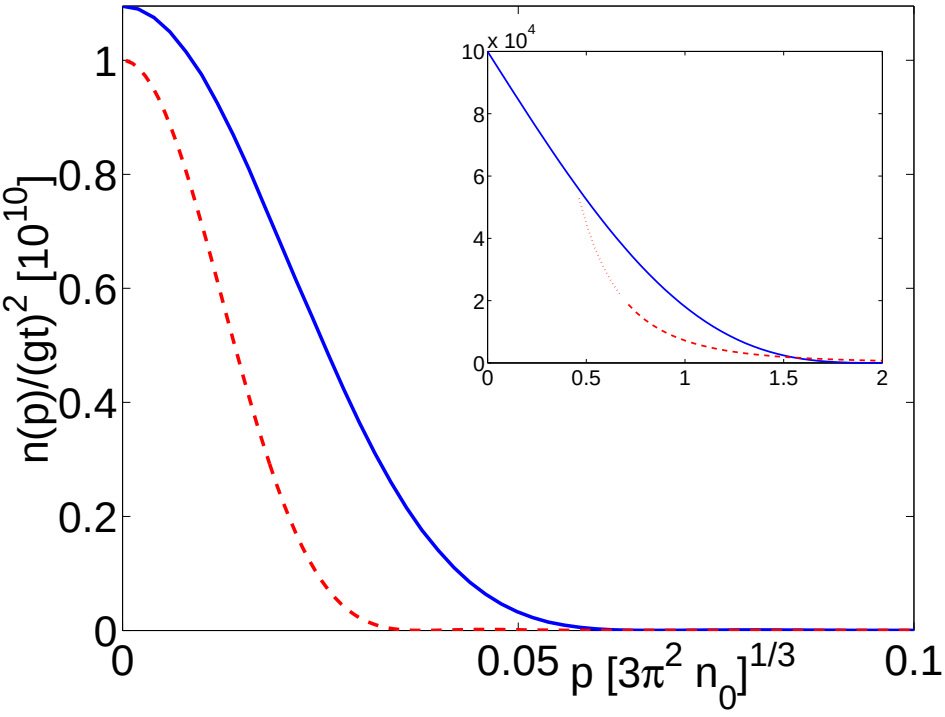

Fig. 7.1: Momentum distribution of molecules formed from a BEC (red dashed line) with $a = 0.1a_{\mathrm{osc}}$ and $T = 0.1T_c$ and a BCS type state with $k_F a = 0.5$ and $a_{\mathrm{osc}} = 5k_F^{-1}(0)$ (blue solid line), both for $N = 10^5$ atoms. The BCS curve has been scaled up by a factor of 20 for easier comparison. The inset shows the noise contribution for BEC (red dashed) and BCS (blue) case. The latter is simply the momentum distribution of molecules formed from a normal Fermi gas. The local density approximation treatment of the noise contribution in the BEC case is not valid for momenta smaller than $2\pi\hbar/\xi$ (indicated by the red dotted line in the inset). Note that the coherent contribution is larger than the noise contribution by five orders of magnitude in the BEC case and three orders of magnitude in the BCS case.

The equations of motion in the interaction picture,

$$i\frac{\partial \hat{a}_{\mathbf{p}}(t)}{\partial t} = g\sum_{\mathbf{k}} e^{i\left(E_{\mathbf{p}}-\epsilon_{\mathbf{p}/2+\mathbf{k}}-\epsilon_{\mathbf{p}/2-\mathbf{k}}\right)t/\hbar}\hat{c}_{\mathbf{p}/2+\mathbf{k}}\hat{c}_{\mathbf{p}/2-\mathbf{k}}, \tag{7.18}$$

are in first order perturbation theory again integrated by treating the operators as constants, leading to

$$\hat{a}_{\mathbf{p}}(t) = \sum_{\mathbf{k}} \Delta(E_p - \epsilon_{\mathbf{p}/2+\mathbf{k}} - \epsilon_{\mathbf{p}/2-\mathbf{k}}, t)\hat{c}_{\mathbf{p}/2+\mathbf{k}}\hat{c}_{\mathbf{p}/2-\mathbf{k}}, \tag{7.19}$$

where we have introduced [5]

$$\Delta(\omega, t) = g\lim_{\eta\downarrow 0}\frac{e^{i\omega t/\hbar}-1}{i\omega+\eta}. \tag{7.20}$$

The condition under which this step is justified is analyzed below. As in the broad resonance case we can insert this expression in $n(\mathbf{p}, t)$ of Eq. (7.5). The calculation of the resulting integrals over expectation values of the atomic state is however considerably subtler than in the broad resonance case.

Repeating the calculation of the broad resonance case that lead to eq. (7.10) with $\hat{a}_{\mathbf{p}}$ now replaced according to eq. (7.19) we find, again to first order in the fluctuations,

$$\begin{aligned} n_{\mathrm{BEC,w.c.}}(\mathbf{p}, t) = N(N-1)\Big|\sum_{\mathbf{k}} \Delta(E_{\mathbf{p}} - \epsilon_{\mathbf{p}/2+\mathbf{k}} - \epsilon_{\mathbf{p}/2-\mathbf{k}}, t)\tilde{\psi}_0(\mathbf{p}/2+\mathbf{k})\tilde{\psi}_0(\mathbf{p}/2-\mathbf{k})\Big|^2 \\ + 4N\sum_{\mathbf{k},j}\frac{V_j}{V}\left|\Delta(E_{\mathbf{p}} - \epsilon_{\mathbf{p}/2+\mathbf{k}} - \epsilon_{\mathbf{p}/2-\mathbf{k}}, t)\right|^2 |\tilde{\psi}_0(\mathbf{p}-\mathbf{k})|^2\langle\hat{c}_{\mathbf{k}}^{(j)\dagger}\hat{c}_{\mathbf{k}}^{(j)}\rangle \\ \equiv n_{\mathrm{coh}}(\mathbf{p}, t) + n_{\mathrm{incoh}}(\mathbf{p}, t). \end{aligned} \tag{7.21}$$

Let us first consider the coherent part $n_{\mathrm{coh}}(\mathbf{p}, t)$. Going over from the summation over momenta to an integral over energies by introducing polar coordinates and making the substitution $E = (\hbar k)^2/M$ we find

$$\begin{aligned} n_{\mathrm{coh}}(\mathbf{p}, t) = \frac{VM^{3/2}}{\pi^2 2^3}\int_0^\infty dE\Delta(\hbar\nu - E, t)\int_0^\pi d\vartheta\sin\vartheta \\ \times\sqrt{E}\tilde{\psi}_0\left(\sqrt{p^2/4 + ME + |p|\sqrt{ME}\cos\vartheta}\right)\tilde{\psi}_0\left(\sqrt{p^2/4 + ME - |p|\sqrt{ME}\cos\vartheta}\right) \end{aligned} \tag{7.22}$$

[5] We denote the function in Eq. (7.20) by Δ because it has properties similar to the usual δ-function. Confusion with the local gap parameter introduced below, which is also denoted by Δ, cannot arise because the first always has energies as its argument while the latter has positions as its argument.

In the limit $t \to \infty$, $\Delta(\hbar\nu - E)$ becomes [88],

$$\lim_{t\to\infty} \Delta(\hbar\nu - E, t) = g\left(\pi\delta(\hbar\nu - E) - i\mathbf{P}\frac{\mathbf{1}}{\hbar\nu - \mathbf{E}}\right) \tag{7.23}$$

where, as usual, **P** means that the integral has to be taken in the sense of the Cauchy-principal value. The real part can be evaluated by making use of the δ-function and for the imaginary part we have to rely on numerical methods to calculate the principal value integral.

Making similar manipulations of the sums over momenta for the incoherent part leads to

$$n_{\rm incoh}(\mathbf{p}, t) = 4N\frac{M^{3/2}}{8\pi^2}\sum_j V_j \int_0^\pi d\vartheta \sin\vartheta$$
$$\times \int_0^\infty dE\, \sqrt{E}|\Delta(\hbar\nu - E, t)|^2 \left|\tilde{\psi}_0\left(\sqrt{p^2/4 + ME - |p|\sqrt{ME}\cos\vartheta}\right)\right|^2 \langle \hat{c}^{(j)\dagger}_{\sqrt{ME}} \hat{c}^{(j)}_{\sqrt{ME}}\rangle. \tag{7.24}$$

In the limit as t goes to infinity we can use the delta function

$$\lim_{t\to\infty} |\Delta(\hbar\nu - E)|^2 = \pi g^2 t\delta(\hbar\nu - E) \tag{7.25}$$

to perform the energy integral.

We find

$$\begin{aligned} n_{\rm BEC,w.c.}(\mathbf{p}, t) &= N(N-1)\frac{V^2M^3g^2}{16\pi^4}\left|\int_0^\infty dE\,\sqrt{E}\left(\pi\delta(\hbar\nu - E) + i\mathbf{P}\frac{1}{\hbar\nu - E}\right)\right. \\ &\times \left.\int_{-1}^1 dz\tilde{\psi}_0\left(\sqrt{p^2/4 + ME - p\sqrt{MEz}}\right)\tilde{\psi}_0\left(\sqrt{p^2/4 + ME + p\sqrt{MEz}}\right)\right|^2 \\ &+ N\delta_{p/2,\sqrt{M\nu}}\frac{3g^2t\sqrt{\nu M^3}R_{TF}^3}{8\pi^2}\int\frac{d^3x}{V}\langle\delta\hat{c}^\dagger_{\mathbf{p}}(\mathbf{x})\delta\hat{c}_{\mathbf{p}}(\mathbf{x})\rangle. \end{aligned} \tag{7.26}$$

In the second term in (7.26) we have defined

$$\begin{aligned} \delta_{p,p'} &= \sqrt{\frac{4\pi V}{3R_{TF}^3}}\int_{-1}^1 dz\left|\tilde{\psi}_0(\sqrt{p^2 + p'^2 - 2pp'z})\right|^2 \\ &= \begin{cases} O(1), & |p - p'| < 2\pi\hbar/R_{\rm TF} \\ 0, & |p - p'| > 2\pi\hbar/R_{\rm TF}. \end{cases} \end{aligned} \tag{7.27}$$

As before, the contribution from the condensate is clearly dominant. The integral in the first term in Eq. (7.26) is proportional to the amplitude for finding an atom

pair with center of mass momentum $\mathbf{p}$ and total kinetic energy $\hbar\nu$. Because $\tilde{\psi}_0$ drops to zero on a scale of $2\pi\hbar/R_{TF}$ this amplitude is essentially zero if $p > 2\pi\hbar/R_{\rm TF}$ or $\hbar\nu > \frac{\pi^2}{MR_{\rm TF}^2}$.

The second term in Eq. (7.26) originates from molecules that are formed from an atom in the condensate and a non-condensed atom. Since the atom momentum $\lesssim 2\pi\hbar/R_{\rm TF}$ in the condensate is very small compared to the momentum $|\mathbf{p}| \sim \hbar/\xi$ of a non-condensed atom, the molecular momentum is essentially due to the non-condensed atom. On the other hand, energy conservation implies that $\hbar\nu + p^2/4M \approx p^2/2M$ if $p \gg 2\pi\hbar/R_{TF}$. Consequently for a given detuning ν, molecules with momenta in a shell of radius $2\sqrt{M\hbar\nu}$ and width $2\pi\hbar/R_{TF}$ are formed from one atom in the condensate and another atom taken from the non-condensed part with a momentum that also lies in a spherical shell in momentum space around $\mathbf{p}$ with thickness $2\pi\hbar/R_{TF}$. Figure 7.2 shows a typical example for the momentum distribution.

Equation (7.26) allows us to extract the criterion for the validity of our approximation, i.e of treating the atomic state as being undepleted. The coherent contribution will only be nonzero if $|\mathbf{p}| \leq 2\pi\hbar/R_{TF}$ and for these momenta the incoherent contribution can be neglected, as we have seen. Requiring that the number of molecules remains much smaller then the initial number of atoms leads to the condition

$$\sqrt{N}g \ll \nu \frac{1}{(R_{TF}/\hbar)^3(M\nu)^{3/2}}. \tag{7.28}$$

In the opposite case $|\mathbf{p}| > 2\pi\hbar/R_{TF}$ the coherent contribution is essentially zero and we need only consider the incoherent contribution. Requiring that the number of molecules with momentum $\mathbf{p}$ be much smaller than the number of non-condensed atoms with that same momentum leads to

$$gt \ll N^{-1}\frac{\nu}{g}\frac{1}{(R_{TF}/\hbar)^3(M\hbar\nu)^{3/2}}. \tag{7.29}$$

7.4 Normal Fermi gas

For a normal Fermi gas we restrict ourselves to the case of zero temperature, $T = 0$. For temperatures T well below the Fermi temperature T_F, the corrections to our results are of order $(T/T_F)^2$ or higher, and do not lead to any qualitatively new effects. We assume that the gas can be described using the local density approximation as described in section 3.2.1.

Using the same perturbation methods as described in the previous section for bosons, we can calculate the momentum distribution of the molecules and their correlation function $g^{(2)}$ for a broad and for a narrow resonance by first calculating

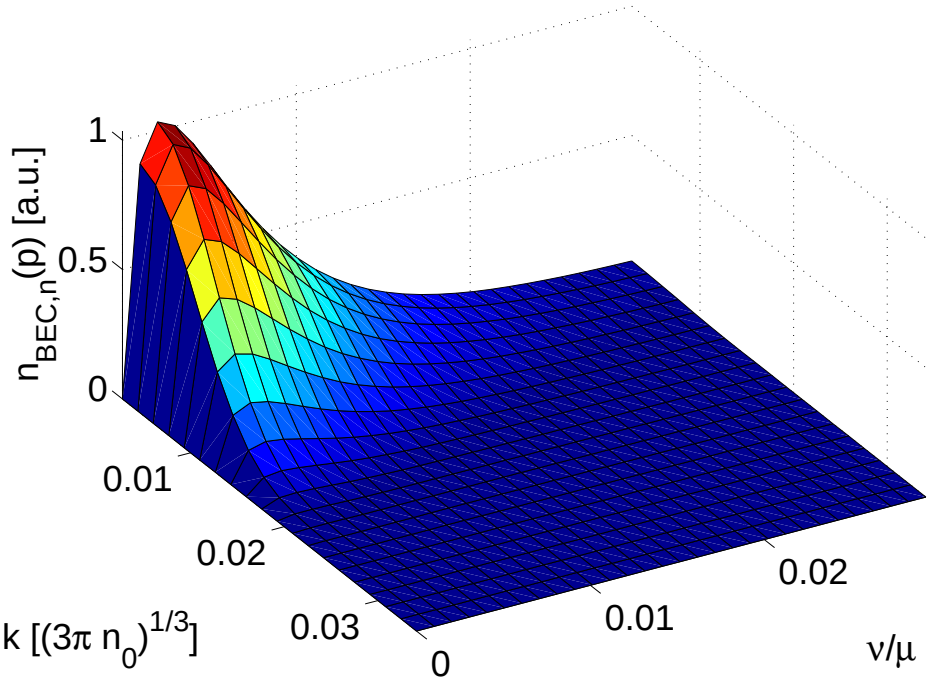

Fig. 7.2: Momentum distribution of molecules formed from a BEC of $N = 10^5$ atoms with scattering length $a = 0.01a_{\mathrm{osc}}$ at $T = 0.1T_c$ for a narrow resonance.

the density of the desired quantity at a position $\mathbf{x}$ and then integrating the result over the volume of the gas.

7.4.1 Strong coupling, $E_{\rm kin} \ll \hbar g \sqrt{N}$

To deal with the case of fermions, we modify Eq. (7.7) by reintroducing the spin of the atoms. In the spirit of the local density approximation we evaluate the resulting expectation value at every point in space in a locally homogeneous system,

$$\sum_{\mathbf{k_1},\mathbf{k_2}} \left\langle \hat{c}^\dagger_{\mathbf{p}/2-\mathbf{k_1}} \hat{c}^\dagger_{\mathbf{p}/2+\mathbf{k_1}} \hat{c}_{\mathbf{p}/2+\mathbf{k_2}} \hat{c}_{\mathbf{p}/2-\mathbf{k_2}} \right\rangle_{\mathbf{x}} = \sum_{\mathbf{k_1},\mathbf{k_2}} \delta_{\mathbf{k_1},\mathbf{k_2}} \Theta(E_F(\mathbf{x}) - \epsilon_{\mathbf{p}/2-\mathbf{k_1}}) \Theta(E_F(\mathbf{x}) - \epsilon_{\mathbf{p}/2+\mathbf{k_2}}). \quad (7.30)$$

The remaining sum counts the number of atom pairs that are eligible to form a molecule based on momentum and spin conservation. This subclass of atom pairs is illustrated in Fig. 7.3(a). The sum can be evaluated in closed form by going over to an integral,

$$F_{\rm s.c.}(\mathbf{p},\mathbf{x}) \equiv \sum_{\mathbf{k}} \Theta(E_F(\mathbf{x}) - \epsilon_{\mathbf{p}/2-\mathbf{k}}) \Theta(\epsilon_F(\mathbf{x}) - E_{\mathbf{p}/2+\mathbf{k}}) = \begin{cases} \frac{\pi k_F^3(\mathbf{x})}{12} \left(16 - 12 \frac{|\mathbf{p}|}{\hbar k_F(\mathbf{x})} + \left(\frac{|\mathbf{p}|}{\hbar k_F(\mathbf{x})} \right)^3 \right), & |\mathbf{p}| \le 2\hbar k_F(\mathbf{x}) \\ 0, & |\mathbf{p}| > 2\hbar k_F(\mathbf{x}) \end{cases} \quad (7.31)$$

Then the momentum distribution of the molecules is found by integrating the local density of molecules over all of space,

$$n_{\rm NFG,s.c.}(\mathbf{p},t) = \int d^3x (gt)^2 F_{\rm s.c.}(\mathbf{p},\mathbf{x}). \quad (7.32)$$

We carry out the integral numerically and the resulting momentum distribution is illustrated in the inset in Fig. 7.1.

The characteristic width of the momentum distribution of the molecules is $\hbar k_F \propto \hbar n_0^{1/3}$, where n_0 is the density of the atoms at the center of trap. This is typically much wider than the distribution found in the BEC case and indicates that the fermions are only correlated over distances of the order of the interparticle spacing. From Eq. (7.32) the number of molecules produced scales linearly with the number of atoms. This is because in contrast to the BEC case, the molecule production is a non-collective effect: Each atom pair is converted into a molecule independently of all the others and there is no collective enhancement.

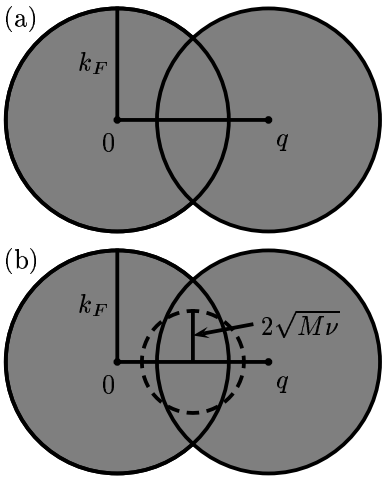

Fig. 7.3: (a) Illustration of the number of atom pairs with center of mass wave vector q. These atoms can be transformed into a molecule of momentum q if energy conservation plays no role. (b) Density of atom pairs with center of mass wave vector q and total kinetic energy $\hbar\nu$. These atom pairs can be converted into a molecule with wave vector q and detuning ν.

Similarly, we can calculate the second order correlations of the molecular field. Considering first a local position $\mathbf{x}$ in the gas we find [6]

$$\begin{aligned} g^{(2)}_{\mathrm{loc}}(\mathbf{p},\mathbf{x},t) &\equiv g^{(2)}_{\mathrm{loc}}(\mathbf{p},t;\mathbf{p},t,\mathbf{x}) \\ &= 2\left(1-\frac{1}{F_b(\mathbf{p},\mathbf{x})}\right). \end{aligned} \tag{7.33}$$

The remaining integration over $\mathbf{x}$ does not change this result in any significant way. As in the case of the BEC, the time dependence in $g^{(2)}(\mathbf{p},\mathbf{x},t)$ cancels at this level of approximation. However, in contrast to the case of a BEC there is some dependence on the momentum left.

The origin of the factor of two in $g^{(2)}(\mathbf{p},\mathbf{x},t)$ is very similar to the situation found in a chaotic light field: The two molecules that are being detected in the measurement of $g^{(2)}$ can be formed from four atoms in two different ways and the two possibilities both give the same contribution. Eq. (7.33) indicates that the statistics of the molecules are super-Poissonian, again similarly to a chaotic field.

By the following argument we can convince ourselves that not only the second-order correlations look thermal, but that the entire counting statistics of each mo-

[6] An expression for the multimode correlation function $g^{(2)}_{\mathrm{loc}}(\mathbf{p_1},t_1;\mathbf{p_2},t_2)$ can very easily be found but the result is lengthy and we refer the interested reader to Ref. [87] for details.

mentum mode is thermal. Each molecular mode characterized by the momentum **p** is coupled to a particular subset of atom pairs selected by momentum conservation. In the short time limit, each atom pair with center of mass momentum **p** is converted into a molecule in the corresponding molecular mode independently of all the other atom pairs and with uncorrelated phases. Thus we expect the number statistics of each molecular mode to be similar to that of a chaotic light field. As explained in chapter 2 the chaotic light field is a model for a thermal light field.

7.4.2 Weak coupling, $E_{kin} \gg \hbar g \sqrt{N}$

In the weak coupling limit we have to insert the fermionic expressions corresponding to Eq. (7.19) in Eq. (7.7). At position **x** we find

$$\langle \hat{a}^\dagger_{\mathbf{p}} \hat{a}_{\mathbf{p}} \rangle = \sum_{\mathbf{k}} |\Delta(E_{\mathbf{p}} - \epsilon_{\mathbf{p}/2+\mathbf{k}} - \epsilon_{\mathbf{p}/2-\mathbf{k}})|^2 \Theta(E_F(\mathbf{x}) - \epsilon_{\mathbf{p}/2-\mathbf{k}}) \Theta(\epsilon_F(\mathbf{x}) - E_{\mathbf{p}/2+\mathbf{k}}) \quad (7.34)$$

Using that $|\Delta(E,t)|^2 \to \pi g^2 t \delta(E)$ we can evaluate the sum in closed form by going over to an integral over energies and after integrating over space we find

$$n_{\mathrm{NFG,w.c.}}(\mathbf{p},t) = \frac{g^2 t}{8\pi} M^{3/2} \nu^{1/2} \int d^3x \quad \max\left(0, \min\left(2, \frac{(\hbar k_F(\mathbf{x}))^2 - p^2/4 - M\nu\hbar}{|\mathbf{p}|\sqrt{M\hbar\nu}}\right)\right). \quad (7.35)$$

The number of molecules produced is proportional to the number of atom pairs that satisfy momentum and energy conservation and hence scales linearly with the number of atoms, indicating that molecule formation is non-collective effect. Figure 7.4 shows the momentum distribution for typical parameters. It is much wider than the momentum distribution for the BEC case in both momentum space and in energy width. As far as their coherence properties are concerned the molecules look very similar to what one finds in the strong coupling regime.

We don't give the lengthy and complicated expression for $g^{(2)}_{\mathrm{loc}}(\mathbf{p}_1, t_1, \mathbf{p}_2, t_2)$ because its qualitative properties are the same as those in the broad resonance case except that the integration is now over pairs of atoms that also satisfy energy conservation. For the particular case of $\mathbf{p}_1 = \mathbf{p}_2 = \mathbf{p}$, we obtain an expression with the exact same form as Eq. (7.33) except that $F_{s.c.}(\mathbf{p}, \mathbf{x})$ must be replaced by

$$F_{w.c.}(\mathbf{p}, \nu, \mathbf{x}) = \begin{cases} \frac{M^{3/2}}{4\pi^2}\sqrt{\hbar\nu}, & \sqrt{M\hbar\nu} \le \hbar k_F(\mathbf{x}) - p/2 \\ \frac{(\hbar k_F(\mathbf{x}))^2 - p^2/4 - M\hbar\nu}{|\mathbf{p}|\sqrt{M\hbar\nu}}, & \hbar k_F(\mathbf{x}) - p/2 \le \sqrt{M\hbar\nu} \le \hbar k_F(\mathbf{x}) + p/2 \\ 0, & \sqrt{M\hbar\nu} \ge \hbar k_F(\mathbf{x}) + p/2 \end{cases} \quad (7.36)$$

which depends on **p** only in the intermediate region of detunings $\hbar k_F(\mathbf{x}) - p/2 \le \sqrt{M\hbar\nu} \le \hbar k_F(\mathbf{x}) + p/2$.

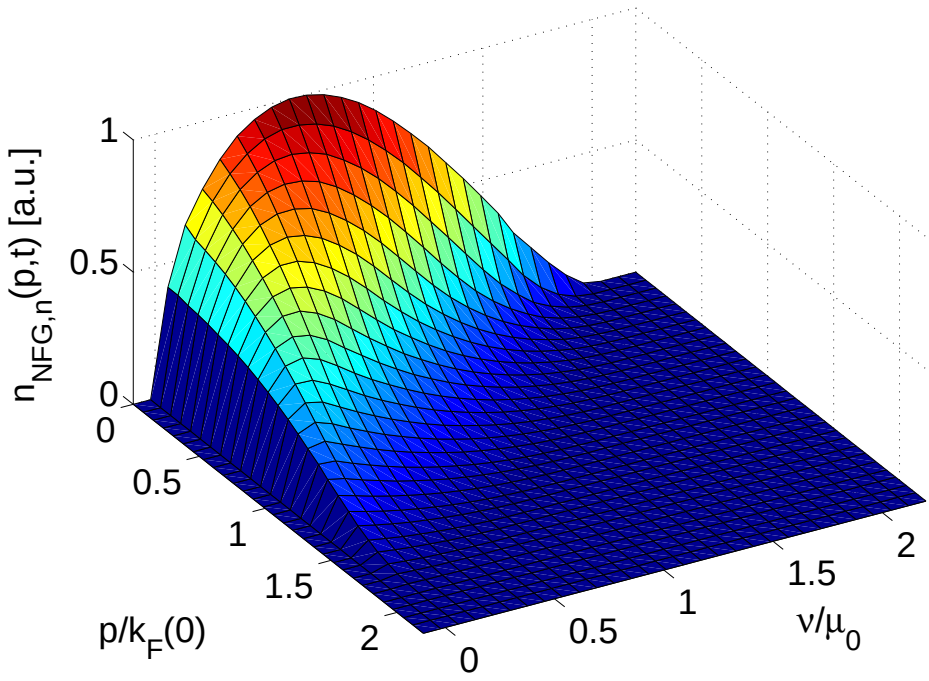

Fig. 7.4: Momentum distribution of molecules produced from a normal Fermi gas in the weak coupling limit for $\hbar g = 10^{-3}\mu$.

7.5 BCS state

We assume that the trapping potential is such that the local density approximation treatment of section 3.2.2 can be applied.

7.5.1 Strong coupling, $E_{kin} \ll \hbar g \sqrt{N}$

We find the momentum distribution of the molecules from the BCS type state by repeating the calculation done in the case of a normal Fermi gas. For the BCS wave function, the relevant atomic expectation values factorize as

$$\begin{aligned}\left\langle \hat{c}^\dagger_{\mathbf{p}/2-\mathbf{k_1},\uparrow} \hat{c}^\dagger_{\mathbf{p}/2+\mathbf{k_1},\downarrow} \hat{c}_{\mathbf{p}/2+\mathbf{k_2},\uparrow} \hat{c}_{\mathbf{p}/2-\mathbf{k_2},\downarrow} \right\rangle = \\ \left\langle \hat{c}^\dagger_{\mathbf{p}/2-\mathbf{k_1},\uparrow} \hat{c}^\dagger_{\mathbf{p}/2+\mathbf{k_1},\downarrow} \right\rangle \left\langle \hat{c}_{\mathbf{p}/2+\mathbf{k_2},\downarrow} \hat{c}_{\mathbf{p}/2-\mathbf{k_2},\uparrow} \right\rangle \\ + \left\langle \hat{c}^\dagger_{\mathbf{p}/2-\mathbf{k_1},\uparrow} \hat{c}_{\mathbf{p}/2+\mathbf{k_2},\downarrow} \right\rangle \left\langle \hat{c}^\dagger_{\mathbf{p}/2+\mathbf{k_1},\downarrow} \hat{c}_{\mathbf{p}/2-\mathbf{k_2},\uparrow} \right\rangle \end{aligned} \quad (7.37)$$

and the momentum distribution of the molecules becomes

$$\begin{aligned} n_{\mathrm{BCS,s.c.}}(\mathbf{p},t) &= (gt)^2 \left[\left| \sum_k \left\langle \hat{c}_{\mathbf{p}/2+\mathbf{k},\downarrow} \hat{c}_{\mathbf{p}/2-\mathbf{k},\uparrow} \right\rangle \right|^2 \right. \\ &\quad \left. + \sum_{\mathbf{k}} \left\langle \hat{c}^\dagger_{\mathbf{p}/2-\mathbf{k},\uparrow} \hat{c}_{\mathbf{p}/2+\mathbf{k},\downarrow} \right\rangle \left\langle \hat{c}^\dagger_{\mathbf{p}/2+\mathbf{k},\downarrow} \hat{c}_{\mathbf{p}/2-\mathbf{k},\uparrow} \right\rangle \right] \quad (7.38) \\ &\approx (gt)^2 \left| \sum_k \left\langle \hat{c}_{\mathbf{p}/2+\mathbf{k},\downarrow} \hat{c}_{\mathbf{p}/2-\mathbf{k},\uparrow} \right\rangle \right|^2 + n_{\mathrm{NFG,s.c.}}(\mathbf{p},t). \quad (7.39) \end{aligned}$$

In going from the first to the second line we have assumed that the interactions are weak enough so that the momentum distribution of the atoms is essentially that of a two component Fermi gas. This is justified because the Cooper pairing only affects the momentum distribution in a small shell of thickness $\hbar/\lambda(r) \ll \hbar k_F(r)$ around the Fermi surface.

The first term involves the square of the pairing field. It is proportional to the square of the number of paired atoms which, below the critical temperature, is a finite fraction of the total number of atoms. This quadratic dependence indicates that it is the result of a collective effect. Naturally, the contribution from the pairing field is of prime interest and we will study it in some more detail.

By going back to the position representation we can write for each term in the sum

$$\left\langle \hat{c}_{\mathbf{p}/2+\mathbf{k},\downarrow} \hat{c}_{\mathbf{p}/2-\mathbf{k},\uparrow} \right\rangle = \int \frac{d^3x}{V} e^{-i\mathbf{p}\cdot\mathbf{x}/\hbar} \int d^3r e^{-i\mathbf{k}\cdot\mathbf{r}/\hbar} \langle \hat{\psi}_\downarrow(\mathbf{x}-\mathbf{r}/2) \hat{\psi}_\uparrow(\mathbf{x}+\mathbf{r}/2) \rangle. \quad (7.40)$$

At every $\mathbf{x}$ the pair correlations decay on a length scale of order $\lambda(\mathbf{x})$. In the local density approximation we can enclose every $\mathbf{x}$ in a box in which the system can be considered homogeneous so that we find for the Fourier transform with respect to the relative coordinate

$$\int d^3r e^{-i\mathbf{k}\cdot\mathbf{r}/\hbar}\langle\hat{\psi}_\downarrow(\mathbf{x}-\mathbf{r}/2)\hat{\psi}_\uparrow(\mathbf{x}+\mathbf{r}/2)\rangle = \langle\hat{c}_{\mathbf{k}\downarrow}\hat{c}_{-\mathbf{k}\uparrow}\rangle\Big|_{\mathbf{x}} \tag{7.41}$$

where we have used that in the BCS state

$$\langle\hat{c}_{\mathbf{p}+\mathbf{k}\downarrow}\hat{c}_{\mathbf{p}-\mathbf{k}\uparrow}\rangle = \delta_{\mathbf{p},0}\langle\hat{c}_{\mathbf{k}\downarrow}\hat{c}_{-\mathbf{k}\uparrow}\rangle$$

The expectation value on the right hand side in Eq. (7.41) is easily evaluated in the Bogoliubov approximation in the locally homogeneous box enclosing x. The sum over the relative momenta $\mathbf{k}$ can then easily be done by using the gap equation and we see that the coherent contribution in the momentum distribution of the molecules is given by the absolute magnitude squared of the Fourier transform of the local gap $\Delta(\mathbf{x})$. Inserting the result into Eq. (7.39) we find

$$n_{\mathrm{BCS,s.c.}}(\mathbf{p},t) = (gt)^2\left[\left|\int d^3x e^{-i\mathbf{x}\cdot\mathbf{p}}\left(1-\frac{2a\Lambda}{\pi}\right)\frac{2\Delta(x)}{U_0}\right|^2 + n_{\mathrm{NFG,s.c.}}(\mathbf{p},t)\right]. \tag{7.42}$$

Following ref. [56] we have replaced the bare background coupling strength by

$$U_0 = U_0\frac{1}{1-\frac{2a\Lambda}{\pi}}, \tag{7.43}$$

where Λ is a momentum cut-off and is of the order of the inverse of the range of the inter-atomic potential.

Using the numerically determined $\Delta(x)$ we can readily perform the remaining Fourier transform in Eq. (7.42). The result of such a calculation is shown in Fig. 7.1. Since the gap parameter changes over distances of order R_{TF} the contribution from the pairing field has a typical width of order $\hbar/R_{TF}$. This is very similar to the BEC case. The background from the unpaired atoms on the other hand has a typical width $\hbar k_F(0) = \hbar(3\pi^2 n_0)^{1/3}$ which is similar to the width of the noise contribution in the BEC case, see inset in Fig. 7.1.

Because of the collective nature of the coherent contribution it dominates over the background, $n_{\mathrm{NFG,s.c.}}$ for strong enough interactions and large enough particle numbers. The narrow width and the collective enhancement of the molecule production are the reasons why the momentum distribution of the molecules is such an excellent indicator of the presence of a superfluid component and the off-diagonal long range order accompanying it.

For weak interactions such that the coherent contribution is small compared to the incoherent contribution, the second order correlations are close to those of a

normal Fermi gas given by Eq. (7.33), $g^{(2)}(\mathbf{p},\mathbf{x},t) \approx 2$. However, in the strongly interacting regime, $k_F|a| \sim 1$, and large N, the coherent contribution from the paired atoms dominates over the incoherent contribution from unpaired atoms. In this limit one finds that the second-order correlation is close to that of the BEC, $g^{(2)}(\mathbf{p},\mathbf{x},t) \approx 1$. The physical reason for this is that at the level of evenorder correlations the pairing field behaves just like the mean field of the condensate. This is clear from the factorization property of the atomic correlation functions, Eq. (7.37), in terms of the normal component of the density and the anomalous density contribution due to the mean field. In this case, the leading order terms in N are given by the anomalous averages. In the strongly interacting limit, the contribution from the 'unpaired' atoms is very similar in nature to the contribution from the fluctuations in the BEC case.

7.5.2 Weak coupling, $E_{\rm kin} \gg \hbar g\sqrt{N}$

A calculation similar to the BEC case leads to

$$n_{\rm BCS,w.c.}(\mathbf{p},t) = \left|\sum_{\mathbf{k}} \Delta(\hbar\nu - (\hbar k)^2/M)\langle \hat{c}_{\mathbf{p}/2+\mathbf{k},\downarrow}\hat{c}_{\mathbf{p}/2-\mathbf{k},\uparrow}\rangle\right|^2 + n_{\rm NFG,w.c.}(\mathbf{p},t), \quad (7.44)$$

where we have assumed again that the gas is weakly interacting. Inserting Eq. (7.20) for Δ in the limit $\nu t \to \infty$ and performing similar manipulations as in the broad resonance case leads to

$$\begin{aligned} n_{\rm BCS,w.c.}(\mathbf{p},t) &= \frac{g^2M^3}{\pi^2\hbar^2p^2}\left|\int_0^\infty dE\,\sqrt{E}\left(\pi\delta(\hbar\nu-E) + i\mathbf{P}\frac{1}{\hbar\nu-E}\right)\right. \\ &\left.\int_0^{R_{\rm TF}} dr r\sin(pr)\langle \hat{c}_{\sqrt{ME},\downarrow}\hat{c}_{-\sqrt{ME},\uparrow}\rangle\right|_r^2 + n_{\rm NFG,w.c.} \quad (7.45) \end{aligned}$$

where again the pairing field $\langle \hat{c}_{k,\downarrow}\hat{c}_{-k,\uparrow}\rangle|_r = u_k(r)v_k(r)$ can be evaluated using the local density approximation. Figure 7.5 shows an example of the pairing field across the trap. Two qualitatively different cases have to be distinguished depending on the strength of the interactions.

If the interactions are fairly strong so that the pairing field, $u_k(r)v_k(r)$, is nonzero in a rather wide region around $k_F(r)$, the pairing field will be a slowly varying function across the atomic cloud. Then the remaining integral in eq. (7.45) can be easily evaluated numerically and we find a momentum distribution of the molecules which is similar to the BEC case. This limit is illustrated in fig. 7.6. The width of the momentum distribution of the molecules is again of order $\hbar/R_{TF}$. It is known that in the strongly interacting limit, the size of the Cooper pairs becomes comparable to the interparticle spacing, $\lambda(r) \sim 1/k_F(r)$. The Cooper pairs

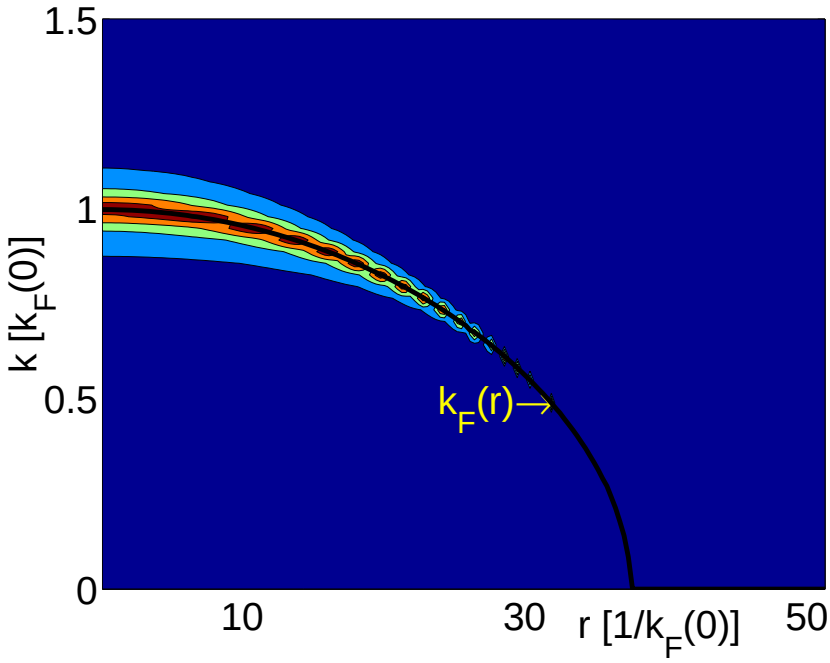

Fig. 7.5: Pairing field $\langle \hat{c}_{\mathbf{k},\downarrow} \hat{c}_{-\mathbf{k},\uparrow} \rangle = u_k v_k$ across the trap for $k_F a = 0.5$ and $a_{\mathrm{osc}} = 5k_F^{-1}(0)$. The black solid line indicates the local Fermi momentum $k_F(r)$.

are no longer delocalized across the extent of the cloud but now approach the limit of localized bosonic "quasi-molecules", i.e. molecules stabilized by the underlying Fermi sea. Thus it is not surprising that the momentum distribution of molecules formed from a BCS type state approaches the one we found in the BEC case.

On the other hand, if the interactions between the atoms are weak the pairing field is a very narrow function of momentum and hence, for fixed momentum, also of position as can be seen from Fig. 7.5. Then the integral in Eq. (7.45) has contributions from a rather narrow region in space only and the momentum distribution will accordingly become wider and smaller.

Probing the BCS system in the narrow resonance regime also yields spatial information about the atomic state. By tuning $\nu = 2\mu_{\rm loc}(r)$ the molecular signal is most sensitive to the pairing field near r and less sensitive to other regions in the trap.

A qualitative difference between the BCS and BEC cases becomes apparent if one looks at the number of molecules as a function of the detuning. While we find that there is only a very narrow distribution of detunings with width $\sim \frac{(\hbar/R_{TF})^2}{2M}$ that leads to molecule formation in the BEC case, molecules are being formed for detunings well below $\nu \sim 2\mu_0$. The non-homogeneity of the trapped atom system manifests itself in a completely different way in the two cases. In the BEC case, the total energy of a particle in the condensate is just the chemical potential while the kinetic energy of a particle is very small compared to the mean field energy in the Thomas Fermi limit. Upon release, the atoms in the condensate all have a spread in kinetic energies that is of the order $\frac{(\hbar/R_{TF})^2}{2M}$ entirely due to zero point motion. On the other hand, in the BCS case the superfluid forms at each position near the local Fermi momentum. Hence, atoms in the BCS state have a large energy spread that is of order $\sim \mu_0$ with the kinetic energies of the paired atoms being centered around $\mu_{\rm loc}(r)$ with a width $\Delta(r)$.

For the second order moment, $g^{(2)}(\mathbf{p}, \mathbf{x}, t)$, the same general arguments that were put forward in the discussion of the strong coupling regime also apply to the weak coupling regime. In the strongly interacting limit, the molecular field is again approximately coherent with a noise contribution from the unpaired fermions.

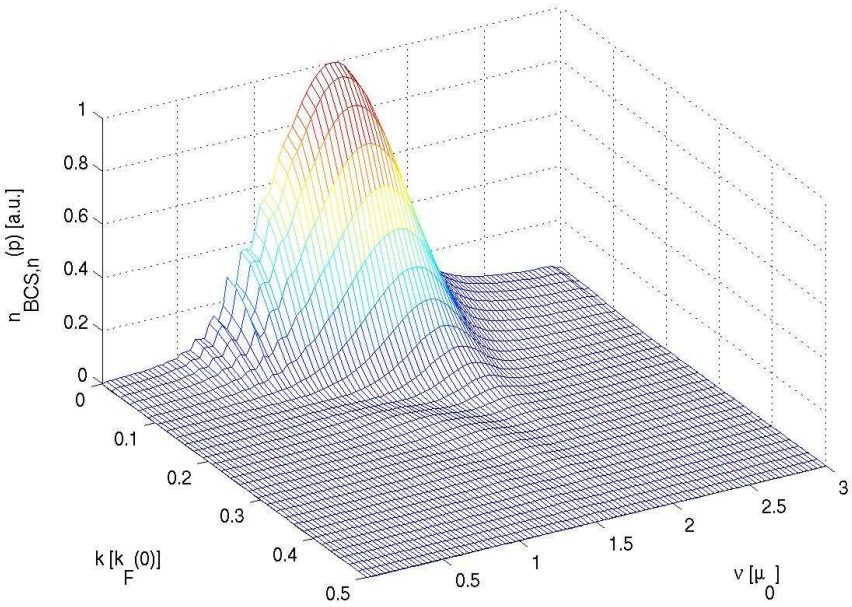

Fig. 7.6: Momentum distribution of molecules formed from a strong coupling ($k_F a = 0.5$) BCS system in the narrow resonance regime as a function of detuning ν for $a_{\mathrm{osc}} = 5k_F^{-1}(0)$. Well below $\hbar\nu = 2\mu$ the figure is a bit noisy because the Fourier transform in eq. (7.45) gets its main contribution from a very narrow region in space where the solution of the gap equation is numerically challenging.

8. FULL COUNTING STATISTICS OF ULTRACOLD MOLECULES

In the previous chapter we have studied the momentum distribution of ultra-cold molecules formed from different atomic states. The multimode theory employed allowed us to study the correlations with spatial resolution. Due to the complexity of the model we were limited to perturbation theory. Such a theory is clearly not well suited to study higher order correlations due to its great complexity.

In this chapter we will take a complementary point of view: We make the single mode approximation for the molecular field which enables us to solve for the system's dynamics exactly by numerically integrating the Schrödinger equation. Thus we have access to all orders of correlation functions and as an example we will calculate the full counting statistics of the molecular field. We analyze how the full counting statistics depends on the statistics and correlations of the atoms. Specifically, we study the three cases of the initial atoms being a BEC, a normal Fermi gas (NFG) and a Fermi gas with superfluid component. On the downside we will no longer be able to say anything about the spatial properties of the molecular correlations.

Besides being interesting in its own right, such an analysis is crucial for an understanding of several recent experiments that used a "projection" onto molecules to detect BCS-type superfluidity in fermionic systems [99, 117]. The results of this chapter confirm that the statistical properties of the molecular field indeed reflect properties of the initial atomic state and are a sensitive probe for superfluidity.

8.1 BEC

The coupling between atoms in a BEC and molecules in the single mode approximation is described by Eq. (3.112) so that, including the detuning between atoms

and molecules ν, the system is described by[1] [61, 5]

$$\hat{H}_{\mathrm{BEC}} = \hbar\nu\hat{a}^\dagger\hat{a} + \hbar g\left(\hat{a}^\dagger\hat{c}^2 + \hat{a}\hat{c}^{\dagger 2}\right), \tag{8.1}$$

where we have omitted the tilde on the effective coupling constant.

We consider the initial state of the system with all atoms in the condensate and no molecules,

$$|\psi(t=0)\rangle = \frac{\hat{c}^{\dagger N_a}}{\sqrt{N_a!}}|0\rangle. \tag{8.2}$$

where $N_a = 2N_{\mathrm{max}}$ is the number of atoms, N_{max} is the maximum possible number of molecules and $|0\rangle$ is the vacuum of both molecules and atoms. For simplicity we only consider the case of even numbers of atoms. The case of an odd number of atoms is qualitatively identical. The Hamiltonian Eq. (8.1) clearly conserves the total number of free and bound atoms, $2\hat{b}^\dagger\hat{b} + \hat{c}^\dagger\hat{c}$. Therefore, the evolution of the system from the initial state Eq. (8.2) can be described in the basis

$$|\phi_n\rangle = \frac{\hat{b}^{\dagger n}\hat{c}^{2n}|\psi(t=0)\rangle}{\mathcal{N}_n}, \quad n = 0, 1, \ldots, N_{\mathrm{max}}, \tag{8.3}$$

with

$$\mathcal{N}_n = \sqrt{\frac{(N_a - 2n)!}{n!N_a!}}$$

a normalization constant. $|\phi_n\rangle$ is a state with n molecules and $2(N_{\mathrm{max}} - n)$ atoms.

Expanding the state of the system on this basis as $|\psi(t)\rangle = \sum_n y_n|\phi_n\rangle$ we can write the Schrödinger equation as

$$i\frac{dy_n}{dt} = g\sqrt{N-n+1}\sqrt{N-n+2}\sqrt{n}y_{n-1} + g\sqrt{N-n}\sqrt{N-n-1}\sqrt{n+1}y_{n+1} + \nu n y_n. \tag{8.4}$$

This set of N_{max} coupled ordinary differential equations is easily solved numerically. We integrate the equations using a fourth order Runge Kutta method with fixed stepsize. In our case, integration using Runge-Kutta has the advantage that we only need to store state vectors. A direct diagonalization of the Hamiltonian on the other hand would require us to store matrices, which leads to serious limitations for the large dimensions of the Hilbert space we need to consider, especially for the fermions below.

From the numerical solution of the Schrödinger equation we then find the molecule statistics $P_n(t) = |y_n(t)|^2$.

[1] The mean field interactions between atoms give rise to a term proportional $\hat{c}^\dagger\hat{c}^\dagger\hat{c}\hat{c}$ which has been neglected in Eq. (8.1). This can be justified as in the previous chapter by assuming that the interactions between the atoms are switched off at $t = 0$ using a Feshbach resonance.

Figure 8.1 shows $P_n(t)$ for 30 initial atom pairs and $\nu = 0$. Starting in the state with zero molecules, a wave-packet-like structure forms and propagates in the direction of increasing n. Near $N_{\max}$ the molecules begin to dissociate back into atom pairs.

We can gain further insight into the short-time dynamics of molecule formation by using first-order perturbation theory [71, 84] similar to the calculations of the previous chapter. We expand the mean number of molecules in a Taylor series around $t = 0$,

$$n(t) = \langle \hat{a}^\dagger \hat{a} \rangle = \sum_{j=0}^{\infty} \frac{t^j}{j!} \frac{\partial^j}{\partial t^j} \langle \hat{a}^\dagger \hat{a} \rangle \Big|_{t=0}. \tag{8.5}$$

We can differentiate under the average sign using the product rule, carefully maintaining the ordering of the operators. Making use of the Heisenberg equations of motion to calculate the derivatives and evaluating the resulting expectation values in the initial state Eq. (8.2) gives

$$n(t) = (gt)^2 2N_{\max}(2N_{\max} - 1) + O((gt)^4) \tag{8.6}$$

and the second factorial moment

$$\begin{aligned} g^{(2)}(t_1, t_2) &\equiv \frac{\langle \hat{b}^\dagger(t_1)\hat{b}^\dagger(t_2)\hat{b}(t_2)\hat{b}(t_1)\rangle}{\langle \hat{b}^\dagger(t_1)\hat{b}(t_1)\rangle\langle \hat{b}^\dagger(t_2)\hat{b}(t_2)\rangle} \\ &= \frac{(2N_{\max} - 2)(2N_{\max} - 3)}{2N_{\max}(2N_{\max} - 1)} \\ &= 1 - \frac{2}{N_{\max}} + O(N_{\max}^{-2}). \end{aligned} \tag{8.7}$$

$n(t)$ is proportional to the square of the number of atoms, which again shows that the molecule production from a BEC is a collective effect. For $N_{\max}$ large enough we have $g^{(2)}(t_1, t_2) \to 1$, the value characteristic of a Glauber coherent field. From $g^{(2)}$ and $n(t)$ we also find the relative width of the molecule number distribution as

$$\frac{\sqrt{\langle (\hat{n} - n)^2 \rangle}}{n} = \sqrt{g^{(2)} + n^{-1} - 1}. \tag{8.8}$$

It approaches $n^{-1/2}$ in the limit of large $N_{\max}$, typical of a Poisson distribution. This confirms that for short enough times, the molecular field is coherent in the sense of quantum optics.

8.2 Normal Fermi gas

Let us now turn to the case of photoassociation from two different species of non-interacting ultra-cold fermions. In the single mode approximation for the

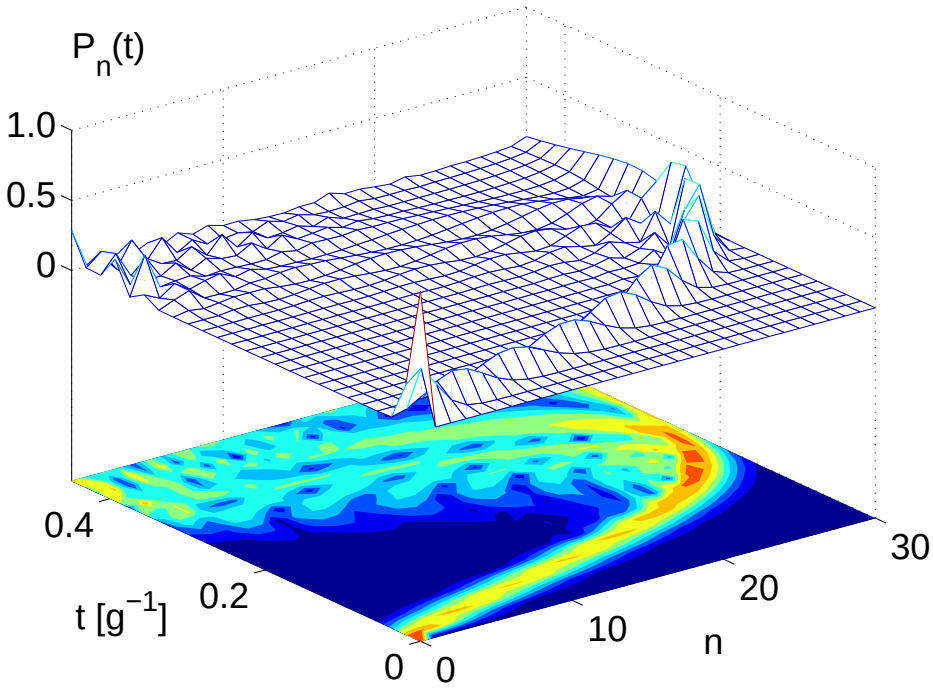

Fig. 8.1: Number statistics of molecules formed from a BEC with $N_{\max} = 30$ and $\nu = 0$.

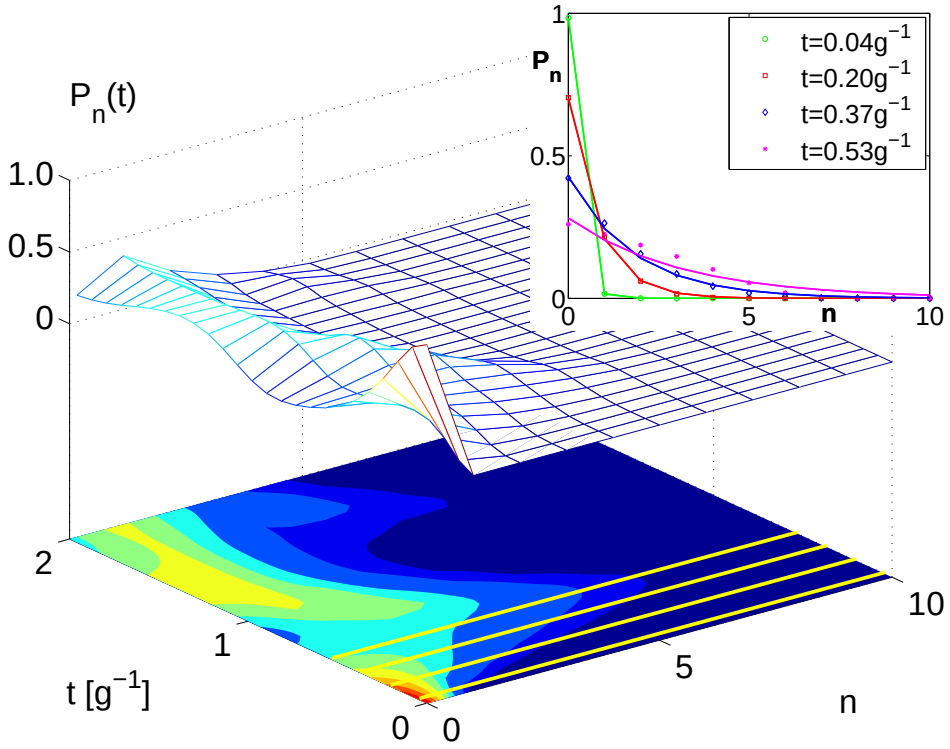

Fig. 8.2: Number statistics of molecules formed from a normal Fermi gas. This simulation is for $N_a = 20$ atoms, the detuning is $\nu = 0$, the Fermi energy is $\mu = 0.1\hbar g$ and the momentum of the i-th pair is $|k_i| = (i-1)2k_F/(N_a/2-1)$. The inset shows fits of the number statistics to thermal distributions for various times as marked by the thick yellow lines in the main figure.

molecules and assuming that the molecules are created at rest the atom-molecule coupling is described by Eq. (5.10). We do not make the degeneracy approximation because the kinetic energies of the atoms are essential in the BCS case studied below. This will also allow us to directly compare the normal Fermi gas results with the BCS results.

Figure 8.2 shows the molecule statistics obtained by a numerical integration of the Schrödinger equation corresponding to the Hamiltonian (5.10). The result is clearly both qualitatively and quantitatively very different from the case of molecule formation from an atomic BEC.

From the Tavis-Cummings model analogy we expect that for short times the statistics of the molecular field should be chaotic, or “thermal”, much like those of a single-mode chaotic light field. This is because each individual atom pair ”emits” a molecule independently and without any phase relation with other pairs. That this is the case is illustrated by the inset of Fig. 8.2, which fits the molecule

statistics at selected short times with chaotic distributions of the form

$$P_{n,\text{thermal}} = \frac{e^{-n/\langle n\rangle}}{\sum_n e^{-n/\langle n\rangle}}. \tag{8.9}$$

The increasing 'pseudo-temperature' $\langle n\rangle$ corresponds to the growing average number of molecules as a function of time.

We can again determine the short-time properties of the molecular field in first-order perturbation theory. Evaluating the relevant atomic expectation values in the appropriately modified Taylor expansion Eq. (8.5) and using a Fermi sea as initial atomic state we find for the mean number of molecules

$$n(t) = (gt)^2 2N_a. \tag{8.10}$$

It is proportional to N_a, in contrast to the BEC result, where n was proportional to N_a^2, see Eq. (8.6). This is another manifestation of the independence of all the atom pairs from each other: While in the BEC case the molecule production is a collective effect with contributions from all possible atom pairs adding constructively, there is no such collective enhancement in the case of Fermions. Each atom can pair up with only one other atom to form a molecule.

For the second factorial moment we find

$$g^{(2)}(t_1, t_2) = 2\left(1 - \frac{1}{2N_a}\right), \tag{8.11}$$

which approaches two in the limit of large atom numbers, typical of a chaotic or thermal field.

8.3 Fermi gas with superfluid component

Unlike repulsive interactions, attractive interactions between fermions have a profound impact on molecule formation. As we have explained in chapter 3 attractive interactions give rise to BCS superfluidity. The molecule formation can be described in exactly the same way as in the previous section albeit with the BCS state as initial state.

In terms of the pseudo spin operators of the previous section the BCS reduced Hamiltonian can be written as [68]

$$\hat{H}_{\text{BCS}} = \hat{H}_{\text{NFG}} - V \sum_{k,k'} \hat{\sigma}_k^+ \hat{\sigma}_{k'}^-, \tag{8.12}$$

and the BCS ground state becomes

$$|\text{BCS}\rangle = \prod_k (u_k + v_k \hat{\sigma}_k^+)|\rangle, \tag{8.13}$$

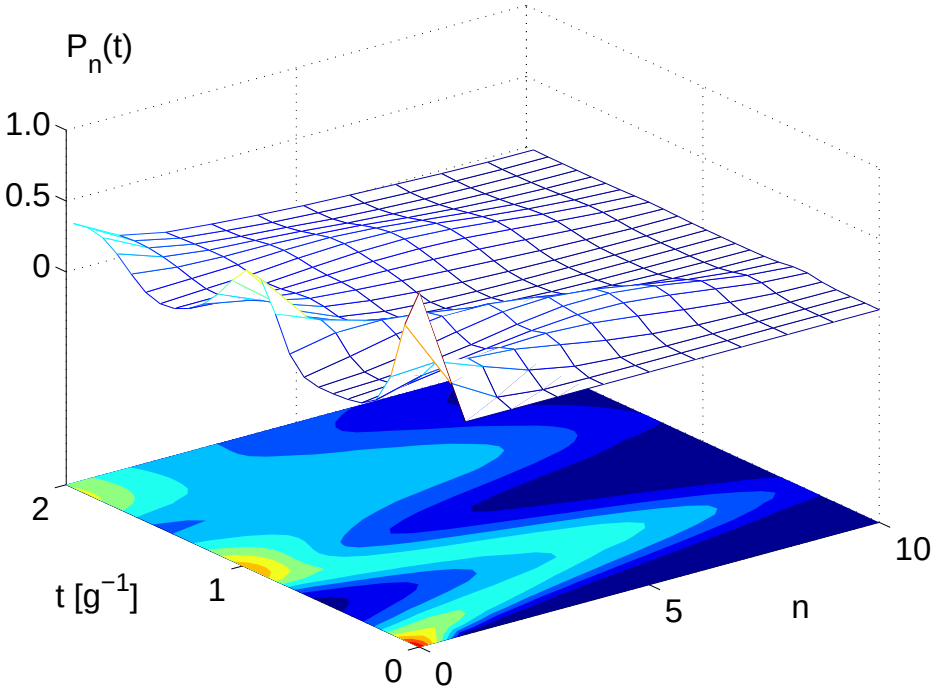

Fig. 8.3: Number statistics of molecules formed from a Fermi gas with pairing correlations. For this simulation the detuning is $\nu = 0$, the Fermi energy is $\mu = 0.1g$ and the background scattering strength is $V = 0.03g$ resulting in $N_a \approx 9.4$ atoms and a gap of $\Delta \approx 0.15g$. The momenta of the atom pairs are distributed as before in the normal Fermi gas case.

with u_k and v_k the Bogoliubov amplitudes of section 3.2.2. The gap equation can be easily solved numerically for the small number of atoms we will be considering. The dynamics is then obtained by a numerical integration of the Schrödinger equation with $|\mathrm{BCS}\rangle$ as the initial atomic state and the molecular field in the vacuum state.

Figure 8.3 shows the resulting molecule statistics for $V = 0.03\hbar g$, which corresponds to $\Delta = 0.15\hbar g = 1.5\mu$ for the system at hand. Such a large background scattering strength was chosen in order for the gap equation to have a positive solution for the small particle numbers to which we are limited by computer memory requirements. Clearly, the molecule production is much more effective than in the case of a normal Fermi gas. The molecules are produced at a higher rate and the maximum number of molecules is larger. The evolution of the number statistics is reminiscent of the BEC case.

The short-time dynamics is again obtained in first-order perturbation theory,

which gives now

$$n(t) = (gt)^2 \left(\sum_{k \neq k'} u_k v_k u_{k'} v_{k'} + \sum_k v_k^2 \right) \tag{8.14}$$

$$\approx (gt)^2 \left[\left(\frac{\Delta}{V} \right)^2 + N_a \right]. \tag{8.15}$$

In addition to the term proportional to N_a representing the incoherent contribution from the individual atom pairs that was already present in the normal Fermi gas, there is now an additional contribution proportional to $(\Delta/V)^2$. Since (Δ/V) can be interpreted as the number of Cooper pairs in the quantum-degenerate Fermi gas, this term can be understood as resulting from the conversion of Cooper pairs into molecules in a collective fashion similar to the BEC case. The collective contribution results naturally from the nonlinear coupling of the atomic field to the molecular field. This nonlinear coupling links higher-order correlations of the molecular field to lower-order correlations of the atomic field, in this case the pairing field of the atoms. For the parameters of Fig. 8.3 $\Delta/V \approx 6.5$ so that the coherent contribution from the Cooper pairs clearly dominates over the incoherent contribution from the unpaired fermions. Note that no signature of that term can be found in the momentum distribution of the atoms themselves. Their momentum distribution is given by $\langle \hat{c}^\dagger_{k,\sigma} \hat{c}_{k,\sigma} \rangle = v_k^2$ and is very similar to that of a normal Fermi gas. The short-time value of $g^{(2)}(t_1, t_2)$, shown in Fig. 8.4, decreases from the value of Eq. (8.11) for a normal Fermi gas at $\Delta = 0$ down to one as Δ increases, underlining the transition from incoherent to coherent molecule production.

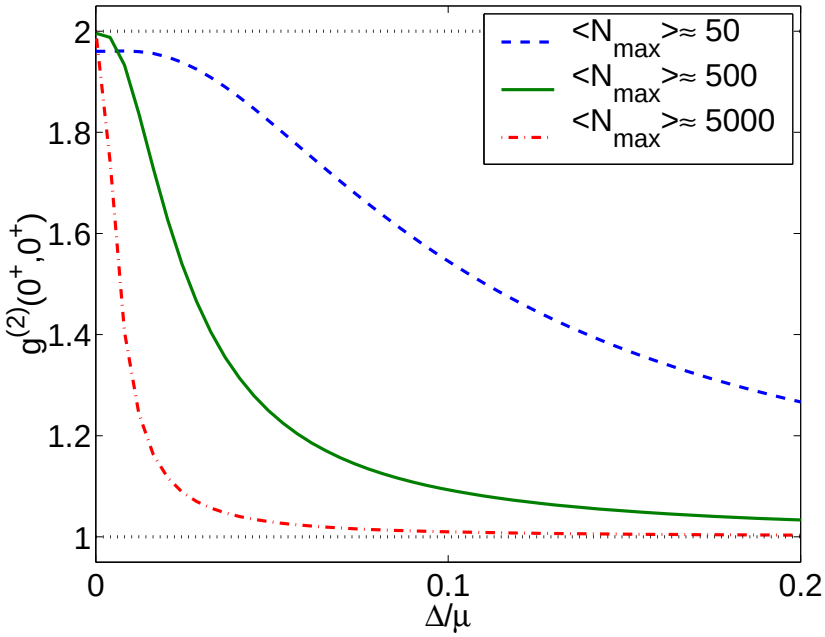

Fig. 8.4: $g^{(2)}(0^+, 0^+)$ as a function of the gap parameter Δ.

9. CONCLUSION

In this dissertation we have studied several approaches to characterize the coherence of ultra-cold atomic systems using methods of nonlinear and quantum optics. A thorough understanding of the coherence properties of ultra-cold atomic systems as well as methods to measure them are crucial for fundamental science as well as for technological applications.

In chapter 6 we have shown how the XFROG method that was first developed for the characterization of ultra-short laser pulses can be adapted for the reconstruction of the condensate wave function of a BEC in the mean field approximation. The role of the gate pulse of the optical XFROG is played by a spatially varying outcoupling potential. As a consequence the method can be implemented with purely linear physics. While in optics one commonly measures the temporal phase, the method yields the spatial phase for ultra-cold atoms.

Considering the specific example of a condensate with a single vortex we have studied the feasibility of the method through numerical simulations. We found that the method can be implemented with currently available experimental technology. As expected from the nonlinear optics experiments, the method is robust against noise in the position of the outcoupling potential and shot to shot fluctuations of the outcoupled intensity. It is insensitive to noise in the overall phase of the BEC.

In the future it will be interesting to see what can be learned about systems that cannot be described by a condensate wave function. Examples are rapidly rotating condensates, highly elongated quasi condensates and one-dimensional Tonks-Giradeau gases. Especially for quasi one-dimensional systems the XFROG method is interesting because for those systems the single shot methods that have been demonstrated in optics [63] can be used. Another future direction would be to adapt the XFROG method to the characterization of the pairing field in a BCS state.

In chapter 7 we have shown that the second order correlations of an ultra-cold atomic gas can be measured using coherent molecule formation. This is particularly relevant to studies of fermionic superfluidity that does not reveal itself in first order correlation functions. We considered the cases of molecule formation from a BEC, a normal Fermi gas and a BCS state. If the coupling between atoms and molecules is much stronger than the kinetic energies the molecules serve as broad-band detectors: While they still contain a good deal of spatial information,

they are not energy selective. If the kinetic energies are much stronger than the coupling the molecules serve as narrow-band detectors.

Using perturbation theory we have calculated the momentum distribution of the molecules. The molecules formed from a BEC have a narrow momentum distribution reflecting the long coherence length of atoms in the condensate of the order of the size of the atomic cloud R_{TF}. Condensed atoms are converted into molecules in a collective fashion: The molecule production rate scales quadratically with the number of atoms. Excitations above the condensate due to finite temperatures and interactions on the other hand give rise to a much broader background with a width of the order of the inverse of the healing length $\hbar/\xi$. The excitations are non-collectively converted into molecules.

Molecules produced from a normal Fermi gas have a broad momentum distribution with width $\sim \hbar k_F \propto \hbar n_0^{-1.3}$ because the atoms are only correlated over distances of the order of the interparticle separation $n_0^{-1/3}$. k_F is the Fermi wave vector in the center of the cloud. The molecule production is non-collective and shares many similarities with the molecule production from the excitations above a BEC.

Molecule formation from a BCS state has two contributions: The unpaired atoms behave very similar to atoms from a normal Fermi gas while the Cooper-pairs lead to collectively formed molecules with a very narrow momentum distribution of the order of the correlation length $\lambda = \frac{\hbar v_F}{\pi\Delta}$ with Δ the gap of the BCS state and v_F the Fermi velocity. Thus the emergence of a narrow peak in the momentum distribution signals the presence superfluidity. One of our main goals for the future is to incorporate more details of the two-body physics of Feshbach resonance. This should allow us to also describe molecules formed by means of sweeps of the magnetic field through the Feshbach resonance.

Chapter 8 is dedicated to the full counting statistics of molecules formed from a BEC, a normal Fermi gas and a BCS state. This is only possible in the single mode approximation for the molecular field because we have to numerically solve the Schrödinger equation in order to get the counting statistics. From the counting statistics we see that the molecules formed from a BEC are in a coherent state while the ones from a normal Fermi gas are in a thermal state. These two results were anticipated based on analogies with quantum optical systems: The molecule formation from a BEC can be mapped onto optical sum frequency generation while the molecule formation from a normal Fermi gas can be mapped onto the Tavis-Cummings model that describes the interaction of an ensemble of two level atoms with a single mode of a quantized light field. The molecules formed from a BCS state go over from one extreme to the other as a function of the gap parameter. For $\Delta = 0$ the BCS state reduces to a normal Fermi gas and for growing Δ more and more atoms form Cooper pairs and the molecular field increasingly resembles

the molecules from a BEC.

10. ZUSAMMENFASSUNG

Kohärenz ist eine sehr wichtige Eigenschaft von Feldern im allgemeinen. Grob gesprochen gibt sie an, zu welchem Grad ein Wellenfeld Interferenz zeigen kann.

Klassische und besonders quantenmechanische Felder können nach ihren Kohärenzeigenschaften klassifiziert werden. So können etwa ein klassisches Lichtfeld, das von einer spektral gefilterten thermischen Lichtquelle emittiert wird, und ein Laser praktisch identische Spektren aufweisen. Die Kohärenzlänge könnte im Prinzip gleich sein, so dass sich auch in einem gewöhnlichen Interferometer keine Unterschiede ergeben. Erst Korrelationen höherer Ordnung, in diesem Fall von mindestens zweiter Ordnung, offenbaren Unterschiede zwischen den beiden.

Besonders für Lichtfelder spielt Kohärenz seit langer Zeit eine große Rolle. Das hängt zum einen damit zusammen, dass wohldefinierte Lichtfelder, insbesondere seit der Erfindung des Lasers, relativ leicht erzeugt werden können und zum anderen ist ein gutes Verständnis der Kohärenzeigenschaften wichtig für viele Anwendungen von Laserlicht in der Grundlagenforschung und in technologischen Anwendungen. Daher ist es nicht verwunderlich, dass eine systematische Kohärenztheorie zuerst für Licht entwickelt wurde: Für klassische Felder durch Wolf [13] und für quantisierte Lichtfelder durch Glauber [47, 46].

Aus der Ähnlichkeit von Materiewellen und Lichtfeldern ergibt sich ganz natürlich die Frage, ob und in welcher Form die optische Kohärenztheorie of Materiefelder ausgedehnt werden kann. Die Übertragung von quantenoptischen Konzepten sollte es erlauben, die Fülle von Zuständen von ultrakalter Materie bezüglich ihrer Kohärenzeigenschaften zu charakterisieren und klassifizieren und einige ihrer Eigenschaften aus der Perspektive einer gut studierten und sehr ausgereiften Theorie zu verstehen. Umgekehrt ergeben sich im Kontext ultrakalter Atome neue Fragestellungen, wie z.B. bezüglich der Kohärenz von Fermionen oder durch die nichtlineare Wechselwirkung der Materiefelder, welche für Photonen in aller Regel sehr schwach ist. Diese neuen Aspekte werfen ein neues Licht auf die quantenoptischen Systeme und führen zu einem tieferen Verständnis derselben.

Das Ziel dieser Dissertation ist es, Methoden aus der nichtlinearen Optik für die Charakterisierung von Kohärenzeigenschaften von ultrakalten Atomen anzupassen. Dazu haben wir die Analogien, die zwischen optischen und atomoptischen Systemen bestehen, im Detail ausgearbeitet und mathematisch formuliert (Kapitel 5). In Kapitel 6 zeigen wir, wie die aus der Physik der ultrakalten Laserpulse be-

kannte XFROG Methode für die Bestimmung der Kondensatwellenfunktion eines BECs benutzt werden kann. Die Kapitel 7 und 8 beschäftigen sich damit, wie die kohärente Bildung von Molekülen dazu benutzt werden kann, Korrelationsfunktionen atomarer Gase von höherer Ordnung zu bestimmen.

10.1 Optische Kohärenztheorie

Selbstverständlich setzt die angestrebte Übertragung optischer Methoden auf Materiefelder eine fundierte Kenntnis der optischen Kohärenztheorie voraus. Daher sind die grundlegenden Tatsachen in Kapitel 2 in einer Weise zusammengestellt, die für die spätere Verallgemeinerung auf Atome geeignet ist und die Gemeinsamkeiten der beiden Fälle klar erkennbar macht.

Wie bereits erwähnt, wurde eine rigorose Kohärenztheorie für klassische Lichtfelder zunächst von E. Wolf formuliert. Der Kontrast des Interferenzmusters bei Überlagerung zweier Felder E_1 und E_2, die z.B. aus dem gleichen Feld an verschiedenen Orten zu verschiedenen Zeiten extrahiert sein könnten, führt Wolf dazu, die Korrelationsfunktion

$$g^{(1)} = \frac{\langle E_1^{(-)} E_2^{(+)} \rangle}{\sqrt{\langle E_1^{(-)} E_1^{(+)} \rangle} \sqrt{\langle E_2^{(-)} E_2^{(+)} \rangle}} \tag{10.1}$$

zu betrachten. Dabei sind $E_{1,2}^{(+)}$ und $E_{1,2}^{(-)}$ der positive und negative Frequenzanteil der Felder E_1 und E_2. Die Mittelwerte $\langle \ldots \rangle$ sind durch die im Vergleich zu den Fluktuationen des Lichtfeldes lange Antwortzeit typischer optischer Detektoren motiviert und sind in Wolfs ursprünglicher Theorie zeitliche Mittelwerte über statistisch stationäre Felder. Eine Erweiterung für Laserpulse ist möglich, indem man die Mittelwerte als Ensemble Mittelwerte interpretiert.

Der Betrag von $g^{(1)}$ bestimmt den Kontrast der Interferenstreifen bei Überlagerung von E_1 und E_2: Ist $|g^{(1)}| = 1$ ist der Kontrast maximal, ist $|g^{(1)}| < 1$ ist der Kontrast reduziert und für $|g^{(1)}| = 0$ werden keine Interferenzstreifen beobachtet. Felder mit $|g^{(1)}| = 1$ heißen demnach kohärent, Felder mit $|g^{(1)}| < 1$ heißen teilweise kohärent und Felder mit $|g^{(1)}| = 0$ heißen inkohärent.

Für quantisierte Lichtfelder ist eine Verschärfung des Kohärenzbegriffes nötig. Der klassische Kohärenzbegriff betrachtet lediglich die Korrelationen der Feldamplitude an zwei Raum-Zeit Punkten während für eine vollständige Charakterisierung der Kohärenz die Korrelationen des Feldes an beliebig vielen verschiedenen Punkten nötig ist. Glauber hat durch eine Analyse des Messprozesses in einem Photodetektor gezeigt, dass Mehrfachkoinzidenz Messungen, die diese Korrelationen messen, durch normalgeordnete Erwartungswerte der Feldamplitude be-

stimmt werden, z.B.

$$g^{(n)}(\mathbf{x_1}t_1,\ldots,\mathbf{x_n}t_n;\mathbf{x_{n+1}}t_{n+1},\ldots,\mathbf{x_{2n}}t_{2n}) = \frac{\langle \hat{E}^{(-)}(\mathbf{x_1},t_1)\ldots\hat{E}^{(-)}(\mathbf{x_n},t_n)\hat{E}^{(+)}(\mathbf{x_{n+1}},t_{n+1})\ldots\hat{E}^{(+)}(\mathbf{x_{2n}},t_{2n})\rangle}{\sqrt{\prod_{j=1,\ldots,2n}\langle \hat{E}^{(-)}(\mathbf{x_j},t_j)\hat{E}^{(+)}(\mathbf{x_j},t_j)\rangle}}. \quad (10.2)$$

Dabei sind $\hat{E}^{(+)}$ und $\hat{E}^{(-)}$ der positive und negative Frequenzanteil der quantisierten Lichtamplitude.

Aufbauend auf diesen Korrelationsfunktionen n-ter Ordnung und motiviert durch die klassische Kohärenztheorie führt Glauber die Kohärenz n-ter Ordnung eines Feldes ein: Ein Feld ist kohärent in n-ter Ordnung wenn alle Korrelationsfunktionen der Ordnung $m \leq n$ in ein Produkt aus $2n$ Funktionen faktorisieren. Klassische Kohärenz entspricht demnach quantenmechanischer Kohärenz erster Ordnung.

Nachdem wir diese Konzepte in Kapitel 2 einführe, disskutieren wir die Kohärenzeigenschaften einiger representativer Zustände des quantisierten Lichtfeldes. Diese Beispiele dienen hauptsächlich dazu, einige Aspekte der quantenoptischen Kohärenztheorie zu erläutern, ein intuitives Verständnis zu entwickeln und um später einige Referenzpunkte zu haben, mit denen die verschiedenen atomaren Zustände und ihre Korrelationen verglichen werden können.

Kohärente Zustände dienen als Beispiel für ein Lichtfeld, das vollständig kohärent, d.h. kohärent in jeder Ordnung ist. Anzahlzustände auf der anderen Seite haben eine wohldefinierte Intensität, zeigen jedoch “anti-bunching” und sind streng genommen lediglich kohärent in erster Ordnung. Im Grenzfall hoher Besetzungszahl nähern sich die Korrelationsfunktionen des Anzahlzustandes denen des kohärenten Zustandes an. Thermische Zustände sind ein gutes Modell für das von einer klassischen thermischen Lichtquelle erzeugte Licht. Thermisches Licht zeigt “bunching”: unmittelbar nach der Detektion eines Photons ist es doppelt so wahrscheinlich, ein weiteres Photon zu detektieren.

Chaotisches Licht ist ein wegen seiner großen Allgemeinheit wichtiges Modell für viele in der Natur vorkommende Lichtfelder. Dabei handelt es sich um die Überlagerung des Lichtes vieler voneinander unabhängiger Strahler. Je nach Wahl der Wahrscheinlichkeitsverteilung der Phasen können z.B. Stoßverbreiterte oder Dopplerverbreiterte Linien modelliert werden. Chaotisches Licht gestattet es, mit sehr wenigen Grundannahmen alle Korrelations- und statistische Eigenschaften des Lichtfeldes zu berechnen. Wie das im Detail erreicht werden kann, ist in Kapitel 2.3 näher beschrieben.

Die Zählstatistik eines Quantenfeldes steht mit seiner Kohärenz in engem Zusammenhang. Die Zählstatistik gibt an, wie wahrscheinlich es ist, eine bestimmte Anzahl von Feldquanten vorzufinden. Die Anzahlstatistik kann sehr leicht für die

aufgeführten Beispiele berechnet werden und ist in den Abbildungen 2.2, 2.3 und 2.4 illustriert.

10.2 Ultrakalte Atome und Moleküle

In Kapitel 3 zeigen wir, wie ultrakalte Atome formal beschrieben werden können, so dass die Ähnlichkeiten zu quantenoptischen Systemen offen zu Tage treten und effektiv ausgenutzt werden können. Der Beschreibung von BECs liegt die Aufspaltung des atomaren Feldoperators in einen Kondensatanteil und Fluktuationen zu Grunde. Diese Aufspaltung kann sehr allgemein aus dem Penrose-Onsager Kriterium für BEC motiviert werden. Für Atome in Fallen ist es wesentlich, die räumliche Inhomogenität einzubauen. Wir zeigen, wie das in einer einfachen Weise durch eine Kombination von lokaler Dichte Approximation für die Fluktuationen und Thomas-Fermi Approximation für das Kondensat erreicht werden kann.

Für Fermionen sind zwei Fälle zu unterscheiden. Sind die Wechselwirkungen zwischen den Atomen abstoßend, so sind die Atome in einem normalen Zustand der durch Landaus Fermi-Flüssigkeitstheorie beschrieben werden kann. Sind die Wechselwirkungen jedoch attraktiv, gehen die Fermionen bei tiefen Temperaturen in einen superfluiden Zustand über. Dieser kann mit Hilfe der Theorie von Bardeen, Cooper und Schrieffer (BCS) beschrieben werden. Auch diese Theorie kann leicht an die räumlich inhomogene Situation in einer Falle angepaßt werden.

Schließlich benötigen wir die Grundlagen von Feshbach Resonanzen, um die Kopplung der Atome and Moleküle beschreiben zu können. Zu diesem Zweck beschreiben wir die wesentlichen Aspekte der relevanten Zwei-Körper Streutheorie für ein System mit zwei Kanälen. Eine Feshbach Resonanz liegt vor, wenn die Energie der kollidierenden Teilchen im einlaufenden Kanal nahe der Energie eines gebundenen Zustandes im geschlossenen Kanal ist. Desweiteren zeigen wir, wie diese Zwei-Körper Physik effektiv in eine Vielteilchentheorie eingebaut werden kann, indem man explizit Operatoren für Moleküle im geschlossenen Kanal einführt. Schliesslich erläutern wir die Einmoden Approximation, die wir später in der Dissertation des öfteren verwenden.

10.3 Kohärenztheorie für ultrakalte Atome

Bis jetzt haben sich die meisten Experimente mit den Kohärenzeigenschaften ultrakalter Gase der ersten Ordnung beschäftig. Diese sind, wie auch im optischen Fall, am leichtesten zugänglich, da sie Messungen der atomaren Dichte erfordern. Viele Experimente wurden in enger Analogie zu konventionellen optischen Experimenten durchgeführt, wie z.B. Youngs Doppelspalt Experiment [4] oder die vielen verschiedenen Experimente mit Atomlasern [11, 69, 10]. Eine weitere Klasse

von Experimenten ziehlt darauf ab, die Kohärenzlänge von eindimensional Quasikondensaten über deren Impulsverteilung, die in engem Zusammenhang mit den Phasenfluktuationen steht, zu bestimmen [101, 42, 103, 54, 36].

Messungen von Korrelationen höherer Ordnung wurden von Greiner et. al. [51] durchgeführt, um Paarkorrelationen in fermionischen Gasen nachzuweisen. Mit einem Atomdetektor basierend auf einem optischen Resonator hoher Güte, der empfindlich genug ist, um einzelne Atome nachzuweisen, ist es in der Gruppe von T. Esslinger gelungen, Korrelationen und die Anzahlstatistik eines Atomlasers zu messen [93, 14].

Auf der theoretischen Seite haben P. Meystre et. al. versucht, eine Kohärenztheorie basierend auf einer Analyse der verschiedenen Atomdetektionsmethoden aufzubauen [48, 49, 98, 97, 104]. Die nähere Betrachtung verschiedener typischer Detektoren zeigt, dass verschiedene Detektoren verschiedene Korrelationen der Atome messen. Detektoren basierend auf Fluoreszenz messen Korrelationen der atomaren Dipoldichte, mit Laserlicht das stark verstimmt ist bezüglich der atomaren Übergangslinie lassen sich Korrelationen der Dichte der Atome im Grundzustand messen und schließlich Detektoren, die Photoionisation ausnutzen, können Korrelationen des atomaren Feldoperators selbst messen. Entsprechend diesen verschiedenen Korrelationsfunktionen ist es zweckmäßig, verschiedene Kohärenzbegriffe einzuführen, denen ähnlich Glaubers Kohärenztheorie die Faktorisierung der jeweiligen Korrelationsfunktionen zu Grunde liegt: Elektronische Kohärenz, Dichtekohärenz und Feldkohärenz.

Da die Methode zur Messung von Korrelationen zweiter Ordnung von atomaren Gasen basierend auf der kohärenten Umwandlung von Atompaaren in Moleküle, die wir weiter unten näher beschreiben, der Idee der Atomdetektion durch Photoionisation sehr ähnlich ist, werden wir sie hier etwas eingehender erläutern. Die Grundidee ist, Atome im internen Zustand $|0\rangle$ mit Hilfe eines klassischen Lichtfeldes in andere interne Zustände zu überführen, die dann als Detektorsignal dienen. Die Kopplung an die Endzustände wird durch einen Wechselwirkungs-Hamiltonoperator der Form

$$\hat{V}_{p.i.} = \sum_j \int d^3x V_{j0}(\mathbf{x})\hat{\psi}_j^\dagger(\mathbf{x})\hat{\psi}_0(\mathbf{x}) + H.C. \tag{10.3}$$

beschrieben, wobei j die verschiedenen Endzustände durchläuft, $\hat{\psi}_j(\mathbf{x})$ der Feldoperator für Atome in diesen Endzuständen ist und $\hat{\psi}(\mathbf{x})$ der Feldoperator für Atome im Anfangszustand $|0\rangle$ ist. Die Kopplungsstärken $V_{j0}(\mathbf{x})$ hängen von der Geometrie der Laser, die die verschiedenen Übergänge treiben ab, und von Eigenschaften der atomaren Zustände. Im Wechselwirkungsbild sind die Endzustände dann

$$\hat{\psi}_j(\mathbf{x}) = -\frac{i}{\hbar}\int dt V_{j0}(\mathbf{x})\hat{\psi}_0(\mathbf{x}), \tag{10.4}$$

so dass Koinzidenzmessungen der Endzustände genau wie im optischen Fall zu normalgeordneten Korrelationsfunktionen von $\hat{\psi}_0$ führen.

10.4 Analogien zwischen atomaren und quantenoptischen Systemen

Es bestehen große Ähnlichkeiten zwischen einer Reihe von quantenoptischen und atomaren Systemen. Indem wir diese Ähnlichkeiten formal ausarbeiten gelingt es, Systeme aus dem Bereich der ultrakalten Atome exakt auf die entsprechenden quantenoptischen Systeme abzubilden. Auf diese Weise ist es möglich, den großen Schatz an Erkenntnissen, der in den letzten 50 Jahren in der Quantenoptik angehäuft wurde, für das Studium ultrakalter Atome nutzbar zu machen und so zumindest qualitativ deren wichtigste Eigenschaften zu verstehen. Zugleich ist es wichtig, die Unterschiede die trotz aller Ähnlichkeit bestehen, klar zu erkennen.

Die de Broglie Wellen nicht entarteter Atome entsprechen klassischem Licht: Die Besetzungszahl einer jeden Mode ist sehr viel kleiner als eins und die Phasen verschiedener atomarer Wellenpakete sind nicht korreliert.

BECs sind in vieler Hinsicht einem Laser ähnlich. Die Kondensatwellenfunktion entspricht der Mode des Laser in einem Resonator. Ein Unterschied zwischen den beiden ist, dass BECs typischerweise eine exakte Anzahl von Bosonen enthalten. Laser auf der anderen Seite sind häufig in einer guten Approximation echte kohärente Zustände, d.h. eine Superposition von verschiedenen Anzahlzuständen. Außerdem sind die Wechselwirkungen zwischen Atomen wesentlich stärker als die zwischen Photonen in einem nichtlinearen Medium.

Für Fermionen ist die Besetzungszahl einer jeden Mode wegen des Paulischen Ausschließungsprinzips auf maximal eins beschränkt. Damit hat jede Mode exakt zwei Zustände, nämlich den besetzten und unbesetzten Zustand und damit liegt es nahe, die Moden des Systems auf effektive Zweiniveauatome abzubilden. Das ist jedoch nicht unmittelbar möglich wegen der Antisymmetry der fermionischen Wellenfunktion unter Teilchenvertauschung. Die Identifikation mit Zweiniveauatomen ist trotzdem möglich, falls die Erzeugungs- und Vernichtungsoperatoren einer Mode immer paarweise auftreten.

Ein Beispiel ist ein System von Fermionen mit zwei verschiedenen internen Zuständen $\uparrow$ und $\downarrow$. In diesem Fall können die fermionischen Erzeugungs- und Vernichtungsoperatoren für die verschiedenen Moden gemäß

$$\hat{\sigma}^x_{\mathbf{k}} = \hat{\sigma}^+_{\mathbf{k}} + \hat{\sigma}^-_{\mathbf{k}}, \quad \hat{\sigma}^y_{\mathbf{k}} = \frac{1}{i}(\hat{\sigma}^+_{\mathbf{k}} - \hat{\sigma}^-_{\mathbf{k}}), \quad \hat{\sigma}^z_{\mathbf{k}} = \hat{c}^\dagger_{\mathbf{k}\uparrow}\hat{c}_{\mathbf{k}\uparrow} - \hat{c}^\dagger_{\mathbf{k}\downarrow}\hat{c}_{\mathbf{k}\downarrow}, \tag{10.5}$$

wobei

$$\hat{\sigma}^+_{\mathbf{k}} = (\hat{\sigma}^-_{\mathbf{k}})^\dagger = \hat{c}^\dagger_{\mathbf{k}\uparrow}\hat{c}_{\mathbf{k}\downarrow}, \tag{10.6}$$

direkt auf die Pauli-Matrizen der effektiven Zweinivauatome abgebildet werden. Dieses Beispiel ist nicht gänzlich trivial da es zeigt, daß die Fermi-Dirac Statistik der Atome keine Rolle spielt, wenn ausschließlich Übergänge zwischen verschiedenen internen Zuständen auftreten, nicht aber Terme der Art $\hat{c}^{\dagger}_{\mathbf{k}'\downarrow}\hat{c}_{\mathbf{k}\uparrow}$.

Ein weiteres Beispiel ist die Abbildung von Paaren von Fermionen in verschiedenen Moden, die wir zur Beschreibung des superfluiden Zustandes in Kapitel 8 verwenden. Die Abbildung auf die effektiven Zweiniveauatome ist in den Gleichungen (5.8) und (5.9) gegeben.

10.5 Rekonstruktion von Kondensatwellenfunktionen mit Hilfe von impulsaufgelösten Kreuzkorrelationen

Die Kondensatwellenfunktion, die ein BEC in der Meanfield-Approximation beschreibt, hat eine Amplitude und eine Phase. Im Gegensatz zur Amplitude, die über die Dichte der Atome bestimmt werden kann, ist die Phase relativ schwer zu messen. Ein ganz ähnliches Problem ergibt sich für ultrakurze Laserpulse. Für diese ist es unzureichend, lediglich die Amplitude der Einhüllenden zu kennen. Für eine vollständige Charakterisierung ist eine Messung des vollständigen Feldes einschließlich der Phase nötig.

Die XFROG Methode, eine spezielle Variante der allgemeinen “Frequency Resolved Optical Gating” (FROG) Methoden, die auf Kreuzkorrelationen beruht, ist eine robuste Lösung des Problems der vollständigen Charakterisierung ultrakurzer Laserpulse. In dieser Methode wird der zu analysierende Puls $\psi(t)$ in einem nichtlinearen Kristall mit einem bekannten Referenzpuls $\psi_{\mathrm{ref}}(t)$ vergleichbarer Länge gemischt und das Spektrum des Summenfrequenzsignals

$$I_{\mathrm{XFROG}}(\omega,\tau) = \left| \int dt e^{-i\omega t}\psi(t)\psi_{\mathrm{ref}}(t-\tau) \right|^2 \tag{10.7}$$

für verschiedene Verzögerungen τ gemessen. Aus dieser sogenannten XFROG-Trace läßt sich der unbekannte Puls $\psi(t)$ numerisch rekonstruieren.

Wie wir in Kapitel 6 im Detail erklären, kann man für Atome in einem BEC mit Kondensatwellenfunktion $\psi(\mathbf{r})$ ein zu Gleichung (10.7) analoges Signal erhalten, indem man die Atome mit einem räumlich veränderlichen Potential

$$\hat{V}_J = \int d^3r V(\mathbf{r}-\mathbf{R})\hat{\psi}^{\dagger}_{\uparrow}(\mathbf{r})\hat{\psi}_{\downarrow}(\mathbf{r}) + H.C. \tag{10.8}$$

aus ihrem ursprünglichen internen Zustand $\downarrow$ in einen anderen internen Zustand $\uparrow$ “auskoppelt”. Die Impulsverteilung der $\uparrow$-Atome,

$$n(\mathbf{q},\mathbf{R}) \propto \left| \int d^3r e^{-i\mathbf{q}\mathbf{r}}\psi(\mathbf{r})V(\mathbf{r}-\mathbf{R}) \right|^2, \tag{10.9}$$

die experimentell zum Beispield durch Flugzeitaufnahmen bestimmt werden kann[1], ist von der gleichen Form wie die XFROG-Trace in Gleichung (10.7), wobei Zeiten in Orte und Frequenzen in Impulse übergehen. Das Auskopplungspotential $V(\mathbf{r} - \mathbf{R})$ spielt die Rolle des bekannten Referenzpulses.

Als Beispiel für die Anwendung dieses Verfahrens rekonstruieren wir in Kapitel 6 die Wellenfunktion eines BEC mit einem quantisierten Wirbel. Der Wirbel führt zu einer nichttrivialen Phasenstruktur: Bei einem Umlauf um das Wirbelzentrum windet sich die Phase um 2π. Wir zeigen, dass Auskopplungspotentiale V mit Abmessungen, wie sie z.B. mit Lasern für einen Raman-Übergang von $\downarrow$ nach $\uparrow$ erreicht werden können, gut geeignet sind, um den Wirbelzustand zu rekonstruieren. Außerdem kann die Anzahl der Verschiebungen $\mathbf{R}$, für die eine Messung der Impulsverteilung durchgeführt wird, ohne zu großen Qualitätsverlust in der Rekonstruktion auf eine praktisch handhabbare Zahl reduziert werden. Die Rekonstruktion ist insensitiv gegenüber Fluktuationen der globalen Phase der Kondensatwellenfunktion und die Robustheit gegenüber Fluktuationen in der relativen Verschiebung R und der Intensität des XFROG Signales ist erstaunlich groß: Fluktuationen in der Intensität von etwa 100% und in der Verschiebung von etwa 10% können bewältigt werden.

10.6 Messung von Korrelationsfunktionen zweiter Ordnung mit Molekülen

Wie erwähnt ist die Messung von Korrelationsfunktionen höherer Ordnung ungleich schwerer als Dichtemessungen. Zugleich sind Korrelationen z.B. zweiter Ordnung jedoch ein sehr wertvolles Mittel, um verschiedene Quantenzustände voneinander zu unterscheiden. So haben etwa ein normales Fermigas ohne superfluiden Anteil und ein BCS-Zustand mit superfluidem Anteil sehr ähnliche Dichte- und Impulsverteilungen, unterscheiden sich jedoch drastisch in ihren Paarkorrelationen. Ein anderes Problem ist, dass die Formulierung und Interpretation einer allgemeinen Kohärenztheorie für Fermionen weit schwieriger ist als für Bosonen.

In Kapitel 7 beschreiben wir eine Methode zur Messung von Korrelationen zweiter Ordnung mit Hilfe von Molekülen, die es erlaubt, diese Schwierigkeiten zu umgehen. Für fermionsche Atome etwa ist die Kopplung von Atomen und Molekülen durch den effektiven Hamiltonoperator in Gleichung (3.108) beschrieben. Daraus ergibt sich, dass die Moleküle an Quadrate des atomaren Feldoperators

[1] Dabei müssen die Wechselwirkungen zwischen den Atomen während der Expansion vernachlässigbar sein, was z.B. mit einer Feshbachresonanz erreicht werden kann. Für Details und weitere Messmethoden siehe Kapitel 6.

koppeln[2],

$$i\hbar\frac{d}{dt}\hat{\varphi}(\mathbf{x}) \approx \hbar g\hat{\psi}_{\uparrow}(\mathbf{x})\hat{\psi}_{\downarrow}(\mathbf{x}). \tag{10.10}$$

Als Konsequenz sind die Korrelationen der Moleküle der n-ten mit atomaren Korrelationen der $2n$-ten Ordnung verknüpft, insbesondere also die Dichte der Moleküle mit atomaren Korrelationen zweiter Ordnung. Desweiteren sind die so gebildeten Moleküle Bosonen und damit kann die Standard Kohärenztheorie auf sie angewendet werden.

Hinsichtlich der Stärke der Kopplung sind zwei Grenzfälle möglich: die Kopplung kann sehr viel stärker oder schwächer sein als die anderen atomaren oder molekularen Energien wie z.B. die kinetische Energie. Im Fall der starken Kopplung können diese anderen Energien vernachlässigt werden und die Moleküle dienen als Breitbanddetektoren: Energieerhaltung ist ähnlich dem Raman-Nath Regime der Lichtstreuung vernachlässigbar. Im umgekehrten Fall können Atome und Moleküle nur dann effektiv ineinander transferiert werden, wenn Energieerhaltung erfüllt ist. In diesem Fall stellen die Moleküle einen schmalbandigen Detektor dar. Diese Energieselektivität kann unter Umständen ausgenutzt werden, um detailliertere Informationen über den atomaren Zustand zu erhalten. Die prinzipiellen Eigenschaften der Moleküle, was ihre Kohärenz anbelangt, ist jedoch in beiden Fällen sehr ähnlich.

In Kapitel 7 betrachten wir zunächst die Bildung von Molekülen aus einem BEC mit Fluktuationen. Der Kondensatanteil führt zu einer sehr scharfen Impulsverteilung mit einer Breite von der Größenordnung $\hbar/R_{\mathrm{TF}}$, wobei R_{TF} die räumliche Ausdehnung des Kondensates ist, siehe Abbildung 7.1. Die Molekülbildungsrate ist proportional dem Quadrat der Anzahl der kondensierten Atome, d.h. Molekülbildung ist ein kollektiver Effekt. Die Fluktuationen auf der anderen Seite führen zu einem breiten Hintergrund in der Impulsverteilung der ebenfalls in Abbildung 7.1 gezeigt ist. Die Breite des Hintergrundes ist von der Größenordnung $\hbar/\xi$, wobei ξ die "healing length" des BECs ist. Die Umwandlung von Fluktuationen in Moleküle skaliert lediglich linear mit der Anzahl der Atome, d.h. sie ist nicht kollektiv verstärkt.

Moleküle gebildet aus einem zweikomponentigen normalen Fermigas sind denen aus Fluktuationen über dem Kondensat gebildeten sehr ähnlich. Ihre Impulsverteilung hat eine Breite von etwa $\hbar n_0^{1/3}$, wobei n_0 die Dichte der Atome ist. Das bedeutet, dass Atompaare nur über Entfernung von der Ordnung des internuklearen Abstandes korreliert sind. Die Molekülbildung ist nichtkollektiv. Wenn man die weiter oben erwähnte Analogie zwischen Paaren von Fermionen und Zweiniveauatomen berücksichtig, kann man die Molekülbildung in diesem Fall als die

[2] In Gleichung (10.10) haben wir die anderen Beiträge zur Dynamik der Moleküle wie kinetische Energie, Fallenpotential und Kollisionen der Einfachheit halber ausgelassen.

inkohärente Emission von Licht von einem Ensemble von Zweiniveauatomen verstehen. Das Molekulare Feld hat dementsprechend die gleichen Eigenschaften wie chaotisches Licht, siehe Kapitel 2.3.

Für den BCS-Zustand hat das molekulare Feld zwei Bestandteile, ähnlich dem obigen BEC Fall. Während die Cooper Paare kollektiv zu Molekülen mit einer scharfen Impulsverteilung mit Breite $\sim \hbar/R_{\mathrm{TF}}$ führen, sind die aus ungepaarten Atome gebildeten Moleküle denen aus einem normalen Fermigas extrem ähnlich. Die Impulsverteilungen im Falle eines normalen Fermigases sowie für den BCS-Zustand sind in Abbildung 7.1 wiedergegeben.

10.7 Zählstatistik der Moleküle

Ausgehend von den Betrachtungen des letzten Abschnittes stellt sich die Frage, wie die Korrelationen höherer Ordnung der Moleküle aussehen, wie sie vom Zustand der Atome abhängen und was man aus ihnen über den Molekülbildungsprozess lernen kann. Zu diesem Zweck betrachten wir in Kapitel 8 ein vereinfachtes Modell für das gekoppelte System von Atomen und Molekülen. In diesem Modell mit lediglich einer Mode für das Molekulare Feld kann die Schrödingergleichung numerisch gelöst werden. Somit können die Korrelationsfunktionen beliebiger Ordnung und die Zählstatistik der Moleküle berechnet werden.

Für die Molekülbildung aus einem BEC vernachlässigen wir außerdem die Fluktuationen über dem Kondensat und beschreiben demgemäß auch die Atome mit nur einer Mode. Das resultierende Modell wird durch den Hamiltonoperator (8.1) beschrieben und entspricht der optischen Summenfrequenzerzeugung. Die Zählstatistik der Moleküle ist in Abbildung 8.1 gezeigt. Bevor alle Atome in Moleküle umgewandelt sind, ist sie der Zählstatistik eines kohärenten Zustandes, d.h. einer Poisson-Verteilung, sehr ähnlich . Das unterstreicht den kohärenten Charakter der Molekülbildung in diesem Fall.

Für ein zweikomponentiges Fermi Gas ist das System in der Einmodenapproximation dem Tavis-Cummings Modell der Resonator Quantenelektrodynamik äquivalent. Dieses System beschreibt die Wechselwirkung eines Ensembles von Zweiniveauatomen mit einer Resonatormode. Demgemäß ist die Molekülbildung für kurze Zeiten chaotisch und die Zählstatistik der Moleküle gut durch eine thermische Verteilung beschrieben, siehe Abbildung 8.2. Für längere Zeiten können sich Korrelationen zwischen den verschiedenen Atompaaren aufbauen die zu einem “Superradiance”-ähnlichen Effekt führen. Dadurch kann die Molekülbildung kollektiv verstärkt werden. Dieser kollektive Superradiance-Effekt wird jedoch durch die verschiedenen kinetischen Energien der Atompaare zerstört. Die kinetischen Energien entsprechen inhomogener Verbreiterung der optischen Übergangsfrequenz im Tavis-Cummings Modell.

Im Fall von Fermionen in einem BCS Zustand finden wir wiederum zwei Beiträge zur Molekülbildung, siehe Abbildung 8.3. Die Cooper Paare werden kollektiv und kohärent in Moleküle umgewandelt und führen zu einer poissonschen Zählstatistik. Die ungepaarten Fermionen auf der anderen Seite sind unabhängig voneinander emittierenden Zweiniveauatomen ähnlich und führen zu einer viel weniger effizienten, inkohärenten Molekülbildung.

Für den BCS Zustand ist es interessant, die Molekülbildung als Funktion des superfluiden Ordnungsparameters Δ zu betrachten. Für $\Delta = 0$ geht der BCS Zustand in ein gewöhnliches Fermigas über und demgemäß ist die Molekülbildung inkohärent und nicht kollektiv. Das wird durch den Kurzzeitlimes der Korrelationsfunktion zweiter Ordnung der Moleküle $\lim_{t\to 0} g^{(2)}(t,t) = 2$ in Abbildung 8.4 bestätigt. Mit wachsendem Δ wird der Anteil der Atome in Cooper Paaren größer und größer und dementsprechend fällt $\lim_{t\to 0} g^{(2)}(t,t)$ vom thermischen Wert zwei auf den für einen kohärenten Zustand typischen Wert eins ab.

BIBLIOGRAPHY

[1] A. A. Abrikosov, L. P. Gorkov, and I. E. Dzyaloshinski. *Methods of quantum field theory in statistical physics*. Dover Publications, New York, 1975.

[2] Ehud Altman, Eugene Demler, and Mikhail D. Lukin. Probing many-body states of ultracold atoms via noise correlations. *Phys. Rev. A*, 70:013603, July 2004.

[3] M. H. Anderson, J. R. Ensher, M. R. Mathews, C. E. Wieman, and E. E. Cornell. Observation of bose-einstein condensation in a dilute atomic vapor. *Science*, 269:198, 1995.

[4] M. R. Andrews, C. G. Townsend, H.-J. Miesner, D. S. Durfee, D. M. Kurn, and W. Ketterle. Observation of interference between two bose condensates. *Science*, 275:637–641, 1997.

[5] J. R. Anglin and A. Vardi. Dynamics of two-mode bose-einstein condensate beyond mean field. *Phys. Rev. A*, 64:013605, 2001.

[6] Radka Bach and Kazimierz Rzażewski. Correlations in atomic systems: Diagnosing coherent superpositions. *Phys. Rev. Lett.*, 92(20):200401, May 2004.

[7] R. A. Barankov and L. S. Levitov. Atom-molecule coexistence and collective dynamics near a feshbach resonance of cold fermions. *Phys. Rev. Lett.*, 93(13):130403, September 2004.

[8] J. Bardeen, L. N. Cooper, and J. R. Schrieffer. Theory of superconductivity. *Phys. Rev.*, 108:1175, 1957.

[9] M. Bartenstein, A. Altmeyer, S. Riedl, S. Jochim, C. Chin, J. Hecker Denschlag, and R. Grimm. Collective excitations of a degenerate gas at the bec-bcs crossover. *Phys. Rev. Lett.*, 92:203201, 2004.

[10] I. Bloch, T. W. Hänsch, and T. Esslinger. Atom laser width cw outcoupling. *Phys. Rev. Lett.*, 82:3008, 1999.

[11] I. Bloch, T. W. Hänsch, and T. Esslinger. Measuring the temporal coherence of an atom laser beam. *Phys. Rev. Lett.*, 87:160404, 2001.

[12] N. N. Bogoliubov. *Zh. Eksp. Teor. Fiz.*, 34:58, 1958.

[13] Max Born and Emil Wolf. *Principles of Optics*. Cambridge University Press, 6th edition edition, 1980.

[14] T. Bourdel, T. Donner, A. Öttl, S. Ritter, M. Köhl, and T. Esslinger. Cavity qec detection of interfering matter waves. *Phys. Rev. A*, 73:043602, 2006.

[15] C. C. Bradley, C. A. Sackett, J. J. Tollett, and R. G. Hulet. Evidence of bose-einstein condensation in an atomic gas with attractive interactions. *Phys. Rev. Lett.*, 75:1687, 1995.

[16] C. Buggle, J. Leonard, W. von Klitzing, and J. T. M. Walraven. Interferometric determination of the s and d-wave scattering amplitudes in rb-87. *Phys. Rev. Lett.*, 93:173202, 2004.

[17] Frank Burgbacher and Jürgen Audretsch. Beam splitter for bose-einstein condensates based on bragg scattering from a cavity mode. *Phys. Rev. A*, 60(5):3385, November 1999.

[18] E. A. Burt, R. W. Christ, C. J. Myatt, M. J. Holland, E. A. Cornell, and C. E. Wieman. Coherence, correlations, and collisions: What one learns about bose-einstein condensates from their decay. *Phys. Rev. Lett.*, 79(3):337, July 1997.

[19] C. Cohen-Tannoudji, J. Dupont-Roc, and G. Grynberg. *Photons and Atoms*. Wiley-Interscience, 1997.

[20] C. Cohen-Tannoudji, J. Dupont-Roc, and G. Grynberg. Wiley-Interscience, 1998.

[21] L. Cacciapuoti, D. Hellweg, M. Kottke, T. Schulte, W. Ertmer, and J. J. Arlt. Second-order correlation function of a phase fluctuating bose-einstein condensate. *Phys. Rev. A*, 68:053612, November 2003.

[22] Kevin E. Cahill and Roy J. Glauber. Density operators for fermions. *Phys. Rev. A*, 59(2):1538, February 1999.

[23] J. L. A. Chilla and O. E. Martinez. *Opt. Lett.*, 16:39, 1991.

[24] C. Chin, M. Bartenstein, A. Altmeyer, S. Riedl, S. Jochim, J. Hecker Denschlag, and R. Grimm. Observation of the pairing gap in a strongly interacting fermi gas. *Science*, 305:1128, 2004.

[25] M. L. Chiofalo, S. J. J. M. F. Kokkelmans, J. N. Milstein, and M. J. Holland. Signatures of resonance superfluidity in a quantum fermi gas. *Phys. Rev. Lett.*, 88(9):090402, 2002.

[26] L. Cooper. Bound electron pairs in a degenerate fermi gas. *Phys. Rev.*, 104:1189, 1956.

[27] K.B. Davis, M. O. Mewes, M. R. Andrews, N. J. van Druten, D. S. Durfee, D. M. Kurn, and W. Ketterle. Bose-einstein condensation in a gas of sodium atoms. *Phys. Rev. Lett.*, 75:3969, 1995.

[28] C. Davisson and L. H. Germer. Diffraction of electrons by a crystal of nickel. *Phys. Rev.*, 30:705–740, 1927.

[29] L. de Broglie. Recherches sur la théorie des quanta, 1924. Paris, Dissertation.

[30] P.G. de Gennes. *Superconductivity of metals and alloys*. W. A. Benjamin, New York, 1966.

[31] K. W. DeLong, R. Trebino, J. Hunter, and W. E. White. Frequency-resolved optical gating with the use of second-harmonic generation. *J. Opt. Soc. Am. B*, 11:2206, 1994.

[32] K. W. DeLong, Rick Trebino, and Daniel J. Kane. Comparison of ultrashort-pulse frequency-resolved-optical-gating traces for three common beam geometries. *J. Opt. Soc. Am. B*, 11:1595, 1994.

[33] Kenneth W. DeLong, David N. Fittinghoff, and Rick Trebino. Practical issues in ultrashort-laser-pulse measurement using frequency-resolved optical gating. *IEEE J. Qantum Electron.*, 32:1253, 1996.

[34] Kenneth W. DeLong and Rick Trebino. Improved ultrahort pulse-retrieval algorithm for frequency-resolved optical gating. *J. Opt. Soc. Am. A*, 11(9):2429, 1994.

[35] Kenneth W. DeLong and Rick Trebino. Improved ultrashort pulse-retrieval algorithm for frequency-resolved optical gating. *J. Opt. Soc. Am. A*, 11(9):2429, 1994.

[36] S. Dettmer, D. Hellweg, P. Ryytty, J. J. Arlt, W. Ertmer, K. Sengstock, D. S. Petrov, G. V. Shlyapnikov, H. Kreutzmann, L. Santos, and M. Lewenstein. Observation of phase fluctuations in elongated bose-einstein condensates. *Phys. Rev. Lett.*, 87(87):160406, 2001.

[37] D. A. Duine and H. T. C. Stoof. Atom-molecule coherence in bose gases. *Phys. Rep.*, 396:115–195, 2004.

[38] S. Durr, T. Volz, N. Syassen, G. Rempe, E. van Kempen, S. Kokkelmans, B. Verhaar, and H. Friedrich. Dissociation of feshbach molecules into different partial waves. *Phys. Rev. A*, 72:052707, 2005.

[39] E. Schrödinger. *Naturwiss.*, 14:664, 1926.

[40] B. Paredes *et al. Nature (London)*, 429:277, 2004.

[41] J. R. Fienup. Phase retrieval algorithms: a comparison. *Appl. Opt.*, 21:2758, 1982.

[42] F. Gerbier, J. H. Thywissen, S. Richard, M. Hugbart, P. Bouyer, and A. Aspect. Momentum distribution and correlation function of quasicondensates in elongated traps. *Phys. Rev. A*, 67:051602, 2003.

[43] A. A. Ginzburg. *Zh. Eksp. Teor. Fiz.*, 32:1442, 1957.

[44] V. L. Ginzburg and L. D. Landau. *Zh. Eksp. Teor. Fiz.*, 20:1064, 1950.

[45] M. Girardeau. Relationship between systems of impenetrable bosons and fermions in one dimension. *J. Math. Phys.*, 1(6):516, 1960.

[46] Roy J. Glauber. Coherent and incoherent states of the radiation field. *Phys. Rev.*, 131(6):2766, September 1963.

[47] Roy J. Glauber. The quantum theory of optical coherence. *Phys. Rev.*, 130(6):2529, June 1963.

[48] E. V. Goldstein and P. Meystre. Atomic detection and matter-wave coherence. *Phys. Rev. Lett.*, 80:5036, 1998.

[49] E. V. Goldstein, O. Zobay, and P. Meystre. Coherence of atomic matter-wave fields. *Phys. Rev. A*, 58:2373, 1998.

[50] L. P. Gor'kov. *Sov. Phys. JETP*, 36:1364, 1959.

[51] M. Greiner, C. A. Regal, J. T. Stewart, and D. S. Jin. Probing pair-correlated fermionic atoms through correlations in atom shot noise. *Phys. Rev. Lett.*, 94:110401, 2005.

[52] Markus Greiner, Olaf Mandel, Tilman Esslinger, Theodor W. Hänsch, and Immanuel Bloch. Quantum phase transition from a superfluid to a mott insulator in a gas of ultracold atoms. *Nature (London)*, 415:39, January 2002.

[53] Markus Greiner, Olaf Mandel, Theodor W. Hänsch, and Immanuel Bloch. Collapse and revival of the matter wave field of a bose-einstein condensate. *Nature (London)*, 419:51, September 2002.

[54] D. Hellweg, L. Cacciapuoti, M. Kottke, T. Schulte, K. Sengstock, W. Ertmer, and J. J. Arlt. Measurement of the spatial correlation function of phase fluctuating bose-einstein condensates. *Phys. Rev. Lett.*, 91:010406, 2003.

[55] D. Hellweg, L. Cacciapuoti, M. Kottke, T. Schulte, K. Sengstock, W. Ertmer, and J. J. Arlt. Measurement of the spatial correlation function of phase fluctuating bose-einstein condensates. *Phys. Rev. Lett.*, 91(1):010406, July 2003.

[56] M. Houbiers, R. Ferwerda, H. T. C. Stoof, W. I. McAlexander, C. A. Sackett, and R. G. Hulet. Superfluid state of atomic ^{6}Li in a magnetic trap. *Phys. Rev. A*, 56(6):4864, December 1997.

[57] Kerson Huang. *Statistical Mechanics*. John Wiley & Sons, New York, 1987.

[58] S. Inouye, M. R. Andrews, J. Stenger, H.-J. Miesner, D. M. Stamper-Kurn, and W. Ketterle. Observation of feshbach resonances in a bose-einstein condensate. *Nature (London)*, 392:151, 1998.

[59] J. D. Jackson. *Classical Electrodynamics*. Wiley, 3rd edition, 1998.

[60] J. Javanainen, M. Kostrun, Y. Zheng, A. Carmichael, U. Shrestha, P. J. Meinel, M. Mackie, O. Dannenberg, and K-A. Suominen. Collective molecule formation in a degenerate fermi gas via a feshbach resonance. *Phys. Rev. Lett.*, 92:200402, May 2004.

[61] Juha Javanainen and Matt Mackie. Coherent photoassociation of a bose-einstein condensate. *Phys. Rev. A*, 59(5):R3186, May 1999.

[62] D. J. Kane and R. Trebino. Characterization of arbitrary femtosecond pulses using frequency-resolved optical gating. *IEEE J. Quantum Electron.*, 29(2):571, 1993.

[63] D. J. Kane and R. Trebino. Single-shot measurement of the intensity and phase of an arbitrary ultrashort pulse by using frequency-resolved optical gating. *Opt. Lett*, 18(10):823, 1993.

[64] M. Kasevich, D. S. Weiss, E. Riis, K. Moler, S. Kasasi, and S. Chu. *Phys. Rev. Lett.*, 66:2297, 1991.

[65] D. W. Keith, C. R. Ekstrom, Q. A. Turchette, and D. E. Pritchard. An interferometer for atoms. *Phys. Rev. Lett.*, 66:2693, 1991.

[66] W. Ketterle, D. S. Durfee, and D. M. Stamper-Kurn. Making, probing and understanding bose-einstein condensates. In M. Inguscio, S. Stringari, and C. E. Wieman, editors, *Bose-Einstein condensation in atomic gases*, pages 67–176. Proceedings of the International School of Physics "Enrico Fermi", Course CXL, IOS Press, Amsterdam, 1999.

[67] J. Kinast, S. L. Hemmer, M. Gehm, A. Turlapov, and J. E. Thomas. Evidence for superfluidity in a resonantly interacting fermi gas. *Phys. Rev. Lett.*, 92:150402, 2004.

[68] Charles Kittel. *Quantum theory of solids*. John Wiley & Sons, 2nd edition edition, 1987.

[69] M. Köhl, T. W. Hänsch, and T. Esslinger. Continous detection of an atom laser beam. *Phys. Rev. A*, 65:021606(R), 2002.

[70] T. Köhler, K. Gorald, and P. S. Julienne. Production of cold molecules via magnetically tunable feshbach resonances. *To appear in Rev. Mod. Phys.*, 2006.

[71] M. Kozierowski and R. Tanaś. Quantum fluctuations in second-harmonic light generation. *Opt. Commun.*, 21(2):229, May 1977.

[72] L. D. Landau, E. M. Lifschitz, and L. P. Pitajewski. *Statistische Physik, Teil 1*. Akademie-Verlag, Berlin, 8th edition, 1987.

[73] L. D. Landau, E. M. Lifshitz, and L. P. Pitaevski. *Statistical Physics, Part 2*. Butterworth-Heinemann, 3rd edition edition, 1980.

[74] Anthony J. Leggett. Bose-einstein condensation in the alkali gases: Some fundamental concepts. *Rev. Mod. Phys.*, 73:307, April 2001.

[75] A. Lenef, T. D. Hammond, E. T. Smith, M. S. Chapman, R. A. Rubenstein, and D. E. Pritchard. Rotation sensing with an atom interferometer. *Phys. Rev. Lett.*, 78:760, 1997.

[76] Elliot H. Lieb. Exact analysis of an interacting bose gas. ii. the excitation spectrum. *Phys. Rev.*, 130:1616, 1963.

[77] Elliot H. Lieb and Werner Liniger. Exact analysis of an interacting bose gas. i. the general solution and the ground state. *Phys. Rev.*, 130:1605, 1963.

[78] E. M. Lifshitz and L. D. Landau. *Quantum Mechanics: Non-relativistic theory*. Butterworth-Heinemann, 3rd edition edition, 1981.

[79] S. Linden, H. Giessen, and J. Kuhl. Xfrog - a new method for amplitude and phase characterization of weak ultrashort pulses. *Phys. Status Solidi B*, 206:119, 1998.

[80] F. London. Macroscopic interpretation of supraconductivity. *Proc. Roy. Soc., London*, 152:24–34, 1935.

[81] F. London and H. London. The electromagnetic equations of the supraconductor. *Proc. Roy. Soc., London*, 149:71–88, 1935.

[82] F. London, H. London, and M. v. Laue. Zur theorie der supraleitung. *Zs. f. Phys.*, 96:359–364, 1935.

[83] Rodney Loudon. *The Quantum Theory of Light*. Oxford Science Publications, 3rd edition edition, 2003.

[84] L. Mandel. Squeezing and photon antibunching in harmonic generation. *Opt. Commun.*, 42(6):437, August 1982.

[85] L. Mandel and E. Wolf. Cambridge University Press, 1995.

[86] M. R. Matthews, B. P. Anderson, P. C. Haljan, D. S. Hall, C. E. Wieman, and E. A. Cornell. Vortices in a bose-einstein condensate. *Phys. Rev. Lett.*, 83:2498, 1999.

[87] D. Meiser, C. P. Search, and P. Meystre. Molecule formation as a diagnostic tool for second order correlations of ultra-cold gases. *Phys. Rev. A*, 71:033621, 2005.

[88] Eugen Merzbacher. *Quantum Mechanics*. John Wiley & Sons, New York, third edition, 1998.

[89] Pierre Meystre and M. Sargent III. *Elements of Quantum Optics*. Springer-Verlag, 3rd edition, 1999.

[90] T. Miyakawa and P. Meystre. Boson-fermion coherence in a spherically symmetric harmonic trap. *Phys. Rev. A*, 71:033624, 2005.

[91] M. Naraschewski and R. J. Glauber. Spatial coherence and density correlations of trapped bose gases. *Phys. Rev. A*, 59(6):4595, June 1999.

[92] Y. Ohashi and A. Griffin. *Phys. Rev. Lett.*, 89:130402, 2002.

[93] A. Öttl, S. Ritter, M. Köhl, and T. Esslinger. Correlations and counting statistics of an atom laser. *Phys. Rev. Lett.*, 95:090404, 2005.

[94] Oliver Penrose and Lars Onsager. Bose-einstein condensation and liquid helium. *Phys. Rev.*, 104(3):576–584, 1956.

[95] C. J. Pethick and H. Smith. *Bose-Einstein condensation in dilute gases*. Cambridge University Publications, 2002.

[96] H. David Politzer. Bose-stimulated scattering off a cold atom trap. *Phys. Rev. A*, 55(2):1140, 1997.

[97] G. Prataviera, E. V. Goldstein, and P. Meystre. Mutual coherence of optical and matter waves. *Phys. Rev. A*, 60:4846, 1999.

[98] G. Prataviera, J. Zapata, and P. Meystre. Higher order mutual coherence of optical and matter waves. *Phys. Rev. A*, 62:023605, 2000.

[99] C. A. Regal, M. Greiner, and D. S. Jin. Observation of resonance condensation of fermionic atom pairs. *Phys. Rev. Lett.*, 92(4):040403, January 2004.

[100] C. A. Regal, M. Greiner, and D. S. Jin. Observation of resonance condensation of fermionic atom pairs. *Phys. Rev. Lett.*, 92:040403, 2004.

[101] S. Richard, F. Gerbier, J. H. Thywissen, M. Hugbart, P. Bouyer, and A. Aspect. Momentum spectroscopy of 1d phase fluctuations in bose-einstein condensates. *Phys. Rev. Lett.*, 91(1):010405, 2003.

[102] Rick Trebino, Kenneth W. DeLong, David N. Fittinghoff, John N. Sweetser, Marco a. Krumbügel, Bruce A. Richman, and Daniel J. Kane. Measuring ultrashort laser pulses in the time-frequency domain using frequency-resolved optical gating. *Rev. Sci. Instrum.*, 68:3277, 1997.

[103] J. E. Simsarian, J. Denschlag, M. Edwards, C. W. Clark, L. Deng, E. W. Hagley, K. Helmerson, S. L. Rolston, and W. D. Phillips. Imaging the phase of an evolving bose-einstein condensate wave function. *Phys. Rev. Lett.*, 85:2040, 2000.

[104] J. J. Slosser and P. Meystre. Coherence in quantum optics. *Am. J. Phys.*, 65:275, 1997.

[105] J. Stenger, S. Inouye, A. P. Chikkatur, D. M. Stamper-Kurn, D. E. Pritschard, and W. Ketterle. *Phys. Rev. Lett.*, 82:4569, 1999.

[106] Greg Taft, Andy Rundquist, Margaret M. Murnane, Ivan P. Christov, Henry C. Kapteyn, Kenneth W. DeLong, David N. Fittinghoff, Marco A. Krumbügel, John N. Sweetser, and Rick Trebino. Measurement of 10-fs laser pulses. *IEEE J. Sel. Top. Quantum Electron.*, 2:575, 1996.

[107] Michael Tavis and Frederick W. Cummings. Exact solution for an n-molecule-radiation-field hamiltonian. *Phys. Rev.*, 170:379, June 1968.

[108] S. T. Thompson, E. Hodby, and C. E. Wieman. Ultracold molecule production via a resonant oscillating magnetic field. *Phys. Rev. Lett.*, 95:190404, 2005.

[109] Eddy Timmermans, Paolo Tommasini, Mahir Hussein, and Arthur Kerman. Feshbach resonances in atomic bose-einstein condensates. *Phys. Rep.*, 315:199–230, 1999.

[110] R. Trebino, editor. *Frequency-Resolved Optical Gating: The Measurement of Ultrashort Laser Pulses*. Kluver, Boston, 2000.

[111] R. Trebino and D. J. Kane. *J. Opt. Soc. Am. A*, 10:1101, 1993.

[112] L. You and Maciej Lewenstein. Near-resonant imaging of trapped cold atomic samples. *J. Res. Natl. Inst. Stand. Technol.*, 101:575, 1996.

[113] L. You, Maciej Lewenstein, Roy J. Glauber, and J. Cooper. Quantum field theory of atoms interacting with photons. III. scattering of weak cw light from cold samples of bosonic atoms. *Phys. Rev. A*, 53(1):329, January 1996.

[114] Eitan Yudilevich, Aharon Levi, G. J. Habetler, and Henry Stark. *J. Opt. Soc. Am. A*, 4(1):236, 1987.

[115] J. Zhang, E. G. M. van Kempen, T. Bourdel, L. Khaykovich, J. Cubizolles, F. Chevy, M. Teichmann, L. Taruell, S. J. J. M. F. Kokkelmans, and C. Salomon. Feshbach resonances of ultracold li-6. *Phys. Rev. A*, 70:030702, 2004.

[116] M. W. Zwierlein, J. R. Abo-Shaeer, A. Schirotzek, C. H. Schunck, and W. Ketterle. Vortices and superfluidity in a strongly interacting fermi gas. *Nature, London*, 435:1047, 2005.

[117] M. W. Zwierlein, C. A. Stan, C. H. Schunck, A. J. Kerman, and W. Ketterle. Condensation of pairs of fermionic atoms near a feshbach resonance. *Phys. Rev. Lett.*, 93:120403, 2004.